Deciphering application potentials and basic principles of neural stem cells - implications for BDNF and CB1

Dissertation

zur Erlangung des Grades

„Doktor der Naturwissenschaften“

am Fachbereich Biologie der

Tina Zimmermann

Mainz, Dezember 2016

Table of contents

1 Summary / Zusammenfassung

1.1 Summary

Stem cells have the remarkable potential to differentiate into multiple cell types during early embryogenesis and adulthood. Given their unique regenerative abilities, stem cells offer new potentials for treating neurodegenerative diseases, such as Huntington's disease (HD). In addition, much work is also needed to detail mechanisms underlying the regulation of neural stem cells (NSCs) in the adult brain and to investigate neuropsychiatric diseases in the context of NSC regulation.

HD is characterized by fatal motoric failures induced by loss of striatal medium spiny neurons. Neuronal cell death has been linked to impaired expression and axonal transport of the neurotrophin BDNF (brain-derived neurotrophic factor). By transplanting embryonic stem cell-derived neural progenitors overexpressing BDNF, we combined cell replacement and BDNF supply as a potential HD therapy approach. Transplantation of purified neural progenitors was analyzed in a quinolinic acid (QA) induced and two genetic HD mouse models (R6/2 and N171-82Q) on the basis of distinct behavioral parameters, including CatWalk gait analysis. Explicit rescue of motor function by BDNF-overexpressing neural progenitors was found in QA-lesioned mice, whereas genetic mouse models displayed only minor improvements. Tumor formation was absent, and regeneration was attributed to enhanced striatal neuron differentiation. Additionally, adult neurogenesis was preserved in a BDNF-dependent manner. Our findings provide significant insight for establishing therapeutic strategies for HD to ameliorate neurodegenerative symptoms.

Adult born neurons in the subgranular zone (SGZ) of the dentate gyrus (DG) are continuously generated and incorporated in the hippocampal neuronal circuitry, yet the molecular mechanism of this process remains still unclear. Adult NSCs contain a functional endocannabinoid system. Endocannabinoids are endogenous lipids, which can bind to and activate the cannabinoid type 1 (CB1) receptor, thereby eliciting multiple cellular responses such as inhibition of neurotransmitter release and activation of different intracellular signaling cascades. To address the direct role of CB1 receptor expressing adult NSCs *in vivo*, we generated the triple-transgenic nestin-CreERT2/R26-STOP-YFP/CB1flox/flox mouse line. Tamoxifen injections induced deletion of the CB1 receptor and expression of yellow fluorescent protein (YFP) specifically in adult nestin-expressing stem cells and their progeny. We found that neural stem cell-specific deletion of the CB1 receptor led to a decrease in

neural stem cell proliferation in the dentate gyrus as reflected by a decreased number of YFP+ and BrdU+ cells. In contrast, the differentiation potential of targeted NSCs was not shifted towards a specific neural lineage. By recording field excitatory postsynaptic potentials in the DG and cornu ammonis 1 (CA1) region, we found that mice with CB1 deficiency specifically in adult-born neurons displayed an impaired long-term potentiation. Furthermore, lack of functional CB1 receptor in NSCs led to a decrease in short-term spatial memory. Additionally, CB1-deficient animals showed an increase in depressive-like behavior. The present study shows that the proliferation of newborn neurons critically depends on CB1 receptor function, reflecting their importance in synaptic transmission processes and their involvement on the behavioral level.

1.2 Zusammenfassung

Stammzellen besitzen die außergewöhnliche Fähigkeit, sich während der Embryogenese oder im Adultstadium in verschiedenste Zelltypen des Körpers zu entwickeln. Aufgrund ihrer einzigartigen regenerativen Eigenschaften können sie als neue Behandlungsmöglichkeiten für neurodegenerative Erkrankungen, wie z.B. die Huntington'sche Erkrankung (*Huntington's disease*, HD), dienen. Ein weiteres großes aktuelles Forschungsgebiet umfasst die Aufklärung der molekularen Regulationsmechanismen neuraler Stammzellen im adulten Gehirn. Dies dient u.a. dazu, die Grundlagen neuropsychiatrischer Erkrankungen im Kontext der Stammzellregulation zu erforschen.

HD ist durch schwerwiegende motorische Störungen charakterisiert, induziert durch das Absterben striataler „medium spiny" Neurone. Der genaue Auslöser des neuronalen Zelltods ist bislang weitgehend ungeklärt; allerdings wurde er mit einer reduzierten Expression und einem verringertem axonalen Transport des Neurotrophins BDNF (*brain-derived neurotrophic factor*) in Verbindung gebracht. In der hier vorliegenden Arbeit wurden Zellersatz und BDNF-Versorgung als potentieller HD Therapieansatz kombiniert. Hierfür wurden aus embryonalen Stammzellen abstammende neuronale Vorläuferzellen, die BDNF überexprimieren, in drei verschiedene HD Mausmodelle transplantiert. Nachfolgend wurden die Auswirkungen der transplantierten Zellen auf das motorische Verhalten im exzitotoxischen Quinolinsäure (*quinolinic acid*, QA) Mausmodell und in zwei genetischen Mausmodellen (R6/2 und N171-82Q) auf Basis bestimmter Verhaltensparameter, inklusive Gangparameter Analyse mit „CatWalk" analysiert. Eine eindeutige „Rettung" der motorischen Funktion durch BDNF-neuronale Progenitoren wurde in QA-läsionierten Mäusen gefunden,

wohingegen die genetischen Mausmodelle nur geringe Verbesserungen zeigten. Histopathologisch wurde eine gesteigerte striatale Differenzierung der BDNF-überexprimierenden Zellen beobachtet, welche die im Vergleich zu Kontrollen erhöhte motorische Regeneration erklärt. Zusätzlich wurde die adulte Neurogenese in einer BDNF-abhängigen Weise erhalten. Ein weiteres wichtiges Charakteristikum der hier angewendeten Stammzelltherapie ist, dass keine Tumorentstehung oder entartetes Zellwachstum beobachtet wurden. Insgesamt liefern unsere Ergebnisse wichtige Erkenntnisse für die Etablierung therapeutischer Strategien für HD, um neurodegenerative Symptome zu lindern.

In der subgranularen Zone (SGZ) des adulten Gyrus Dentatus (DG) werden kontinuierlich neue Neurone generiert und in die hippokampalen Schaltkreise integriert, jedoch ist der molekulare Mechanismus dieses Prozesses weitgehend unklar. Wie die meisten Neurone besitzen adulte neurale Stammzellen (*neural stem cells*, NSCs) ein funktionelles Endocannabinoid-System. Endocannabinoide sind endogene Lipide, die an den Cannabinoid Typ 1 (CB1)-Rezeptor binden und diesen aktivieren können, wodurch multiple zelluläre Reaktionen wie die Hemmung der Neurotransmitter-Freisetzung und eine Aktivierung verschiedener intrazellulärer Signalkaskaden hervorgerufen werden können. In der hier vorliegenden Arbeit wurde die dreifach transgene Mauslinie nestin-CreERT2/R26-STOP-YFP/CB1flox/flox generiert, um die direkte Rolle des CB1-Rezeptors, der in adulten neuralen Stammzellen exprimiert wird, zu untersuchen. Durch Tamoxifen-Injektion kam es zur induzierten Deletion des CB1-Rezeptorgens und der Expression von gelbem Fluoreszenzprotein (YFP) spezifisch in adulten Nestin-exprimierenden Stammzellen und deren zellulären Nachkommen. Die neurale stammzellspezifische Inaktivierung des CB1-Rezeptors führte zu einer Abnahme der YFP- und BrdU-positiven Zellen und damit zu einer Abnahme der neuralen Stammzellproliferation im DG. Im Gegensatz dazu wurde das Differenzierungspotential der rekombinierten NSCs nicht in eine spezifische neurale Differenzierungsrichtung verschoben. Durch elektrophysiologische Messungen von Feld-exzitatorischen postsynaptischen Potentialen in der DG- und Cornu Ammonis 1 (CA1) Region wurde beobachtet, dass Mäuse mit einer spezifischen CB1-Rezeptor-Defizienz in adult-geborenen Neuronen eine beeinträchtigte Langzeitpotenzierung zeigten. Darüber hinaus führte der Mangel an funktionellem CB1-Rezeptor in adulten Stammzellen zu einer Abnahme des kurzzeitigen räumlichen Gedächtnisses. Zusätzlich zeigten CB1-Rezeptor-defiziente Tiere eine Zunahme depressionsähnlichen Verhaltens. Die vorliegende Studie zeigt, dass die Proliferation von neugeborenen Neuronen entscheidend von der Funktionalität des CB1-Rezeptors abhängt, welches ihre Bedeutung für synaptische Übertragungsprozesse und ihre Beteiligung auf der Verhaltensebene widerspiegelt.

2 Introduction

2.1 Stem cells

Every organ and tissue in our bodies originates from stem cells. Highly specialized cells arise from an initial pool of stem cells generated shortly after fertilization. Throughout our lives we still rely on residing stem cells to replace cells after injury or to replenish lost cells, like skin, hair or blood.

Stem cells are characterized by two key properties:

1) The ability to self-renew by division

If the division yields two identical copies, the division is called symmetric. Asymmetric division includes the generation of one new stem cell and a daughter (progenitor) cell with limited self-renewal capacities.

2) The potency to differentiate (‘multipotency’)

The potential to differentiate into different cell types can be divided into categories of potency. The fertilized egg (zygote) and the subsequent first divisions are termed *totipotent*. The zygote, the ultimate stem cell, can produce an entire organism including the trophoblast/placenta. Further divisions lead to the morula and the blastocyst stage, where a cavity forms and cells accumulate to the inner cell mass (Figure 1). Embryonic stem cells (ESCs) are obtained from the inner cell mass. The ESCs are termed *pluripotent*, which means being able to generate all different types of cells in the body, namely the three germ layers: the endoderm, mesoderm and ectoderm. Human ESCs are derived from blastocysts that were created by *in vitro* fertilization (IVF) for assisted reproduction. Somatic/adult stem cells are called *multipotent*, since they are already specialized and can produce restricted cell types within a particular tissue/organ. Finally, differentiated somatic cells are called *unipotent*.

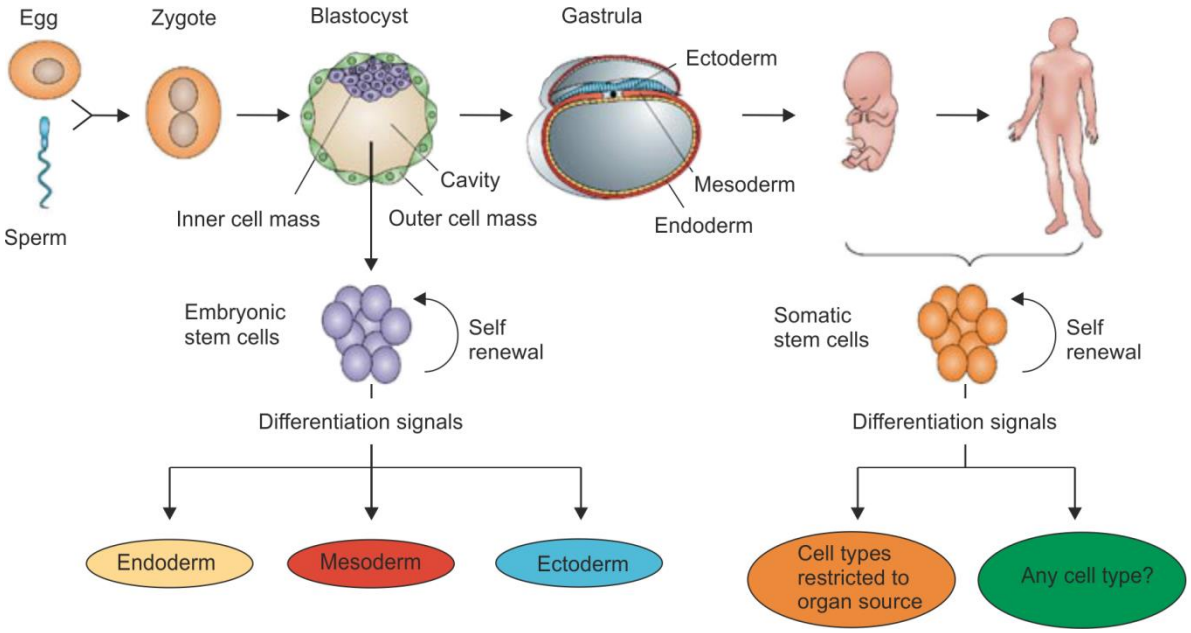

Figure 1. Derivation of embryonic and adult (somatic) stem cells (O'Connor and Crystal, 2006). During human fertilization sperm and egg cells fuse, generating a diploid zygote. After multiple cell divisions the blastocyst stage includes a blastocyst cavity, outer and inner cell mass. Embryonic stem cells are derived from the inner cell mass. After isolation they can self-renew and differentiate into all three germ layers: endoderm, mesoderm, and ectoderm. Upon implantation, the gastrula contains all three germ layers in utero. Somatic stem cells can be found in fetal and post-natal tissue. They are also capable of self-renewal and differentiation into cell types from the organ from which we they are derived.

One of the most prevalent topics in stem cell research includes the study of induced pluripotent stem cells (iPSCs). Somatic cells (for example skin cells) can be reprogrammed by the introduction of four reprogramming genes to become pluripotent, behave like an embryonic stem cell, and develop into all cell types of the body. In 2006, Shinya Yamanaka made the ground-breaking discovery that won him the Nobel Prize in Physiology or Medicine six years later (Takahashi and Yamanaka, 2006). IPSCs from patients that carry specific mutations can be used for modelling a distinct disease in the dish, which can serve for drug testing or discovering new mechanisms to better understand the disease. IPSCs can be generated from any genotype, which has opened new avenues for personalized medicine, because the risk of rejection of patient-specific stem cells after transplantation may be minimized.

2.1.1 Embryonic stem cells

ESCs are derived from the inner cell mass of a blastocyst (Evans and Kaufman, 1981; Martin, 1981) and can give rise to all cell types from the three germ layers. The first human ESC cultures have been isolated by Thomson and colleagues in 1998 (Thomson et al.,

1998). In cell culture, they can be expanded almost indefinitely, comprising a proper cell population to model development in the dish, to study disease states and to generate implantable cells to treat incurable diseases.

ESCs can be genetically modified to express a gene of interest or to carry a mutation for a gene knock out. To generate knock out or knock-in cells ESCs are electroporated with a vector containing a targeting sequence. This gene sequence is then integrated into the genome by homologous recombination (Thomas and Capecchi, 1987). ESCs can also be used to create genetically modified mice. Genetically altered mouse ESCs are re-injected into the blastocyst and returned to the uterus of a female mouse to develop into a foetus with a mixture of cells, resulting in a chimera (Capecchi, 1989; Doetschman et al., 1987). The offspring of those chimeras contains genes from originally modified ESCs. The discovery was rewarded with the Nobel Prize in Physiology or Medicine 2007 for Mario R. Capecchi, Sir Martin J. Evans and Oliver Smithies.

In vitro, mouse ESCs are cultured on mouse embryonic fibroblasts (Figure 2A) in the presence of calf serum and a differentiation-inhibiting cytokine, leukemia inhibitory factor (LIF) (Smith et al., 1988; Williams et al., 1988). Human ESCs need basic fibroblast growth factor 2 (FGF2) to keep pluripotency. Both types of ESCs express pluripotency factors Octamer binding transcription factor 4 (Oct4) (Okamoto et al., 1990; Scholer et al., 1990), SRY-box transcription factor 2 (Sox2) (Ambrosetti et al., 1997), Nanog (Chambers et al., 2003), and a suite of transcription factors (Esrrb, Klf4, Klf2, and Tbx3 (Nichols and Smith, 2012)). Sox2 is also expressed later in all neuroectodermal cells, representing also a marker for adult neural stem cells *in vivo*. In this state, ESCs are pluripotent, which can also be identified by injecting ESCs into immune-comprised mice for the formation of a benign tumour, called teratoma, in which tissue derived from all three germ layers can be found (Stevens and Varnum, 1974).

To initiate differentiation of ESCs *in vitro*, they can be cultured as embryoid bodies (EBs), recapitulating embryonic development as non-adherent cultures in the absence of LIF or FGF2. The EBs are comprised of aggregates of differentiating ESCs and consist of ectoderm, mesoderm, and endoderm (Desbaillets et al., 2000) (Figure 2B).

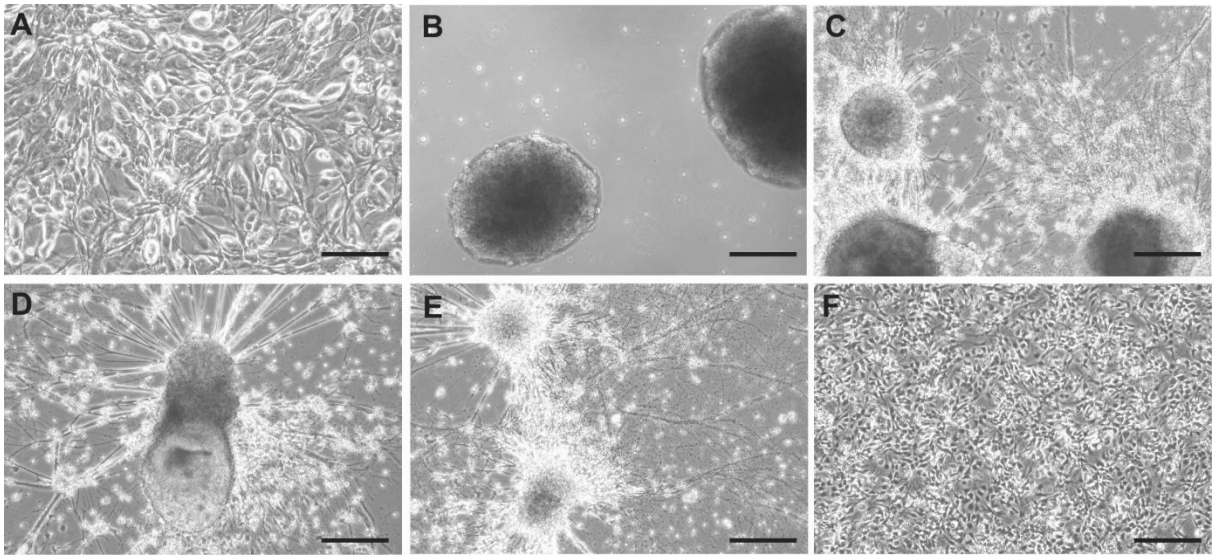

Figure 2. Recapitulating embryogenesis *in vitro*. Brightfield micrographs of mouse embryonic stem cells (ESCs) in culture (unpublished images). ESCs are cultured on mouse embryonic fibroblasts (A). In non-adherent culture conditions embryoid bodies (B) form and start differentiating in adherent dishes (C). After differentiation for several days (D, E) by using the lineage selection protocol (Butenschon et al., 2016), neuronal progenitor cells are formed (F). Scale bar, 200 µm.

By using specific growth factors and signaling molecules ESCs can differentiate into cardiogenic (Wobus et al., 1991)(Maltsev et al., 1993; Maltsev et al., 1994), myogenic (Rohwedel et al., 1994), adipocytic (Dani et al., 1997), chondrogenic (Kramer et al., 2000), osteogenic (Hegert et al., 2002), hematopoetic (Schmitt et al., 1991), insulinproducing (Schroeder et al., 2006), and epithelial cell types (Bagutti et al., 1996). Just recently, researchers have created artificial oocytes from fibroblasts (via iPSCs) *in vitro* (Hikabe et al., 2016). Neural cell types have also been shown to be differentiated from ESCs (Fraichard et al., 1995; Strubing et al., 1995). The differentiation to neuronal cell types is controlled by an intrinsic predefined mechanism *in vivo*. It has been shown in Xenopus that the neuroectoderm will develop from ectoderm through a default mechanism (Hemmati-Brivanlou and Melton, 1997).

In general, three different strategies have been developed:

1) To obtain neurons of different specifications, ESCs are cultured as a monolayer culture in the addition of growth factors or signaling molecules (Gerrard et al., 2005; Itsykson et al., 2005; Perrier et al., 2004; Reubinoff et al., 2001)

2) To induce the differentiation into neurons by co-culturing ESCs with stromal cells/astrocytes (Kawasaki et al., 2000)

3) To select neural precursor cells by letting ESCs form EBs in the presence of serum or defined media (Tropepe et al., 2001; Zhou et al., 2008)

With these protocols it has been possible to obtain neurons of different specifications, such as dopaminergic (Kawasaki et al., 2000; Lee et al., 2000), serotonergic (Barberi et al., 2003), and motor neurons (Li et al., 2005; Wichterle and Peljto, 2008). When EBs are cultured in the presence of retinoic acid (RA), a high number of neurons can be generated (Bain et al., 1995). Leschik et al. used this approach in a combination of overexpressing BDNF in ESCs and obtained an enriched population of GABAergic neurons (Leschik et al., 2013).

Finally, the lineage selection protocol allows for generation of a high number of neural precursor cells from EBs in the presence of FGF-2 (Figure 2C-F). Here, survival and proliferation of ectodermal neural precursor cells are favoured in contrast to mesodermal and endodermal cell differentiation (Okabe et al., 1996). Terminal differentiation into neurons is induced by withdrawal of FGF-2 (Figure 2G). We were using this protocol in Chapter 3 to derive telencephalic precursor cells *in vitro*, which then can be transplanted into Huntington's disease mouse models to obtain medium spiny neurons *in vivo*.

Current challenges facing applied ESC research include their pluripotency and their highly tumorigenic potential if not fully differentiated before transplantation, which could result in dysontogenetic tumors, teratomas or teratocarcinomas (Asano et al., 2003; Langa et al., 2000; Reubinoff et al., 2001).

2.1.2 Adult stem cells

Various types of adult stem cells have been identified in distinct organs and tissues, creating stem cell niches in the entire body (Figure 3). Adult stem cells form different kinds of tissues or some of the cells of a particular tissue. Mesenchymal stem cells generate cartilage, bone, tendon, ligaments, muscle, skin, and fat cells. In contrast, hematopoietic stem cells form blood cells only, while neural stem cells give rise to cells in the adult nervous system, such as neurons, astrocytes, and oligodendrocytes (Gage, 2000).

Blood, skin, and intestines are the classic regenerative tissues, whereas the brain regenerates poorly.

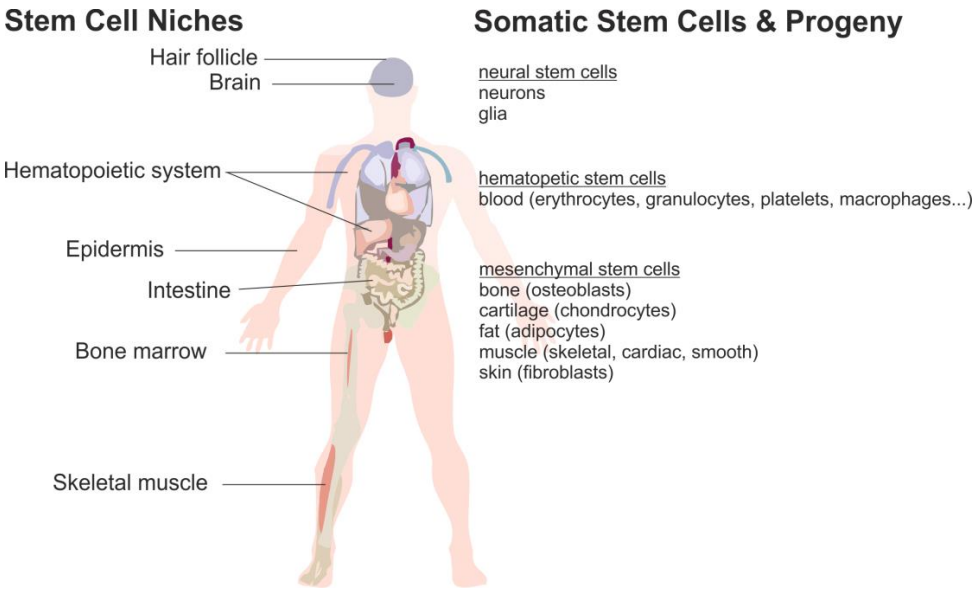

Figure 3. Overview of somatic stem cell niches, stem cell types and their progeny (modified from (Sun and Lai, 2013)).

2.1.2.1 Adult neural stem cells

Adult-born neurons are continuously generated in neurogenic regions in the mammalian brain throughout life, in the subgranular zone (SGZ) of the hippocampal dentate gyrus (DG) and in the subventricular zone (SVZ) of the lateral ventricle (Altman and Das, 1965) (Figure 4).

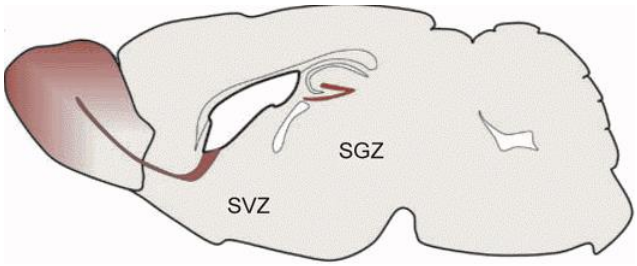

Figure 4. Neurogenic niches in the adult brain. The subventricular zone (SVZ) of the lateral ventricles and the subgranular zone (SGZ) of the dentate gyrus give rise to newborn neurons (Ma et al., 2009).

In the SGZ, new granule neurons are generated and incorporated in the hippocampal circuitry. Subsequently, they regulate multiple physiological functions (Kee et al., 2007). In the SVZ, stem cells generate transiently amplifying progenitor cells, which give rise to migratory progenitors travelling along the rostral migratory stream (RMS) to the olfactory bulb. Here, they terminally differentiate into local interneurons and integrate into the network (Doetsch et al., 1999).

Adult neurogenesis itself is a complex process in the neural stem cell niche and is regulated at many stages of cell development. A self-renewing precursor cells divides either symmetrical or asymmetrical, giving rise to progeny, which can become neuronal or glial. A part of the daughter cells survives and migrates. Differentiation includes dendrite and axon extension and formation of synapses. Finally, newborn neurons integrate into the existing network and establish new connections.

Despite the two niches SGZ and SVZ, the hypothalamus has been identified as a neurogenic region. The presence of BrdU (Bromdesoxyuridin)-incorporating cells has been confirmed, but neurogenesis occurs at a lower rate than in the SVZ or SGZ, and the identification of the exact cell of origin of newborn neurons is still under debate (Cheng, 2013; Evans et al., 2002).

Under normal conditions, the adult brain appears to be essentially non-neurogenic. However, under the condition of acute cell death (e.g. ischemia) in the striatum of mice, reactive neurogenesis seems to be possible, even though the response does not seem to originate from local stem cells rather based on precursor cells recruited from the SVZ (Arvidsson et al., 2002; Thored et al., 2006). Further studies have shown that overexpression of BDNF in the SVZ can lead to striatal neurogenesis as well (Benraiss et al., 2001; Chmielnicki et al., 2004), thus creating a neurogenic permissiveness.

To gain insights about function and properties of adult neural stem cells for the situation *in vivo*, neural stem cells can be studied *in vitro*. They can be isolated from the niche and propagated and differentiated *in vitro* as adherent cultures or as floating aggregates, the neurospheres (Ray et al., 1993; Reynolds and Weiss, 1992). Major conclusions about stemness, self-renewal, and multipotency were drawn from these techniques. However, they have to be cultured in the presence of FGF-2 and epidermal growth factor (EGF), resulting in an artificial system, which can only serve as a model for the *in vivo* situation.

The unique microenvironment in the SGZ regulates activation, development, and maintenance of adult neural precursor cells by a number of signaling molecules (Mu et al., 2010). In Chapter 4 we are going to assess the influence of the CB1 receptor on the process of adult neurogenesis in the SGZ.

2.2 Aims of the thesis

Stem cells are a powerful tool to study neural development, to model a disease or to serve as a therapy for diseases of the central nervous system. This thesis pursues two main aims: first, the regenerative potential of neurally differentiated embryonic stem cells (ESCs) genetically modified to overexpress BDNF in mouse models of Huntington's disease and second, the functional role of the CB1 receptor in adult neural stem cells (NSCs) of the hippocampus.

Regarding the first aim, we established a combination therapy approach composed of cellular replacement by ESC-derived neural progenitors linked to BDNF supply for Huntington's disease (HD). HD is a neurodegenerative disease characterized by dramatic motor dysfunction, cognitive decline, and psychiatric symptoms, which lead to progressive dementia and death. To date, treatment has been regarded only as symptomatic and cell transplantation might be a suitable alternative. The transplanted cells might replace degenerated neurons and improve functional behavior by re-establishing neuronal circuits. For this reason, we have generated BDNF overexpressing mouse ESCs by knock-in technology that display an enhanced neuronal differentiation *in vitro*. In the present study, we grafted cells into three different mouse models for HD, assessed the efficient regeneration with multiple behavioral tests and analyzed the cells for potential tumor formation, survival, differentiation, and the effect on endogenous adult NSCs in the subventricular zone (SVZ) (Chapter 3). The results obtained in this study are of high impact for therapeutic interventions, as they add knowledge to former and future cell replacement approaches in HD patients.

The second chapter of this thesis (Chapter 4) aimed at understanding to what extent adult NSCs in the neurogenic niche in the subgranular zone (SGZ) of the hippocampus are regulated by the CB1 receptor. The unique microenvironment has been shown to modulate activation, development, and maintenance of adult neural precursor cells by a number of signaling molecules. Since CB1 deletion in all cells of the nervous system caused a decrease in adult neurogenesis and a reduced differentiation into the glial lineage, we were interested to know if this process is regulated by a direct (CB1 on adult NSCs) or an indirect (CB1 on surrounding neurons and astrocytes) mechanism. We used triple transgenic mice to specifically delete CB1 on adult NSCs and assessed the rate of proliferation and differentiation of neuronal progenitors. Furthermore, we were interested, whether this loss of CB1 receptor only in adult NSCs in the SGZ leads to alterations in synaptic plasticity in the hippocampal circuit and to behavioural deteriorations, such as depression-like behavior and

memory. With this approach we shed light on the exact role of CB1 receptor on adult NSCs in regulating adult neurogenesis and behavior.

3 Cell replacement therapy with BDNF-overexpressing stem cells in mouse models of HD

3.1 Introduction

3.1.1 Huntington's disease

Huntington's disease (HD) is the most common monogenic neurological disorder in the developed world (Fisher and Hayden, 2014) and is a devastating condition for patients and their families. Prevalence studies show that 1 in 7,300 individuals are affected in Western populations (Fisher and Hayden, 2014). HD is also known as Huntington's chorea (involuntary muscle jerks and twitches), while chorea was first defined by Paracelsus (1493–1541) to define this movement disorder. HD is known since the last 17th century, but it has been first classically described by George Huntington in 1872 (Huntington, 1872). HD is a neurodegenerative disease, which is characterized by dramatic motor dysfunction, cognitive decline, and psychiatric symptoms, leading to progressive dementia and death approximately 15-20 years after onset (Landles and Bates, 2004). It is an autosomal dominant inheritable disease, caused by an expanded CAG (cytosine adenine guanine) trinucleotide repeat in the huntingtin (HTT) gene, leading to an increased number of poly-glutamine repeats in the encoded protein (Group, 1993). The gene HTT is located at chromosome 4p16.3 (Group, 1993). The length of the CAG trinucleotide repeat in this segment can be determined in any individual - healthy, at risk, or clinically diagnosed with HD - by a polymerase chain reaction (PCR) assay with specific primers. The age of motor onset is dependent on the number of CAG repeats, with higher numbers of repeats causing earlier onset and faster progression (Langbehn et al., 2010).

Average CAG repeats in HTT in healthy individuals are 18.4–18.7 repeats in people of European descent, whereas HD patients carry more than 36 CAG repeats (Squitieri et al., 1994). The history of clinical HD (Figure 5) is characterized by a pre-manifest period (Ross et al., 2014), where no symptoms can be detected.

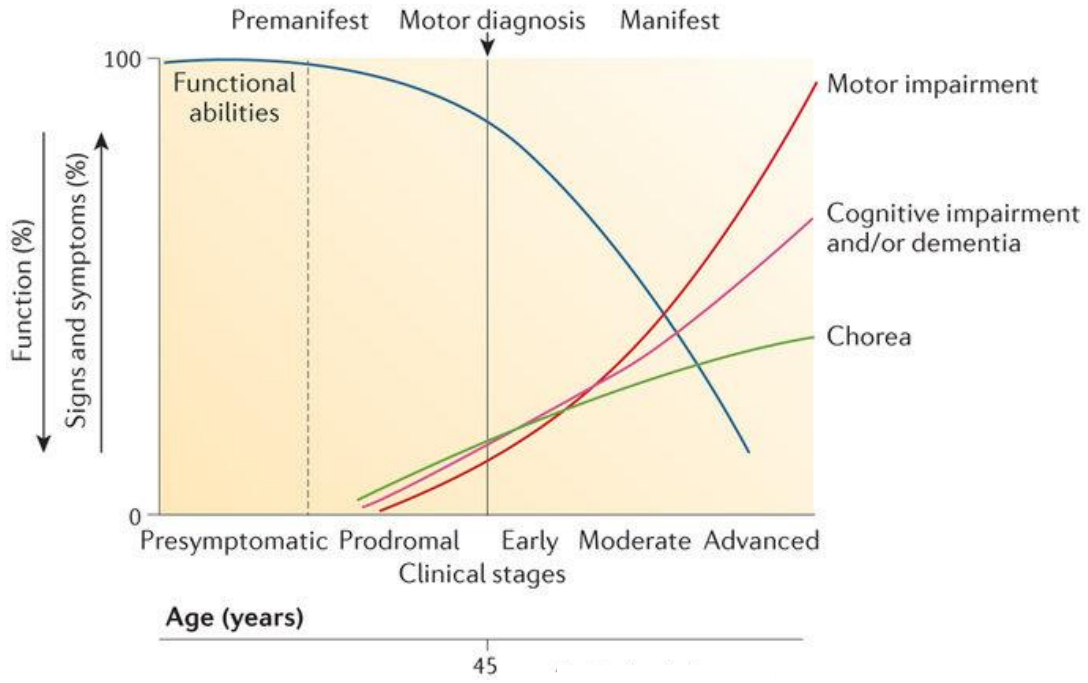

Figure 5. Natural history of clinical Huntington's disease (HD). The pre-manifest period occurs before diagnosable symptoms of HD. The manifest phase involves slow progression of motor and cognitive difficulties and Chorea is observed (Bates et al., 2015).

In the prodromal phase, subtle motor, cognitive, and behavioral changes are detected and often precede a formal clinical diagnosis. The mean age of disease onset is 45, but there is substantial inter-individual variability, which also depends on the CAG repeat length. Signs and symptoms develop over the course of the disease, such as progressive dementia, gradual impairment of the mental processes involved in comprehension, reasoning, judgment, and memory. Patients become unable to walk, have poor dietary intake, they cease to talk, and become unable to care for themselves. They potentially require long-term institutional care. Most HD patients eventually die from aspiration pneumonia because of difficulties to swallow (Bates et al., 2015).

The protein huntingtin consists of 3,144 amino acids and has a molecular weight of 348 kDa. It is expressed at varying levels in cells throughout the whole body. In the cell, it is found in the cytoplasm and the nucleus, shuttling between both compartments. The normal functions of huntingtin are not well understood, however, it has been implicated in the development of the nervous system, in brain-derived neurotrophic factor (BDNF) production and transport, and in cell adhesion (Zuccato and Cattaneo, 2014).

HD is primarily a toxic gain-of-function disease, and chronic expression of mutant HTT leads to multiple pathological events in the cell (Figure 6).

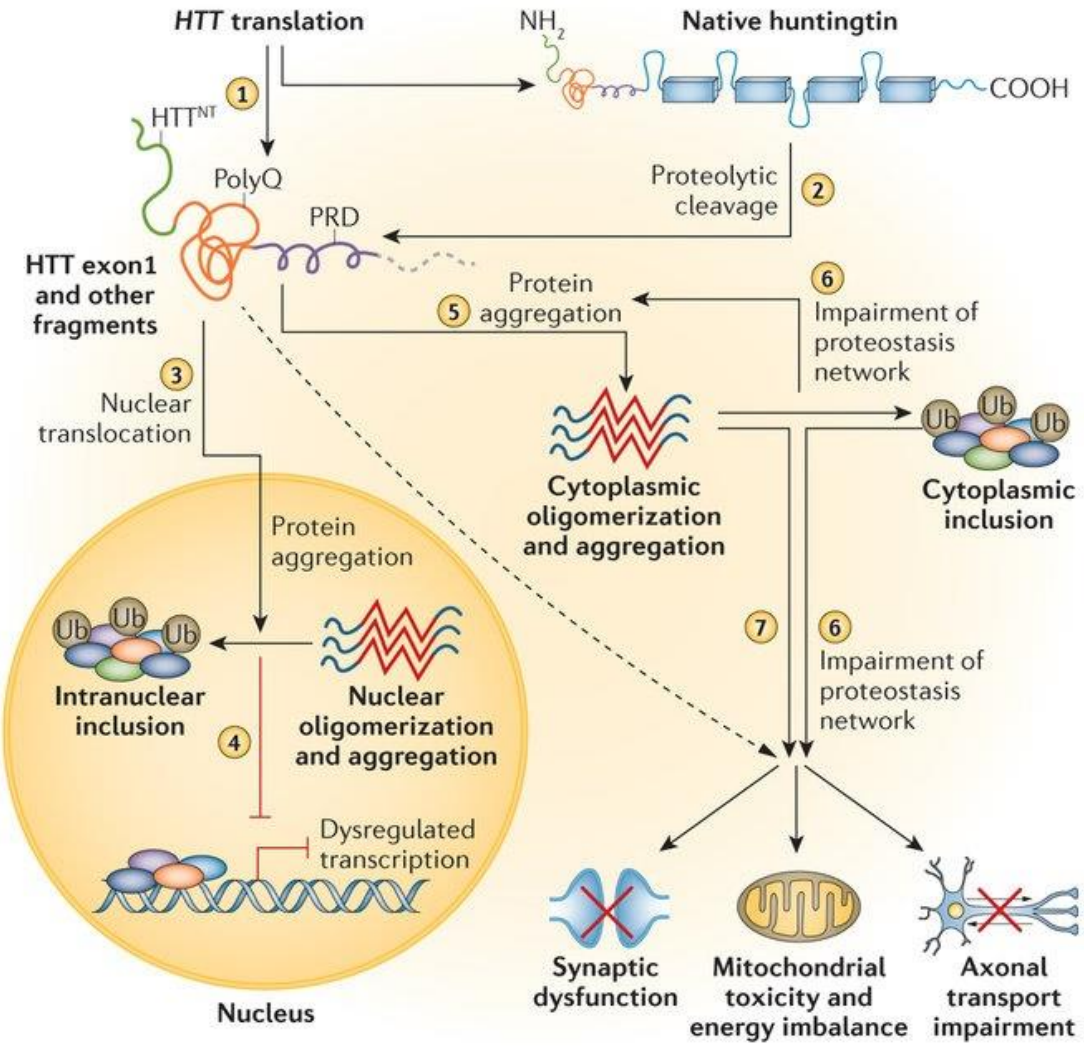

Figure 6. Pathological events in a cell of HD (Bates et al., 2015). Translation of HTT leads to production of full-length huntingtin and HTT exon1 fragment (1) and full-length native huntingtin is cleaved to generate protein fragments (2). These fragments enter the nucleus (3), aggregate, and form inclusions, leading to a transcriptional dysregulation (4). In the cytoplasm, huntingtin fragments generate massive huntingtin-rich inclusions (5). These aggregates lead to impairments of the proteostasis network (6), and further result in synaptic dysfunction, mitochondrial toxicity, and a decreased rate of axonal transport (7).

Nuclear HTT aggregates are multiple micrometres in diameter, contain >100,000,000 molecules of HTT-related peptides (Wetzel and Mishra, 2014), and lead to dysregulated transcription. Cytoplasmic aggregates interfere with the proteostasis network and lead to synaptic dysfunction, mitochondrial toxicity, and axonal transport impairment.

The pathology of HD consists of prominent cell loss in the brain and atrophy in the caudate nucleus and putamen. Especially GABAergic medium spiny neurons of the striatum are particularly vulnerable to mutant HTT-induced harm and are primarily responsible for typical HD symptoms (Reiner et al., 1988). Additionally, GABAergic neurons degenerate in other areas of the brain, such as the substantia nigra (pars reticulata), the subthalamic nucleus,

the thalamus, the hippocampus, and also in cortical areas (Vonsattel et al., 1985). This leads to shrinkage of the striatum, to enlarged lateral ventricles, and to cortical atrophy. The striatum is an important brain structure that initiates and modulates voluntary movements and influences emotional and cognitive behavior (Alexander et al., 1990). It is comprised of the caudate nucleus and the putamen that are connected with the substantia nigra (pars compacta and pars reticulata). The putamen is primarily involved in motor control by projecting to the supplementary motor area and premotor cortex. The caudate nucleus is connected with the lateral orbitofrontal cortex mediating limbic functions such as motivation, emotion, and reward. It also projects to the dorsolateral prefrontal cortex, which is involved in cognitive functions (Alexander et al., 1990).

How mutant HTT protein causes neuronal dysfunction and neurodegeneration has not yet been understood in detail, but depletion of neurotrophins, especially BDNF, is a prominent feature of HD and a high priority therapeutic target (Sari, 2011).

3.1.2 BDNF

Brain-derived neurotrophic factor (BDNF) is a key regulator of neuronal circuit development and function. It promotes cell survival and differentiation, and is essential for neurite outgrowth and synaptogenesis (Huang and Reichardt, 2001). BDNF is a member of the neurotrophins, a group of polypeptide growth factors (Binder and Scharfman, 2004). The group includes nerve growth factor (NGF) and neurotrophin (NT)-3 and NT-4/5. BDNF binds with high-affinity to tropomyosin-receptor kinase B (TrkB) receptor (Squinto et al., 1991) and with low affinity to p75 neurotrophin receptor (p75NTR) (Curtis et al., 1995). Activation of the TrkB receptor leads to dimerization of the receptor and autophosphorylation of tyrosine residues. Src homology 2 domain-containing adapter protein (Shc) and phospholipase C (PLC) dock at the domain and activate intracellular signaling cascades such as Ras, phosphoinositide 3-kinase (PI3K) and PLC (Kaplan and Miller, 2000), which are involved in multiple aspects of neuronal survival and neurite outgrowth (Dimitropoulou and Bixby, 2000; Vaillant et al., 1999). Activation of p75NTR is important for pro- and anti-trophic processes, such as neurite outgrowth and apoptosis (Kaplan and Miller, 2000). Since BDNF plays a role in neuronal survival and apoptosis, numerous studies have focused on the role of BDNF in development. BNDF knock-out mice die shortly after birth, emphasizing the importance of BDNF for postnatal survival. Surviving mice show poorer peripheral nervous system development, but display mild deficiencies in central nervous system (CNS) development (Jones et al., 1994). Infusion of BDNF in the adult brain has been shown to promote

neurogenesis (Pencea et al., 2001; Scharfman et al., 2005) in multiple brain regions, such as hippocampus, septum, thalamus, hypothalamus, and striatum. In the developing striatum, selective removal of TrkB from the lateral ganglionic eminence led to a loss of medium spiny neurons and an increase in apoptosis in the subventricular zone (Baydyuk et al., 2011), highlighting the significance of BDNF for striatal cell survival and development. Furthermore, conditional deletion of BDNF from postmitotic neurons resulted in smaller striatal neurons, fewer dendritic segments, and reduced spine density (Rauskolb et al., 2010), thus underlining the role of BDNF in neuronal maturation. Striatal neurons require BDNF to survive, which is mainly produced in the cortex and transported anterogradely to the striatum via corticostriatal afferents. It facilitates glutamate release and controls striatal output. This process is regulated by wildtype HTT, which upregulates transcription of BDNF (Zuccato et al., 2001) (Figure 7).

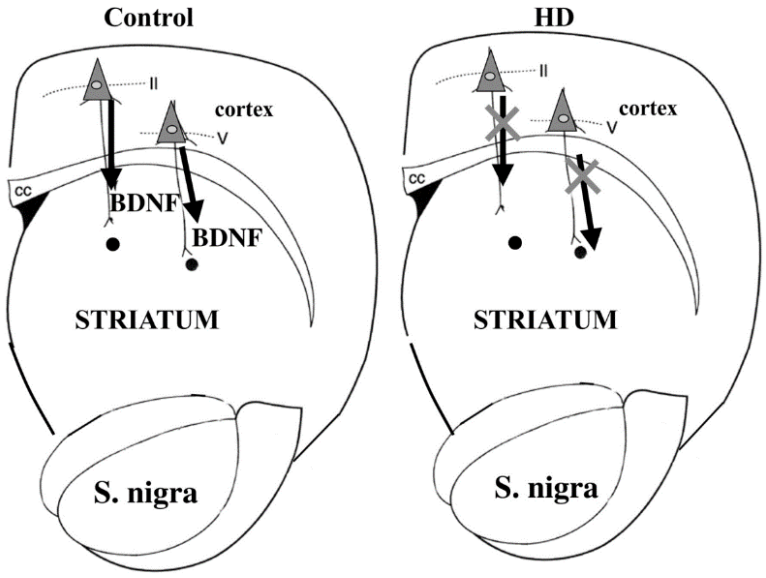

Figure 7. BDNF is transported anterogradely from the cortex to the striatum via the corticostriatal afferents (Control). In HD, loss of wildtype huntingtin results in a decreased production and transport of BDNF to the striatum resulting in increased vulnerability of striatal neurons (Cattaneo, 2003).

In HD mouse models, BDNF or BDNF/TrkB signaling is strongly reduced due to a mutant HTT-mediated mechanism (Plotkin et al., 2014; Zuccato and Cattaneo, 2009). Besides causing changes in vesicular transport of BDNF (Gauthier et al., 2004), mutant HTT has also been described to cause transcriptional downregulation of the BDNF gene through translocation of RE1 silencing transcription factor (REST) to the nucleus (Buckley et al., 2010). In addition to HD mouse models, a systematic and quantitative assessment of BDNF levels in human cerebral cortex samples, examined post-mortem, confirmed that the production of this neurotrophin was impaired in the brains of HD patients (Zuccato et al.,

2008). As striatal medium spiny neurons (MSNs) depend on BDNF activity, a number of studies intended striatal neuroprotection by providing exogenous BDNF delivered to the diseased rodent striatum either by adeno-associated viral transfer or by the transplantation of diverse genetically-modified cell types (e.g. fibroblasts) (Connor et al., 2016; Sari, 2011). Altogether, these studies showed enhanced neuroprotection, but no or only mild effects on long-term functional improvement in HD rodent models.

3.1.3 Huntington's disease mouse models

At present, a variety of different HD mouse models exists, chemically- or genetically-induced, which match with some aspects of HD pathology. However, to date, none of them perfectly recapitulates human neuropathological hallmarks as well as progressive cognitive and motor impairments.

Genetic models are divided into three groups depending on how they were generated. First, N-terminal transgenic animals carry the 5' portion of the human HTT gene with CAG repeats. In contrast, full-length transgenic models carry the full- length HTT sequence and CAG repeats, encoding for polyglutamines. Third, in knock-in models, the HD mutation is engineered by directly introducing CAG repeats of varying length into the mouse huntingtin genomic locus. All HD mouse models differ in their CAG repeat numbers, size and species of origin of the huntingtin protein, the promoters that drive huntingtin expression, and the background strain (Menalled, 2014).

So far, genetic HD mouse models were only used in a few cell transplantation studies. Instead in most cases, cell transplantation was mainly performed in toxin-lesioned mice, where vast neurodegeneration occurs. This is clearly an advantage over genetic mouse models, which harbour less neurotoxicity. In contrast, genetic accuracy is missing in toxin-induced lesions, and therefore, it is questionable whether this represents an appropriate model system to test therapeutics for human pathology. For this reason, we decided to use for our cell-transplantation approach, besides the toxin-lesioned model with quinolinic acid (QA), the two widely used transgenic mouse lines R6/2 and N171-82Q, which differ in their extent of pathological features and degree of impairment (Ramaswamy et al., 2007).

The induction of an excitotoxic lesion in the striatum of healthy rodents is generally obtained by injection of QA, which acts as a N-methyl-D-aspartat (NMDA) receptor agonist. Overstimulation leads to a selective degeneration of striatal medium-sized GABA (gamma-aminobutyric acid)-ergic projection neurons and spares GABAergic interneurons and

dopaminergic and serotonergic afferent projections (Beal et al., 1991). The lesion leads to striatal shrinkage, enlargement of the lateral ventricles, and reactive gliosis (Beal et al., 1989), secreting also neurotrophic factors and creating a permissive environment for transplantation of cells. Animals with a unilaterally lesioned striatum display hyperkinesia and HD-like behaviors (Bernreuther et al., 2006; Giralt et al., 2010; Pineda et al., 2007). However, dyskinesia and chorea-like movements are missing. It is rather an acute model and does not resemble the progressive development of HD (Sanberg and Coyle, 1984).

One of the most extensively studied mouse models for HD is the R6/2 mouse line. It is one of the fastest progressing mouse models (life span: 12 weeks) and displays behavioral deficits such as ataxia, tremor, and cognitive impairments. The R6/2 mouse line expresses mutant human exon 1 HTT (Mangiarini et al., 1996) with 145 CAG repeats under the control of 1 kb of the human huntingtin promoter. Motor deficits can be seen from 5 weeks of age on, even if drastic motor impairments are obvious from 8 weeks of age on. Neuropathologically, massive huntingtin aggregates can be found in the striatum. Surprisingly, these animals display only 25% neuronal cell death in the striatum (Stack et al., 2005). R6/2 mice primarily die of metabolic deterioration and/or epileptic seizures.

Another N-terminal-HTT transgenic mouse is the N171-82Q line (Schilling et al., 1999), which expresses a 171 amino acid mutant HTT fragment with 82 CAG repeats under the regulation of the mouse prion promoter, directing expression primarily in the brain. This mouse model (life span: 21 weeks) shows a delayed onset of disease compared to the R6/2 line, since it contains less CAG repeats. From 11 weeks of age on N171-82Q mice display resting tremor, hypokinesia, and impairment in Rotarod performance (McBride et al., 2006). Neuropathological hallmarks are comprised of massive huntingtin aggregates in the cortex and selective neuronal death in the striatum. At the age of 16 weeks, 25% of neurons in the striatum are lost, and the striatal volume is decreased by 20% (McBride et al., 2006).

To date, no perfect mouse model, which models all neuropathological and progressive cognitive and motor impairments of the human HD, exists. A perfect model should have the following features: robust phenotype, fast disease onset and progressive course, well-defined behavior impairments, neuropathological hallmarks resembling the human disease, and limited variability. To mimic all features of HD, we used all three mouse models for our transplantation therapy approach.

3.1.4 Cell replacement therapy

For more than two decades, scientists have used different neural cell sources to find a promising cell replacement therapy for the loss of striatal neurons in HD. Cell transplantation represents a promising therapeutic strategy, which aims to replace striatal neurons. It has yielded some preliminary, but only modest and short-lived clinical benefits when using fetal neural cells (Bachoud-Levi et al., 2006; Gallina et al., 2010). Therefore, specifically ESCs and iPSCs are considered to be an appropriate cell source, as ESCs can be differentiated *in vitro* into a MSN-like phenotype (Aubry et al., 2008; Danjo et al., 2011; Ma et al., 2012b; Shin et al., 2012). However, their long-term survival, long-term functional improvement and safety *in vivo* still need to be proven.

In the present study, we aimed at establishing a combination therapy approach, composed of cellular replacement by ESC-derived neural progenitors linked to BDNF supply. For this reason, we have generated BDNF overexpressing mouse ESCs by knock-in technology that display an enhanced neuronal and GABAergic differentiation *in vitro* (Leschik et al., 2013). Very recently, we could show that polysialylated-neural cell adhesion molecule (PSA-NCAM) positive progenitors derived from these ESCs led to functional improvement when transplanted into mice with contusion spinal cord injury (Butenschon et al., 2016). With small modifications to the published protocol, which comprises magnetic-activated cell sorting (MACS) technology for purification, we tested in this study the efficiency and safety in three divergent HD mouse models.

3.2 Materials and Methods

3.2.1 Production of ESCs

Recombinant ESCs had been obtained by knock-in targeting strategy into the Rosa26 (R26) locus. The targeting vector R26-BDNF-GFP (Figure 8) contained the coding sequence of mouse pre-pro-BDNF-GFP (fused to the long 3' untranslated region (UTR) of the BDNF gene), which has been produced and published by Leschik and colleagues (Leschik et al., 2013). The ubiquitous CAG promoter (cytomegalovirus enhancer element and the chicken β-actin promoter) was placed upstream of the coding sequence. Furthermore, a floxed-stop cassette was introduced as a transcriptional blocker, which included a neomycin resistance gene.

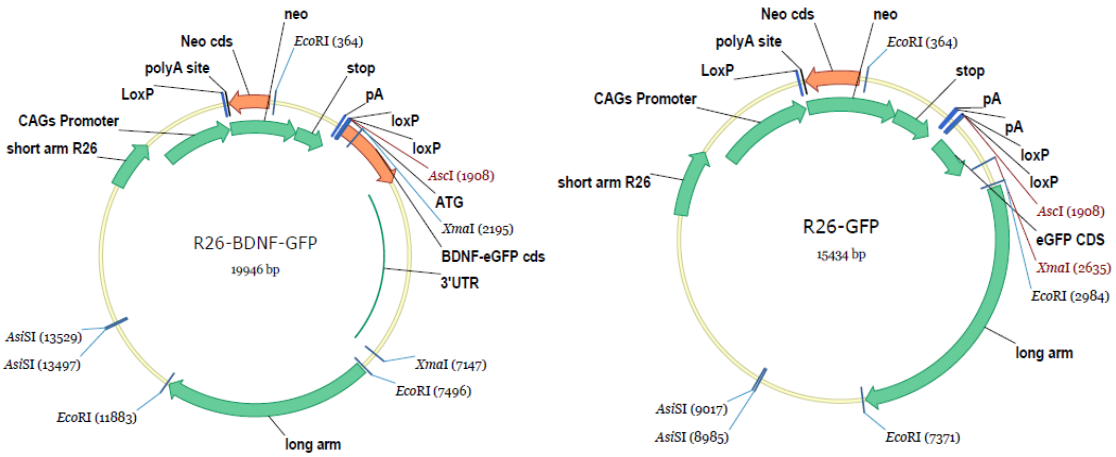

Figure 8. Plasmid maps of R26-BDNF-GFP and R26-GFP. R26, ROSA26 locus; CAG, cytomegalovirus enhancer/chicken β-actin promoter; neo cds, neomycin resistance coding sequence; floxed stop, transcriptional terminator flanked by loxP sites; polyA site, polyadenylation site; BDNF-eGFP cds, brain-derived neurotrophic factor coding sequence; 3'UTR, untranslated region; eGFP cds, enhanced green fluorescent protein. Vector backbone: pBluescript II KS (Stratagene).

For this thesis, we modified the vector by deleting the coding sequence of mouse pre-pro-BDNF-GFP and by introducing the green fluorescent protein (GFP) coding sequence, respectively. The GFP coding sequence was produced by PCR from the R26-BDNF-GFP vector. The resulting fragment was cloned into pCR™2.1-TOPO® TA cloning vector (Invitrogen, Carlsbad, CA, USA). The TOPO-GFP vector was then digested with restriction enzymes XmaI and AscI and the resulting GFP fragment purified. The R26-BDNF-GFP was also digested with XmaI and AscI and the resulting vector backbone purified. Finally, the GFP fragment was ligated into the R26 vector backbone and sequenced. DNA construct design was performed using Vector NTI software (Invitrogen, Carlsbad, CA, USA).

The target construct R26-GFP (Figure 8) was linearized by AsisI digestion and V6.5 or Bl6 ESCs were electroporated. Neomycin resistant target clones were picked and DNA extracted. In a PCR screen for GFP homologous recombined clones were selected and Southern blotting was performed as described previously (Sambrook and Russell, 2001) after EcoRI restriction digest of genomic DNA. The hybridization probe (5') was produced by PCR. Sequence of the 5' probe fw: 5'-CAGGCAAAAAGGGGAGACCA-3', 5' probe rev: 5'-CGTTGGGCCTAACTCGAGTC-3'. Successful recombined clones were electroporated with pCrepac and subsequently selected with puromycin. Expression of Cre recombinase led to excision of the floxed neo-stop cassette and to transcriptional activation of the GFP sequence. Puromycin-resistant clones were clonally expanded and screened for GFP fluorescence. To finish, a Southern blot with the 5' probe and neo probe was performed. Sequence of the neo probe fw: 5'-TGCTCGACGTTGTCACTGAAGC-3', Neo probe rev: 5'-TACCGTAAAGCACGAGGAAGC-3'.

3.2.2 Differentiation and purification of ESCs by MACS

ESCs were maintained on mitomycin-treated feeder cells (mouse embryonic fibroblasts) and cultured in the presence of LIF according to standard protocols (Hogan, 1994). For differentiation, cells were cultured for two passages on gelatin (stage 1) and then differentiated according to the protocol of Bernreuther et al. (Bernreuther et al., 2006). This protocol includes EB formation of ESCs (stage 2), selection of nestin-positive cells from plated EBs (stage 3) and expansion of nestin-positive cells (stage 4). EB formation was induced by plating 2.5 x 10^4 cells/cm² on non-adherent bacterial plastic dishes (Starlab) in ES culture medium without LIF. Embryoid bodies kept in suspension culture for 4 days were plated onto a tissue culture surface (Starlab). On the next day, the medium was switched to (insulin, transferrin, selenium chloride, fibronectin) ITSFn medium and nestin-positive cells were selected for 10 days with a medium change every other day. Cells maintained in ITSFn medium were dissociated and replated at a density of 1.5 x 10^5 cells/cm^2 on precoated poly-ornithin/laminin dishes. The expansion medium containing bFGF was changed every 2 days. See a list of ESC culture and differentiation reagents below (Table 1).

Table 1. List of ESC culture and differentiation reagents.

Medium	Components	Final concentration	Company	Catalog number
ESC culture medium	DMEM	1x	Sigma	D5671
	FBS	10%	PAA	A15-101
	Non-essential AA	0.1 mM	Invitrogen	11140035
	Sodium Pyruvate	1 mM	Sigma	S8636
	2-Mercaptoethanol	0.1 mM	Sigma	M7522
	L-Glutamine	2 mM	Sigma	G7513
	Pen/Strep	100 U/ml	Sigma	P0781
	LIF	recombinant LIF from supernatant of transfected HEK cells (kind gift from Ari Weissmann)		
ITSFn medium	DMEM/F12 with Glutamax	1x	Invitrogen	10565-018
	Fibronectin	5 µg/ml	Sigma	F2006
	Insulin	5 µg/ml	Sigma	I4011
	Transferrin	50 µg/ml	Sigma	T8158
	Selenium Chloride	30 nM	Sigma	323527
	L-Glutamine	2 mM	Sigma	G7513
	Pen/Strep	100 U/ml	Sigma	P0781
Expansion medium	DMEM/F12 with Glutamax	1x	Invitrogen	10565-018
	bFGF	10 ng/ml	Sigma	F0291
	B27	1x	Invitrogen	17504-044
	L-Glutamine	2 mM	Sigma	G7513
	Pen/Strep	100 U/ml	Sigma	P0781
Gelatin		0.1%	Sigma	1393
Poly-L-ornithine hydrobromide (poly-O)		10 mg/ml	Sigma	P3655
Laminin		1 µg/ml	Sigma	L2020

After 6 days expansion of nestin-positive cells, cells were enriched for PSA-NCAM positive cells and depleted for stage-specific embryonic antigen 1 (SSEA-1) positive cells by MACS (Figure 9, Table 2) (Miltenyi Biotec, Bergisch Gladbach, Germany) as described previously (Butenschon et al., 2016).

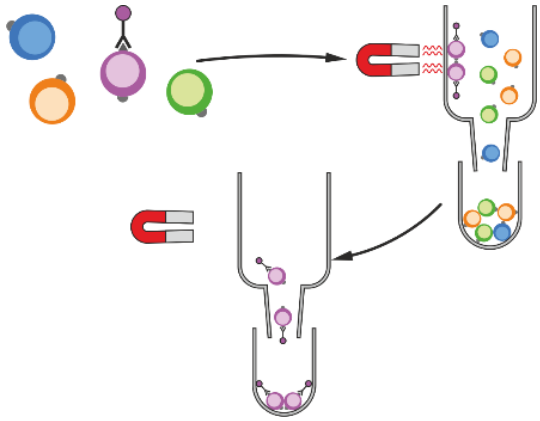

Figure 9. Magnetic-activated cell sorting principle. Cells were labeled with magnetic beads with specific antibodies against SSEA-1 and PSA-NCAM and isolated through columns placed in a magnetic field of a separator (picture modified from Miltenyi Biotec).

Table 2. List of microbeads for MACS.

Microbeads	Company	Catalog number
anti-SSEA-1 Micro Beads	Miltenyi	130-094-530
anti-PSA-NCAM-APC Micro Bead Kit	Miltenyi	130-097-859

Successful sorting was verified via flow cytometric analysis. SSEA-1^{-}/PSA-NCAM^{+} sorted cells were plated onto poly-ornithin/laminin coated dishes at a density of 2.0 x 10^5 cells/cm^2 in DMEM/F12/Glutamax supplemented with B27 and differentiated for 3 days by the omission of FGF2. To ensure cell detection after transplantation, cells were treated with 5 µM BrdU (Sigma Aldrich) for 48 h before transplantation.

3.2.3 Animals

Animals were single housed in a temperature- and humidity-controlled room with a 12 h/12 h light/dark cycle (lights on 5 am - 5 pm) and had access to food and water *ad libitum*. All experiments were carried out in accordance with the European Community's Council Directive of 22 September 2010 (2010/63EU) and were approved by the local animal care committee (Landesuntersuchungsamt Koblenz, permit number G 12-1-097). This study was performed on male C57BL/6J mice (Harlan Laboratories), lesioned with quinolinic acid (Sigma Aldrich), male R6/2 mice (Jackson's laboratories, mouse strain stock number: 002810) and wild-type littermates maintained on the F1 hybrid B6CBA strain and N171-82Q mice (Jackson's laboratories, mouse strain stock number: 003627) and wild-type littermates maintained on the F1 hybrid B6C3H strain. Animals were subjected to genotyping to confirm the presence of the transgene with the mutated huntingtin. CAG repeat sizes were determined from genomic DNA by Laragen Inc. (Culver City, CA). The N171-82Q mice used in this study had a mean CAG repeat length of 84.00 ± 0.06 and the R6/2 mice used in this study a mean CAG repeat length of 167.40 ± 0.91. There was no difference in CAG repeats between transgenic groups. For randomization littermates were split among groups. Experimenters were blind to the genotype of mice and to the treatment.

3.2.4 Quinolinic acid lesion and cell transplantation

Mice were anaesthetized with isoflurane anesthesia and received a subcutaneous injection of buprenorphine (0.05 mg/kg) after the surgery. Mice that were lesioned before the cell transplantation received an additional injection of midazolam (50 mg/kg), to reduce quinolinic

acid-induced seizures after waking up from surgery. One week before transplantation, the right striatum (0.0 mm AP, −2.0 mm ML, −3.0 mm DV from bregma) of C57BL6/J mice was lesioned by stereotactic injection of 1 µl 60 nmol quinolinic acid (Sigma, P63204). ESCs, differentiated for 3 days to yield neural progenitor cells (NPCs), were trypsinized and resuspended at a concentration of 100,000 cells/µl in HBSS (Hanks' balanced salt solution) without Ca^{2+} and Mg^{2+} (Gibco, 14175-046). Before transplantation, viability (>95%) of NPCs was validated by Trypan blue exclusion. 1 µl of the cell suspension was injected either in the right striatum of quinolinic acid lesioned mice (same coordinates as for lesioning) or bilaterally in transgenic mice (0.0 mm AP, ±2.0 mm ML, −3.0 DV from bregma) with a flow rate of 500 nl/min with a 26G beveled NanoFil needle. The injection needle was left in place for additional 5 min and then slowly removed. Sham-injected animals received an injection of 1 µl HBSS instead of the cell suspension.

3.2.5 Behavioral assays

All behavioral tests were performed during the light phase of the cycle, starting at 8 am. QA-lesioned and transgenic (R6/2 or N171-82Q) animals had been randomized into treatment groups before transplantation.

3.2.3.1 Body Weight

Body weight was measured once per week to observe any possible weight loss because of tumor formation of transplanted cells, or as a measure of physical recovery.

3.2.3.2 Rotation Test

To assess the functional lesion of the right striatum, mice were injected intraperitoneally with apomorphine (Sigma) at a concentration of 2 mg/kg body weight and immediately placed in an acrylic cylinder (20 cm diameter, 25 cm tall) in an Open Field box. The behavior of the mouse was video recorded for 45 min. 5 min after the injection, rotations were counted for 30 min with EthoVision. Net rotations were calculated: number of ipsilateral rotations − number of contralateral rotations.

3.2.3.3 Rotarod

The rotarod apparatus (Ugo Basile) was used to measure motor coordination and balance. Mice were placed on the rotarod at an accelerating speed ranging from 4 to 40 rpm over 5 min. Mice received three trials per day with a rest period of at least 1 hour in between trials for three consecutive days. On the third day (testing day) the maximum latency to fall off the rotarod for each mouse was recorded. The testing day was repeated every 2 weeks.

3.2.3.4 Quantitative gait analysis using the CatWalk system

CatWalk XT 9 (Noldus, The Netherlands) was used to assess gait and locomotion. Mice traversed a green illuminated glass plate, the reflected light from the paws that touch the glass was captured with a high-speed video camera and the illuminated paw prints were recorded. The recorded section was 9 mm long and automatic detection settings were applied. The intensity threshold was set to 0.25, the camera gain was set to 37.5. The testing was performed in the dark. Animals were placed on the glass plate and allowed to explore the walkway freely for 3 min. Then the runs were acquired, while the animal was running back and forth voluntarily. The maximum variation was set to 20% and the three fastest trials were used for subsequent analysis.

The following parameters were analyzed (RF= right forepaw, RH= right hindpaw, LF= left forepaw, LH= left hindpaw):

Temporal parameters: walk speed (distance of the runway divided by the time needed to cross), cadence (number of steps per second), stance duration (average time in seconds that the paw is in contact with the glass plate), swing duration (average time in seconds that the paw is not in contact with the glass plate) and swing speed. Individual paw statistics: maximum contact area, maximum intensity, print area, print width, print length. Comparative paw statistics: stride length (distance between successive placements of the same paw), duty cycle (percentage of time the paw accounts for the total step cycle of the paw), base of support (average distance between front paws or hind paws).

3.2.3.5 Open Field

Mice were placed in the center of a white box (40 x 40 x 40 cm) illuminated at 90 lux and their behavior was video recorded for 10 min and tracked using EthoVision (Noldus). The distance moved was analyzed.

3.2.3.6 Grip Strength

To measure forelimb grip strength, a mouse was suspended by the tail and lowered towards the apparatus (Ugo Basile) until it grasped a handle with both front paws. The mouse was pulled back until it released its grip from the handle. All mice were tested for five consecutive trials, the peak pull-force (g) was recorded and the mean pull-force of all five trials was calculated.

3.2.3.7 Hindlimb Clasping

A marker for disease progression of neurodegeneration in R6/2 mice is hindlimb clasping. Mice were taken by the tail and lifted up in the air for 30 sec (Lee et al., 2009). The foot-clasping time was scored as the following: no clasping equals a score of 0, 0 to 5 sec a score of 1, 5 to 10 sec a score of 2, and more than 10 sec a score of 3.

3.2.6 Immunofluorescent staining

For immunocytochemistry, cells were fixed 15 min with 4% paraformaldehyde (PFA) and washed with phosphate buffered saline (PBS). Coverslips were rinsed for 5 min in 0.2% PBS-Triton X-100 (TX) and blocked with 4% goat serum for 20 min. Cells were incubated with primary antibodies in 4% goat serum overnight at 4°C. The second day, coverslips were washed three times for 5 min with PBS and incubated with the secondary antibody for 2 h at room temperature. Afterwards, cells were washed, counterstained with 4',6-diamidino-2-phenylindole (DAPI) and mounted on (SuperFrostPlus, Menzel, Braunschweig, Germany) slides with Mowiol (Sigma Aldrich).

The following primary antibodies were used: mouse anti-nestin (1:200), mouse anti-PSA-NCAM (1:100), mouse anti-microtubule-associated protein 2 (MAP2, 1:200), mouse anti-oligodendrocyte transcription factor 2 (OLIG2*,* 1:1000, all Merck Milipore), rabbit anti-KI67 (1:500), guinea pig anti-doublecortin (DCX, 1:500), rabbit anti-glial fibrillary acidic protein (GFAP, 1:1000) and rabbit anti-forkhead box protein G1 (FOXG1, 1:500), rabbit anti-BDNF (1:100, all Abcam, Cambridge, UK). Prior to immunostaining with anti-BDNF antibody, antigen retrieval at 98°C in sodium citrate buffer (10 mM sodium citrate, 0.05% Tween 20, pH 6.0) was performed. For PSA-NCAM staining, all buffers were used without TX.

For immunohistochemistry*,* mice were perfused transcardially with PBS followed by 4% PFA, brains were removed, post-fixed overnight in 4% PFA and treated with 30% sucrose for 48 h.

Then brains were sectioned 30 µm thick in coronal plane and stored at 4°C in cryoprotection solution until use. Sections were blocked in PBS containing 5% normal donkey serum (NDS), 2.5% bovine serum albumin (BSA) and 0.3% TX for 90 min and incubated with the respective primary antibody in PBS containing 1% NDS, 0.1% BSA and 0.3% TX overnight: goat anti-dopamine- and cAMP-regulated neuronal phosphoprotein (DARPP32) (1:50, Santa Cruz Biotechnologies Inc., Santa Cruz, CA, USA) or guinea pig anti-DCX (1:500, Abcam). For double staining with BrdU, sections were washed 5 min with 0.2% tris buffered saline (TBS)-TX and incubated in 1 N HCl for 1 h at 37°C to denature DNA, followed by 3 x 5 min washes with TBS. Brain slices were then blocked in TBS with 1% NDS, 0.1% BSA and 0.3% TX for 90 min and incubated with the primary antibodies in blocking buffer overnight at 4°C. On the next day, appropriate secondary antibodies were applied for 2 h. To visualize cell nuclei in non-BrdU treated sections, brain slices were incubated with DAPI for 5 min, washed with PBS and mounted with Mowiol onto slides. The following primary antibodies were used: rat anti-BrdU (1:500), rabbit anti-FOXP1 (1:500), rabbit anti-GFAP (1:1000), rabbit anti- S100 calcium-binding protein B (S100B) (1:500, all Abcam), rabbit polyclonal anti-MAP2, 1:200 (Merck Milipore), and rabbit anti-aspartoacylase (ASPA) (1:1000, kind gift from Matthias Klugmann, Sydney, Australia).

The respective secondary antibodies were applied: goat anti-mouse IgM or donkey anti-mouse, goat anti-rabbit, goat anti-guinea pig, donkey anti-goat or goat anti-rat AlexaFluor546 and goat anti-mouse, anti-rabbit or anti-rat AlexaFluor647 (all 1:1000; Invitrogen). See a list of all used antibodies and working dilutions below.

Table 3. List of antibodies.

Antibody	Species	Dilution	Company	Catalog number
NESTIN	mouse	1:200	Merck Milipore	MAB353
PSA-NCAM	mouse	1:100	Merck Milipore	MAB5324
MAP2	mouse	1:200	Merck Milipore	MAB3418
OLIG2	mouse	1:1000	Merck Milipore	MABN50
KI67	rabbit	1:500	Abcam	ab15580
DCX	guinea pig	1:500	Abcam	ab2253
GFAP	rabbit	1:1000	Abcam	ab7260
FOXG1	rabbit	1:500	Abcam	ab18259
DARPP32	goat	1:50	Santa Cruz	sc-8483
BrdU	rat	1:500	Abcam	ab6326
FOXP1	rabbit	1:500	Abcam	ab16645
S100B	rabbit	1:500	Abcam	ab41548
ASPA	rabbit	1:1000	kind gift from Matthias Klugmann	
anti-mouse IgM AlexaFluor546	goat	1:1000	Invitrogen	A-21045
anti-mouse IgG AlexaFluor546	donkey	1:1000	Invitrogen	A-10036
anti-rabbit IgG AlexaFluor546	goat	1:1000	Invitrogen	A-11010
anti-guinea pig IgG AlexaFluor546	goat	1:1000	Invitrogen	A-11074
anti-goat IgG AlexaFluor546	donkey	1:1000	Invitrogen	A-11056
anti-rat IgG AlexaFluor546	goat	1:1000	Invitrogen	A-11081
anti-mouse IgG AlexaFluor647	goat	1:1000	Invitrogen	A-21235
anti-rabbit IgG AlexaFluor647	goat	1:1000	Invitrogen	A-21244
anti-rat IgG AlexaFluor647	goat	1:1000	Invitrogen	A-21247

3.2.7 Flow cytometric analysis

To determine the amount of PSA-NCAM and SSEA-1 positive cells in the expansion culture, cells were analyzed via flow cytometry and immunofluorescence. The following antibodies were used: primary mouse IgM monoclonal PSA-NCAM (1:100, Chemicon, Billerica, MA) or primary mouse IgM monoclonal SSEA-1 (1:50, Developmental Studies Hybridoma Bank, University of Iowa, USA), secondary antibody anti-mouse AlexaFluor546 IgM (1:1000, Invitrogen, Carlsbad, CA, USA). For flow cytometric analysis before MACS purification, cells were trypsinized and gently triturated. Cells were filtered through a 30 µm pre-separation filter to obtain single cell suspensions. 1 x10^6 cells were fixed 15 min with 4% PFA, washed and incubated with the primary antibody for 1 h. Subsequently, cells were incubated with the secondary antibody for 45 min. All washing and incubation steps were performed in 0.5% BSA/PBS at room temperature.

Cell analysis was performed at the Core Facility Flow Cytometry at the Institute of Molecular Bioscience (IMB) in Mainz. Stained cells were analyzed on a flow cytometer (BD

LSRFortessa™). PSA-NCAM and SSEA-1 positivity was determined according to negative controls where no primary antibody was used and by comparing to undifferentiated ES cells, which do not express PSA-NCAM, but SSEA-1.

3.2.8 Microscopic analysis of histology

Slides were observed under a Leica DM5500 (Leica Camera, Wetzlar, Germany) fluorescence microscope or a Zeiss Axiovert LSM 710 (Carl Zeiss, Oberkochen, Germany) laser scanning confocal microscope. For laser scanning confocal microscopy, z-stacks with optical sections of 1 µm of the graft were recorded.

Lesion volume and cell survival were assessed based on the Cavalieri principle of stereology. Lesion size was determined by staining every 10th brain section of the entire striatum of QA-lesioned animals for DARPP32, a medium spiny neuron marker. The lesion area was outlined on digitized images and measured by ImageJ, National Institutes of Health, Bethesda, MD, USA. The lesion volume was calculated by multiplying the distance between sections (300 µm), number of sections and the measured area. Transplanted cells were quantified by staining marked cells with a BrdU antibody. Positive cells were counted in every 6th section (180 µm apart) and calculated for the whole graft. For each parameter four animals were analyzed.

To dissect the differentiation pattern of transplanted cells, BrdU positive cells and BrdU cells positive for the respective cell fate marker were counted in 2 sections of each graft in eight animals per group, analyzing at least 1000 cells per marker and animal.

For evaluation of endogenous precursor proliferation, every 10th brain section was immunostained with DCX and DAPI, and positive cells in the ipsilateral dorsolateral subventricular zone (SVZ) were counted.

3.2.9 Statistical analysis

Data are represented as the mean ± standard error of the mean (SEM). Statistical analysis was done using GraphPad Prism 4 (GraphPad Software Inc, La Jolla, CA, USA) and IBM SPSS Statistics 22v software (IBM Corporation, Armonk, NY, USA). For analysis of behavior over time, analysis of variance (ANOVA) with repeated measures and consecutive Tukey's post hoc tests (for significant group differences) or simple effects analysis with Sidak correction (for significant group x time interaction) was conducted. The factors were groups x

time. Motor behavior at distinct time points was analyzed with one-way ANOVA with post-hoc Tukey's test. For analysis of immunostaining of cells *in-vitro*, two-way ANOVA followed by Bonferroni's corrected multiple comparisons was applied. When comparing only two groups in immunohistology (BDNF-GFP NPCs and GFP NPCs), the two-tailed unpaired Student's t-test was applied. For lesion volume (three groups) and endogenous precursor proliferation (four groups), one-way ANOVA with post-hoc Tukey's or Dunnett's test was used. Differences were assumed to be significant if $p<0.05$.

3.3 Results

3.3.1 Generation of recombinant ESCs expressing GFP

Previously, BDNF-GFP expressing ESCs via homologous recombination have been generated in our lab (Leschik et al., 2013). To use these cells in transplantation studies we needed to produce proper control cells via knock-in targeting strategy into the Rosa26 locus (Figure 10A). Therefore, the same targeting vector with the GFP instead of the BDNF coding sequence was produced by the cloning strategy described in material and methods (3.2.1).

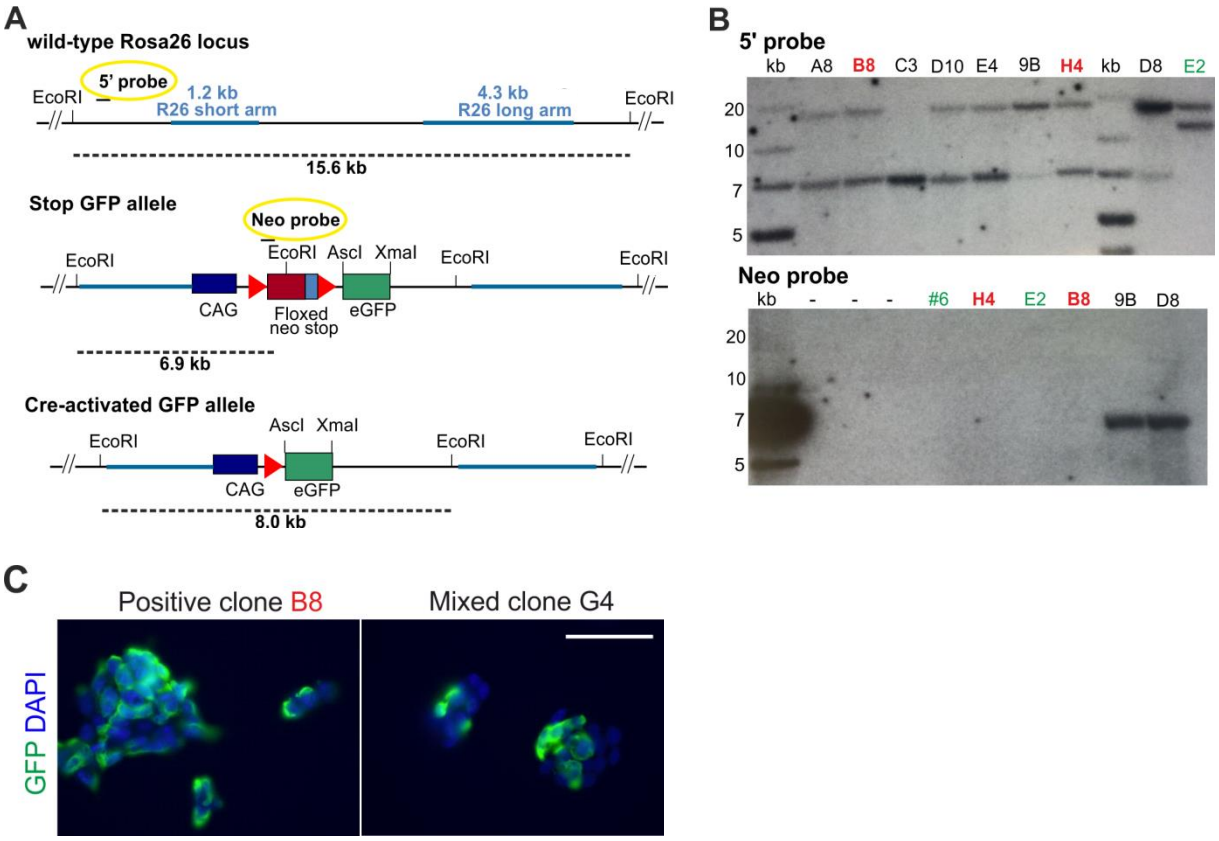

Figure 10. Schematic representation of gene targeting of a GFP-encoding allele into the Rosa26 locus and analysis of ESC clones. (A) Overview of recombination steps in alleles of ESCs, positions of hybridization probes for Southern blotting and lengths of generated fragments (modified from (Leschik et al., 2013)). (B) Southern blots of newly generated GFP ESCs with either 5' probe or neo probe. Red: newly generated control GFP clones, green: existing BDNF-GFP clones. (C) Fluorescent micrograph depicting a positive clone (B8) and a mixed clone (G4) after homologous recombination Scale bar, 50 µm.

After electroporating V6.5 or Bl6 #6 ESCs with the R26-GFP vector and homologous recombination we obtained clones with a stop GFP allele (recombination efficiency V6.5: 5.0%, Bl6 #6: 9.3%). GFP expression was transcriptionally blocked by a stop cassette with a neomycin resistance gene, which allowed selection with G148 for positive clones. By using

the Cre recombinase expressing plasmid pCrepac and subsequent selection with puromycin, the floxed stop cassette was excised and GFP activated. Picked clones were clonally expanded and checked on Southern blot with the 5' probe and neo probe for successful recombination (Figure 10B). The 5' probe hybridized to EcoRI digested DNA from target clones with the heterozygous Cre-activated GFP allele and the neo probe to the heterozygous stop-GFP allele. Target clones contained the 15.6 kb and the 8.0 kb fragment (5' probe). Clones A8, B8, D10, E4, 9B, H4, and D8 were selected as positive. As a control, clone E2 (BDNF-GFP ESC, green) depicts the fragment sizes 15.6 and 12.3 kb (see also (Leschik et al., 2013). When testing four of the positive 5' clones (H4, B8, 9B, D8) with the neo probe to verify excision of the stop cassette, only clones H4 and B8 were negative for the 6.9 kb fragment. Clones 9B and D8 were discarded. Here, BDNF-GFP clones (green) E2 and #6 were used as controls. Finally, clones were examined for GFP fluorescence (Figure 10C. The positive clone B8 showed GFP fluorescence in every cell (DAPI stained), whereas a mixed clone showed cells positive and negative for GFP. The here generated clone H4 and the previously produced BDNF-GFP clone #6 were used for differentiation to NPCs and subsequent transplantation into the spinal cord (Butenschon et al., 2016), the background of those cells was exclusively Bl6. In this thesis, the GFP clone B8 and the previously produced BDNF-GFP clone E2 (background V6.5 (Sv129/Bl6 hybrid)) were used for transplantation in different HD mouse models.

3.3.2 Efficient *in vitro* preparation and purification of neural precursor cells for transplantation

Mouse ESCs either overexpressing BDNF-GFP or GFP as control were differentiated as described previously via an EB protocol followed by neural lineage selection (Butenschon et al., 2016) with one further differentiation step (for details see materials and methods 3.2.2). Cells were enriched for the intermediate neural progenitor marker PSA-NCAM and depleted of undifferentiated ESCs positive for SSEA-1 by MACS (Figure 11).

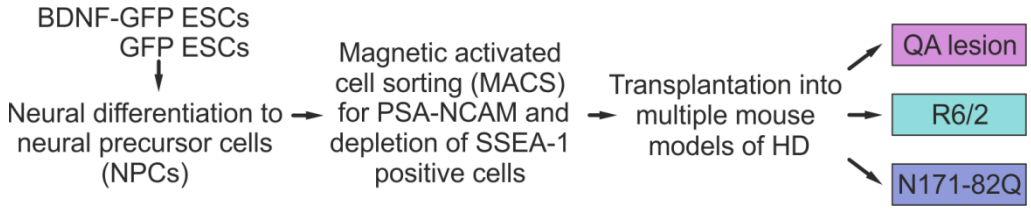

Figure 11. General concept of the study. BDNF-GFP and GFP ESCs were differentiated to NPCs and sorted by MACS for a PSA-NCAM$^+$/SSEA-1$^-$ population. After three days of differentiation, cells were transplanted into the striatum of three different HD mouse models: the QA lesioned, the R6/2 and the N171-82Q mouse model.

On day 24 of differentiation, flow cytometric analysis showed that 50.8% of all cells were PSA-NCAM positive (Figure 12A), and 5.07% positive for SSEA-1 Figure 12B). To obtain a pure neural population for transplantation, the PSA-NCAM positive fraction was enriched by MACS, and the undifferentiated ES cells positive for SSEA-1 were removed. After MACS, all cells were positive for PSA-NCAM, and no SSEA-1 positive cells were detected (Figure 12A,B).

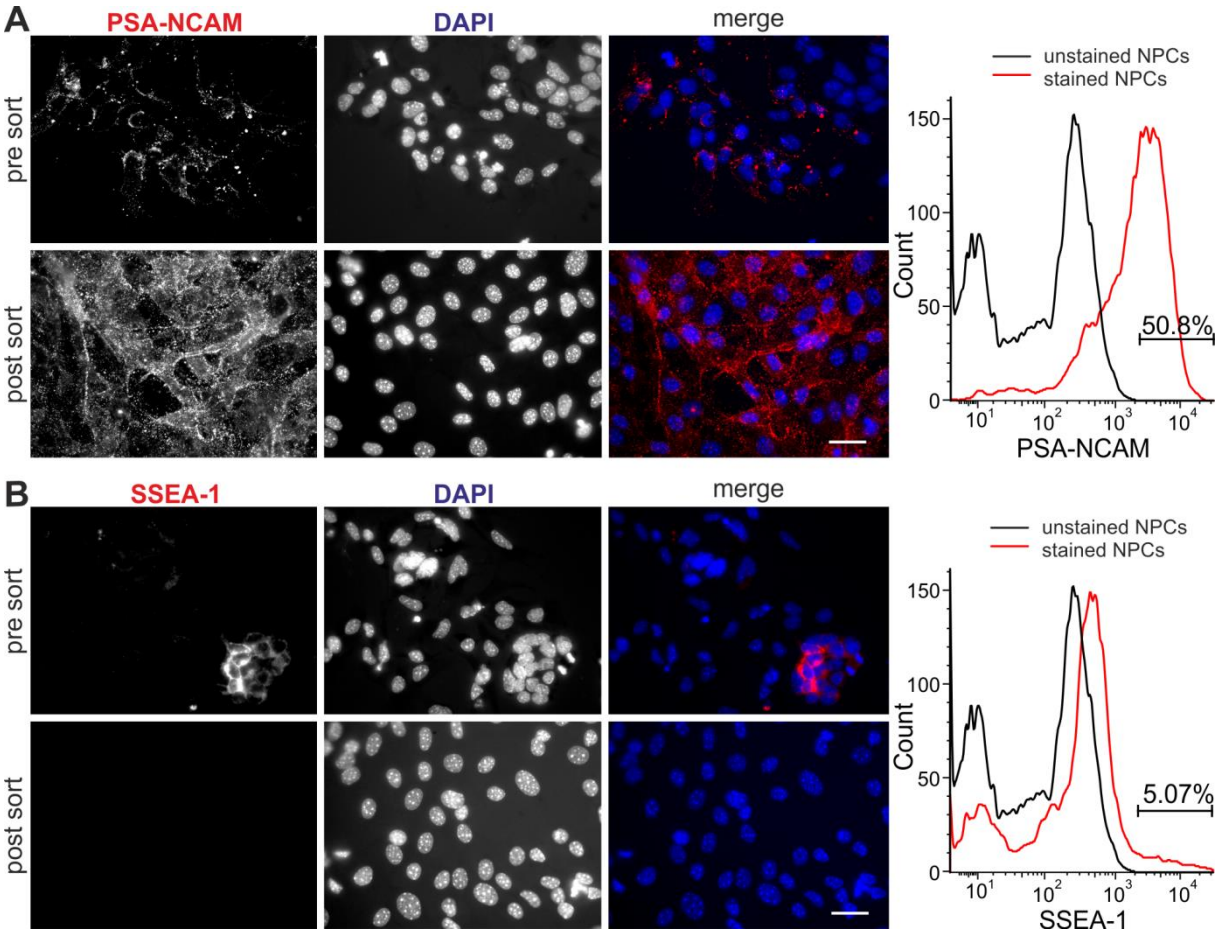

Figure 12. Immunocytochemistry and flow cytometric analysis of NPCs before and after MACS. Before MACS, 50.8% of all cells were positive for PSA-NCAM (A, pre sort) and 5.07% positive for SSEA-1 (B, pre sort). After MACS, immunofluorescence showed that cells are positive for PSA-NCAM (A, post sort) and negative for SSEA-1 (B, post sort). Scale bar, 25 µm.

Cells were replated, and differentiation was induced by removal of FGF2. Three days later, cells were analyzed by staining for multiple markers to ensure that BDNF-GFP and GFP cells were in the same stage of differentiation prior to transplantation (Figure 13A, B).

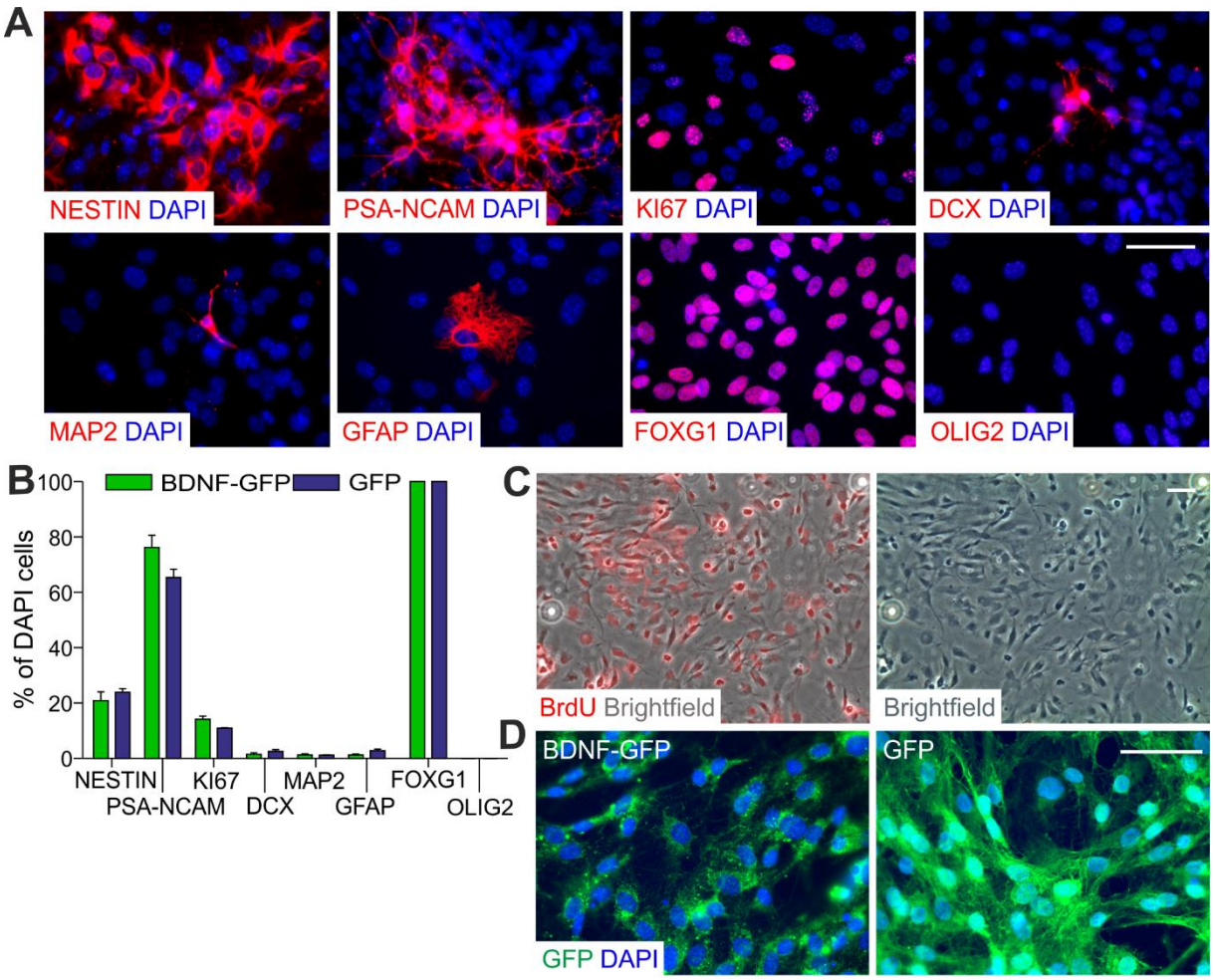

Figure 13. BDNF-GFP and GFP cells do not differ in expression of neural, glial and neuronal markers before transplantation. (A) Generation of NPCs was analyzed after MACS and three subsequent days of differentiation by immunostaining for NESTIN, PSA-NCAM, KI67, DCX, MAP2, GFAP, FOXG1, and OLIG2 (BDNF-GFP cells, all stained in red). (B) Respective percentages of marker expression of all cells (DAPI). No significant difference (p=0.3656) between BDNF-GFP and GFP cells was detected (n=3 independent experiments). (C) Overlay of fluorescent and brightfield microscopic images demonstrates that all cells were labelled with BrdU and hence proliferative. (D) Anti-GFP immunocytochemistry of purified BDNF-GFP NPCs shows the vesicular distribution of BDNF-GFP throughout the cell, whereas in GFP NPCs, GFP is detected in the whole cytoplasm. Scale bar, 50 µm.

Cultured cells (n=3 independent experiments) expressed the neural stem cell markers NESTIN (20.9 ± 3.2% BDNF-GFP, 23.9 ± 1.4% GFP cells) and PSA-NCAM (76.2 ± 4.4% BDNF-GFP and 65.4 ± 3.1% GFP cells). Only 1.5 ± 0.6% of BDNF-GFP and 2.5 ± 0.7% of GFP cells were positive for DCX. All neural progenitors expressed FOXG1, one of the earliest markers of the telencephalic lineage. Few cells expressed the neuronal marker MAP2 (1.3 ± 0.3% BDNF-GFP and 1.2 ± 0.1% GFP) and the astrocytic marker GFAP (1.3 ± 0.3% BDNF-GFP and 2.8 ± 0.6% GFP), whereas no cells expressed the oligodendrocytic marker OLIG2. A fraction of proliferating cells was detectable by the M-phase marker KI67 (14.1 ± 1.2% BDNF-GFP and 10.9 ± 0.2% GFP NPCs), but all cells were positive for BrdU (Figure 13C). No significant differences for any marker were detected between the two

groups of cells. *In vitro*, BDNF-GFP cells were detectable with GFP immunostaining (Figure 13D) and showed BDNF-GFP positive vesicular structures, while GFP NPCs displayed a uniform staining of the whole cell. As already shown by Butenschön et al. (Butenschon et al., 2016), BDNF-GFP signal was barely detectable *in vivo*. Therefore, BrdU was used to label cells for transplantation, which was carried out in three different HD mouse models: QA lesion, R6/2 and N171-82Q. Figure 14 depicts the experimental outline of the transplantation studies with subsequent behavioral assays.

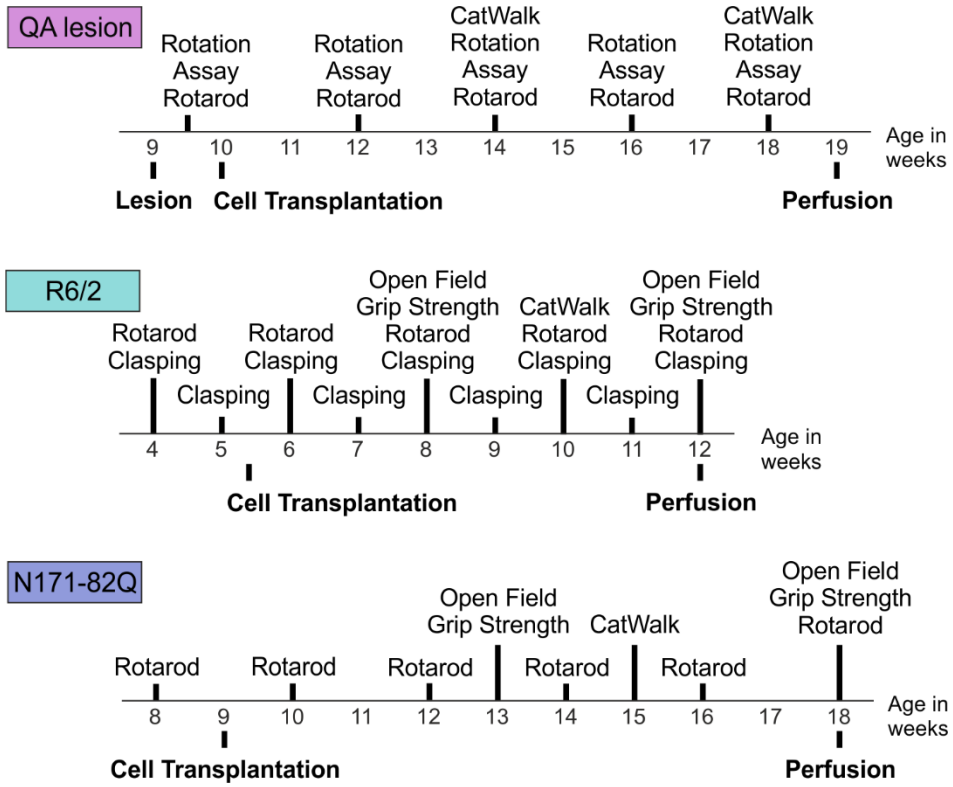

Figure 14. Experimental timeline. Overview of mouse models and respective behavioral assays at distinct time points of age.

3.3.3 BDNF-GFP cells induce locomotor recovery in QA-lesioned mice

First, we addressed the functional effect of transplanting BDNF-GFP NPCs into the chemical HD mouse model with QA-induced lesion (Figure 15). Therefore, NPCs were transplanted at an animal age of 10 weeks, and groups (n=10/group) were tested every other week for apomorphine-induced rotations.

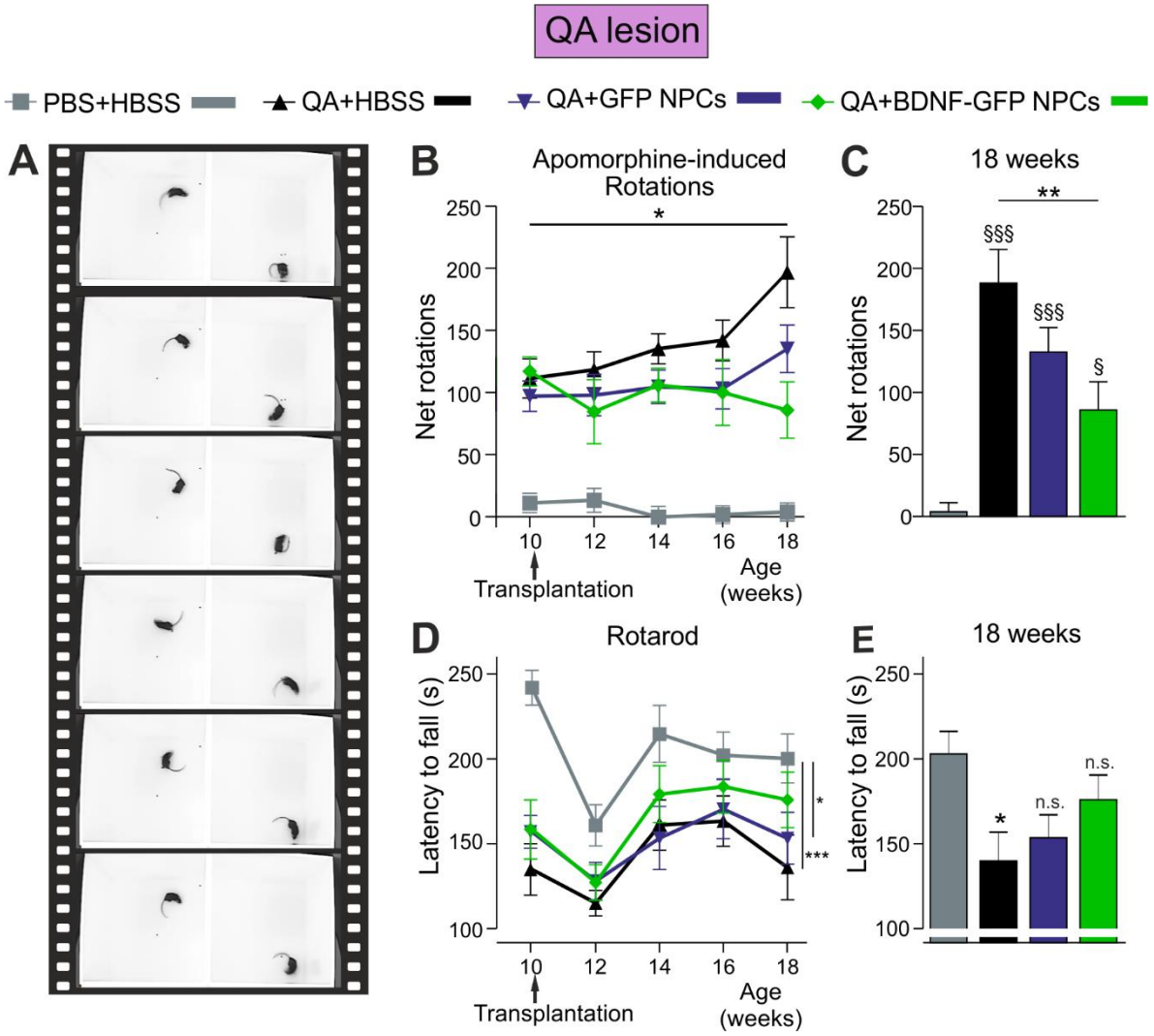

F

CatWalk

		parameters significantly different between QA- and non-lesioned
		paw: partial rescue by NPCs
14 weeks	Walk speed	-
	Swing	LH: GFP
	Swing speed	LF: GFP, BDNF-GFP LH: GFP
18 weeks	Walk speed	-
	Swing	-
	Swing speed	-
	Cadence	-
	Stride length	-
	Stand	-
	Duty Cycle	RH: GFP, BDNF-GFP

Figure 15. BDNF-GFP cells improve locomotor function in QA lesioned mice 8 weeks after transplantation. (A) QA-lesioned mice display rotation behavior in the open field after injection of apomorphine. (B) Analysis of rotational behavior in response to apomorphine. At all time points, non-lesioned animals (PBS+HBSS) displayed significant fewer rotations (*p<0.05) than QA-lesioned (QA+HBSS, QA+GFP NPCs and QA+BDNF-GFP NPCs) animals. (C) At an age of 18 weeks (8 weeks after transplantation), all lesioned groups were different from the non-lesioned group (QA+HBSS: p<0.001, QA+GFP NPCs: p<0.001, QA+BDNF-GFP NPCs: p=0.03). However, BDNF-GFP NPCs showed a highly significant decrease in net rotations compared to untreated, lesioned animals (**p=0.005). Values represent mean ± SEM, §§§p<0.001, §p<0.05 vs PBS+HBSS. (D) Analysis of motor behavior on the Rotarod. An overall group effect was observed (p=0.006), without a significant

interaction for cell groups x time (p=0.076). BDNF-GFP NPCs did not differ from non-lesioned animals (p=0.144), but GFP NPC grafted (p=0.022) and non-grafted animals (p=0.009) were significantly different from non-lesioned animals. *p<0.05 and ***p<0.001. (E) Analysis of Rotarod performance at an age of 18 weeks (8 weeks after transplantation). Only lesioned, non-grafted animals were significantly different to non-lesioned mice (p=0.023), showing a beneficial effect of transplanted cells on Rotarod performance. *p<0.05 vs PBS+HBSS. (F) List of affected CatWalk gait parameters, analyzed by one-way ANOVA with post-hoc Tukey's test between groups for each paw. At 14 weeks of age, the following parameters were significantly different (p<0.05) between lesioned and non-lesioned animals: walk speed, swing and swing speed. NPCs affected beneficially swing and swing speed. At 18 weeks of age, the following parameters were additionally significantly different: cadence, stride length, stand and duty cycle. RF= right forepaw, RH= right hindpaw, LF= left forepaw, LH= left hindpaw. Explanatory graphs and statistics: supplemental Figure S1. Data represent mean (n=10 animals) ± SEM.

Immediately prior to transplantation, animals of all QA-lesioned groups displayed similar numbers of net rotations, which were significantly different from those mice that had only received a PBS injection instead of QA (p<0.001). After transplantation and repeated testing over time, QA-lesioned animals (QA+HBSS, QA+GFP NPCs and QA+BDNF-GFP NPCs) exhibited significant higher net rotations at all time points than non-lesioned animals (PBS+HBSS) (Figure 15A and B). Recovery became significant 8 weeks after transplantation (age of 18 weeks), when animals in the BDNF-GFP transplant group displayed 85 ± 22.65 net rotations compared to 132.6 ± 19.84 in the QA-HBSS group (p=0.005) (Figure 15C). GFP cell transplanted animals did not display significant improvement of locomotor function compared to control animals (QA+HBSS) 8 weeks after transplantation.

Rotarod data showed similar results, with BDNF-GFP cells improving motor function of QA-lesioned mice (Figure 15D). Mice with BDNF-GFP transplants improved in their latency to fall and were not significantly different (p=0.144) when compared to non-lesioned control animals during repeated testing. In contrast, GFP transplants did not ameliorate motor function over time, as they still differed significantly from the non-lesioned control group with p=0.022 during repeated testing. However, when looking at a single time point at 18 weeks of age (8 weeks after transplantation), the mean latency of 153.2 ± 13.61 s detected for the GFP cell transplanted group did not significantly differ anymore from non-lesioned control animals (PBS+HBSS; 202.8 ± 13.31 s latency) (Figure 15E). This means that also GFP cells exerted a significant functional recovery, which was similar to the improvement of BDNF-GFP cell transplanted animals at 8 weeks after transplantation, as no significant difference between both groups was detected. Only HBSS-vehicle treated QA-animals still displayed significantly lower motor performance than the healthy control group (p=0.023).

In addition to the analysis of motor performance by the Rotation and the Rotarod assay, we established the use of the CatWalk gait system in the QA-lesion HD model. Figure 15F further demonstrates qualitatively in tabular representation which gait parameters of which paw could be partially rescued by either or both types of NPCs. Figure 16 graphically

demonstrates distinct gait parameters, which were significantly affected in QA-lesioned mice compared to non-lesioned control animals.

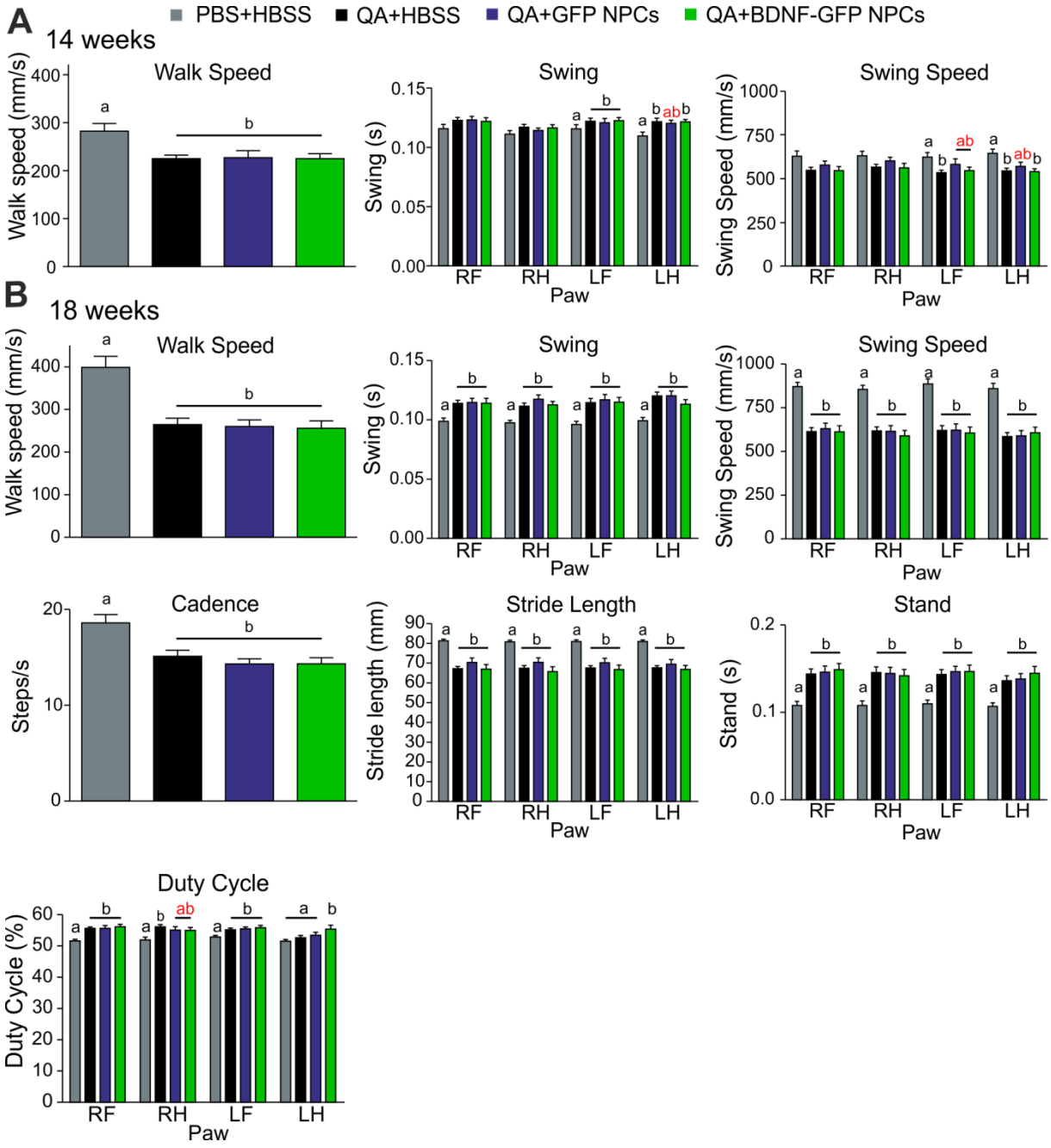

Figure 16. Affected CatWalk parameters of QA lesioned mice. Detailed graphs for the table in Figure 11F. An influence of NPCs can be seen at 14 weeks of age (A) and 18 weeks of age (B). One-way ANOVA with post-hoc Tukey's test between groups for each paw (n=10-12). Data represent mean ± SEM. Values of bars with a different letter (a or b) were significantly different ($p<0.05$) from each other. Values of bars with the same letter (a or b) were not significantly different from each other, hence values of bars marked with "ab" (marked in red) are not significantly different from either a or b, thereby indicating a partial/incomplete rescue of the phenotype.
RF= right forepaw, RH= right hindpaw, LF= left forepaw, LH=left hindpaw.

At 14 weeks of age, QA-lesioned mice displayed significantly reduced walk speed (PBS+HBSS: 282.4 ± 16.2 mm/s, QA+HBSS: 225.3 ± 7.4 mm/s, p=0.009) and swing speed (e.g. PBS+HBSS(left forepaw, LF): 623.7 ± 25.9 mm/s, QA+HBSS(LF): 534.7 ± 14.0 mm/s, p(LF)=0.038) and enhanced swing (e.g. PBS+HBSS(left hindpaw, LH): 0.1095 ± 0.0032 s, QA+HBSS(LH): 0.1215 ± 0.0030 s, p(LH)= p=0.018) compared to non-lesioned control mice. At 18 weeks of age, additionally cadence (PBS+HBSS: 18.6 ± 0.86 steps/s, QA+HBSS: 15.11 ± 0.62 steps/s, p= p=0.005) and stride length (e.g. PBS+HBSS(right forepaw, RF): 81.28 ± 0.80 mm, QA+HBSS(RF): 67.13 ± 1.19 mm, p(RF)=0.0001) were significantly reduced, whereas stand (e.g. PBS+HBSS(RF): 0.1079 ± 0.0047 s, QA+HBSS(RF): 0.1440 ± 0.0057 s, p(RF)=0.001) and duty cycle (e.g. PBS+HBSS(RF): 51.60 ± 0.51%, QA+HBSS(RF): 55.60 ± 0.47%, p(RF)=0.001) were significantly enhanced. In general, measuring at 14 weeks of age (4 weeks after transplantation) seemed to be more effective than at a later time point. Here, swing (QA+GFP NPCs (LH): 0.1201 ± 0.0027 s, p(LH) vs PBS+HBSS(LH)=0.057) and swing speed (e.g. QA+GFP NPCs (LF): 582.00 ± 31.69 mm/s, p(LF) vs PBS+HBSS(LF)=0.109, QA+BDNF-GFP NPCs (LF): 546.59 ± 19.60 mm/s, p(LF) vs PBS+HBSS(LF)=0.596) were improved by either GFPcells alone or both cell types, which was not measurable anymore at 18 weeks of age. At this time point, only duty cycle was positively affected by GFP and BDNF-GFP NPCs (QA+GFP NPCs: 55.05 ± 3.54%, p vs PBS+HBSS=0.088, QA+BDNF-GFP NPCs: 54.97 ± 3.05%, p vs PBS+HBSS=0.100).

3.3.4 CatWalk gait parameters of the R6/2 model are affected by transplantation of NPCs

Next, we asked how transplantation of NPCs affects pathology in the transgenic R6/2 mouse model of HD. The middle panel of Figure 14 describes the experimental outline with cell transplantation into R6/2 animals (n=10-12/group) at 5 weeks of age and consecutive behavioral assays until the age of 12 weeks. Rotarod and hindlimb clasping, the two mainly used assays for functional assessment of the R6/2 line, revealed no differences between NPC transplanted animals and vehicle control R6/2 animals (Figure 17A, B).

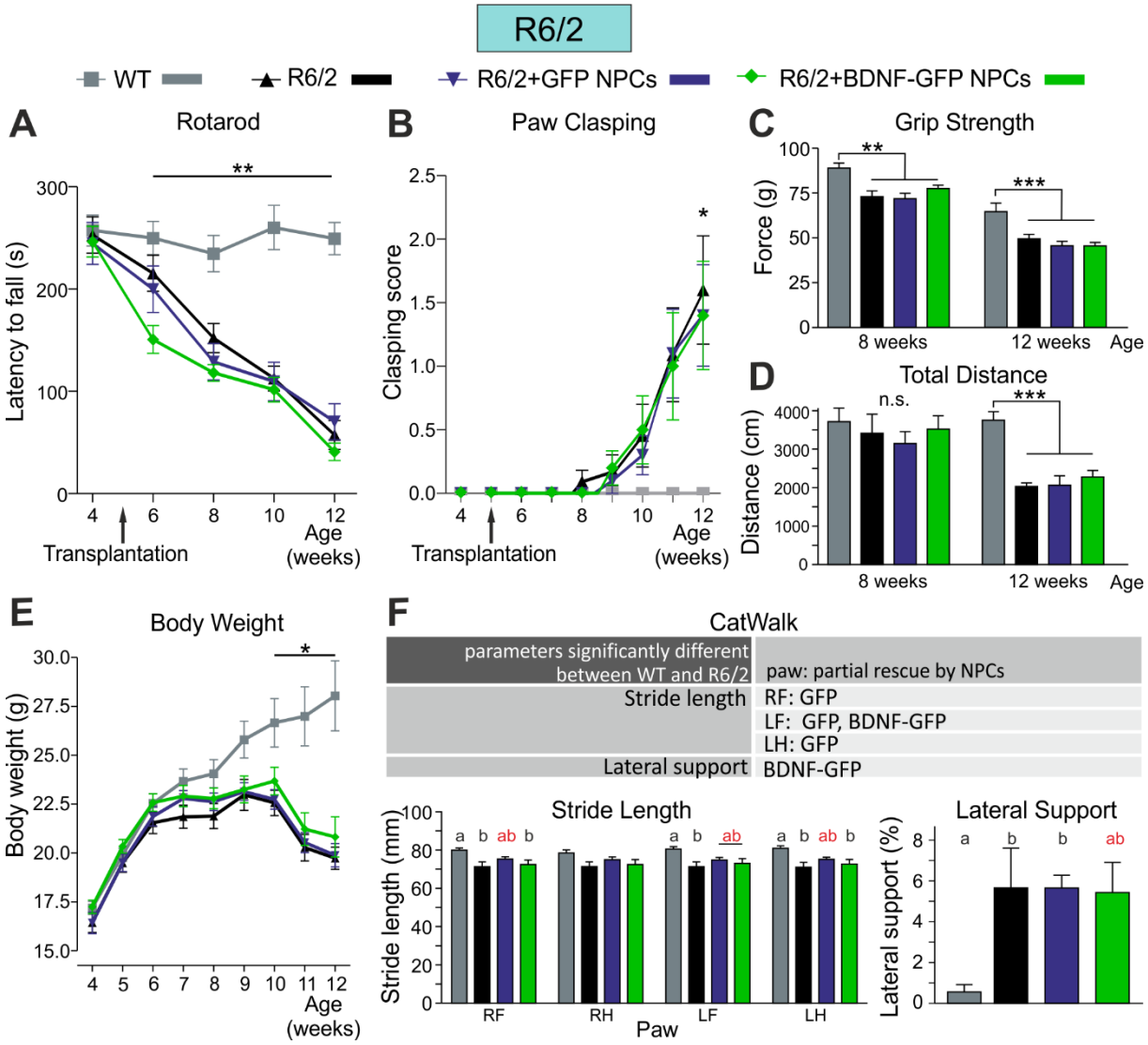

Figure 17. Few gait parameters of the R6/2 model are affected by transplantation of NPCs. (A) Behavioral performance on the Rotarod was assessed every 2 weeks. R6/2 mice show significantly lower latency to fall from the Rotarod for compared to wildtype mice after transplantation starting at 6 weeks of age (**p<0.01). No effect of transplanted NPCs on transgenic R6/2 mice was observed at any time point. (B) Paw Clasping was analyzed weekly. R6/2 mice had a significantly higher clasping score compared to wildtype animals at 12 weeks of age. Cell transplantation did not have any effect on performance in the paw clasping test. (C) Grip Strength of wildtype and R6/2 mice was measured at 8 and 12 weeks of age. Non-treated and grafted R6/2 mice displayed a significant decrease in Grip Strength at both time points. No effect of transplanted NPCs was observed. (D) Quantification of total distance of wildtype and R6/2 mice in the Open Field. (E) Body weight was measured weekly. ANOVA with repeated measures (cell groups x time, p=0.001) and consecutive simple effects analysis with Sidak correction show a significant decrease of body weight in all transgenic R6/2 compared to wildtype animals from 10 weeks of age on. (F) Gait parameters of R6/2 mice were analyzed on the CatWalk at 10 weeks of age, revealing differences in stride length and lateral support. Stride length of R6/2 mice was partially rescued by transplantation of NPCs, except for the right hind paw. Lateral support of R6/2 mice was partially decreased when BDNF-GFP NPCs were transplanted. Values of bars with a different letter (a or b) were significantly different (p<0.05) from each other. Values of bars with the same letter (a or b) were not significantly different from each other, hence values of bars marked with “ab” (marked in red) are not significantly different from either a or b, which indicates a partial/incomplete rescue of the phenotype. Data represent mean (n=10-12 animals) ± SEM, *p<0.05 and **p<0.01, ***p<0.001 vs WT, n.s. not significant. RF= right forepaw, RH= right hindpaw, LF= left forepaw, LH= left hindpaw.

Similar results were obtained with the Grip Strength and Open Field test. Only the wildtype group behaved significantly different as compared to the transplanted and non-transplanted R6/2 groups in both tests (Figure 17C,D). Furthermore, body weight, an increase of which can be taken as a measure of physical recovery, was unchanged between R6/2 groups (Figure 17E). However, when we tested animals in the CatWalk gait system, we detected functional improvements in certain parameters after cell transplantation. Partial rescue effects in stride length (e.g. WT(LF): 80.46 ± 1.22 mm, TG(LF): 71.18 ± 2.59 mm, p(LF)= 0.014) were detected in animals that had received GFP (LF: 74.74 ± 1.36 mm, p(LF) vs WT=0.231) or BDNF-GFP (LF: 72.97 ± 2.54 mm, p(LF) vs WT=0.071) cell transplants. In contrast, lateral support (WT: 0.55 ± 0.36%, TG: 5.67 ± 1.94%, p=0.041) was partially rescued only by BDNF-GFP cells (5.43 ± 1.47%, p vs WT=0.064) (Figure 17F).

3.3.5 Transplantation of NPCs into the N171-82Q mouse model exerts beneficial effects in the CatWalk test

Similar to cell transplantation into R6/2 mice, the robust Rotarod assay as well as the Grip Strength test revealed no differential effects by transplanted NPCs compared to vehicle-injected N171-82Q animals (n=10-12/group) (Figure 18A, B; experimental outline Figure 14, lower panel). Furthermore, the Open Field test did not result in significant reduction of moved distance in transgenic compared to wildtype animals (Figure 18C) and the lack of body weight gain in transgenic animals could not be rescued (Figure 18D). Hence, a visible improvement due to NPC transplantation was not detectable.

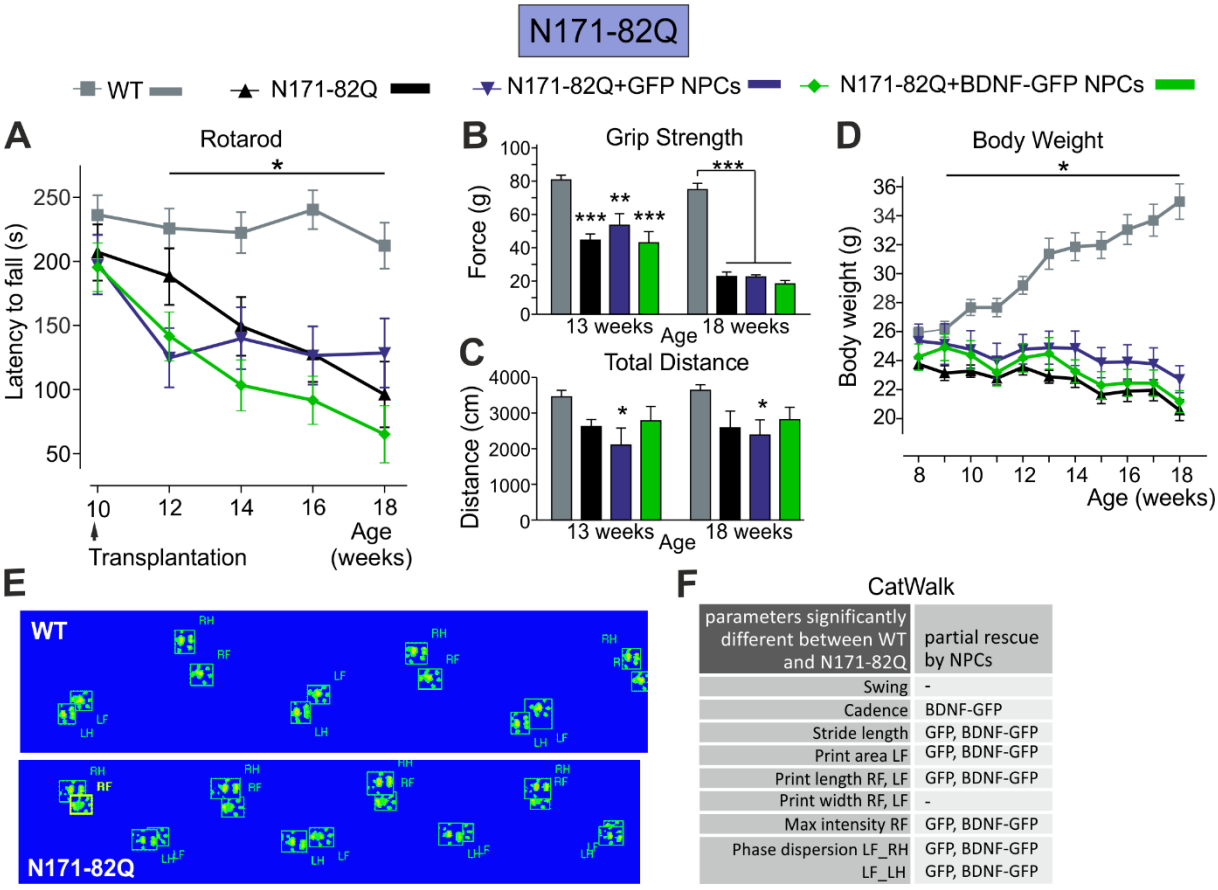

parameters significantly different between WT and N171-82Q	partial rescue by NPCs
Swing	-
Cadence	BDNF-GFP
Stride length	GFP, BDNF-GFP
Print area LF	GFP, BDNF-GFP
Print length RF, LF	GFP, BDNF-GFP
Print width RF, LF	-
Max intensity RF	GFP, BDNF-GFP
Phase dispersion LF_RH	GFP, BDNF-GFP
LF_LH	GFP, BDNF-GFP

Figure 18. Transplantation of NPCs into the N171-82Q mouse model exerts beneficial effects in the CatWalk test. (A) Analysis of motor behavior on the Rotarod. N171-82Q mice showed a significant decrease in the latency to fall compared to wildtype animals from 12 weeks of age on. No difference between NPC transplanted and non-transplanted mice was detected. (B) Grip Strength of transgenic animals was not influenced by transplantation of NPCs at 13 or 18 weeks of age, but was lower than in wildtype. (C) Total distance moved in the Open Field was not changed in transgenic animals compared to wildtype mice at 13 or 18 weeks of age. Transplantation of GFP NPCs in transgenic N171-82Q animals reduced the distance moved at both time points compared to wildtype mice, but had no effect when comparing to transgenic N171-82Q mice. (D) Weekly body weight measurement showed a slow loss of body weight in transgenic animals, whereas wildtype mice gained body weight over time (ANOVA with repeated measures (cell groups x time, p=0.001) and consecutive simple effects analysis with Sidak correction) from 9 weeks of age on. No difference was detected between transplanted and non-transplanted animals. (E) Footprints of WT and N171-82Q mice were detected with the CatWalk system. (F) Overview of different gait parameters as quantified by the CatWalk test ($p<0.05$). NPCs affected positively altered cadence, stride length, print area, print length, maximum intensity of distinct paws and phase dispersion. Explanatory graphs see Figure 15. Data represent estimated marginal mean (A) or mean (B-D) (n=10-12 animals) ± SEM, *$p<0.05$ and **$p<0.01$, ***$p<0.001$ vs WT, n.s. not significant. RF= right forepaw, RH= right hindpaw, LF= left forepaw, LH= left hindpaw.

In order to identify the occurrence of subtler motor effects after cell transplantation, we also established the CatWalk gait system for the analysis of the N171-82Q mouse line. Indeed, we uncovered many gait parameters, which were significantly different in N171-82Q transgenic and wildtype mice (Figure 19).

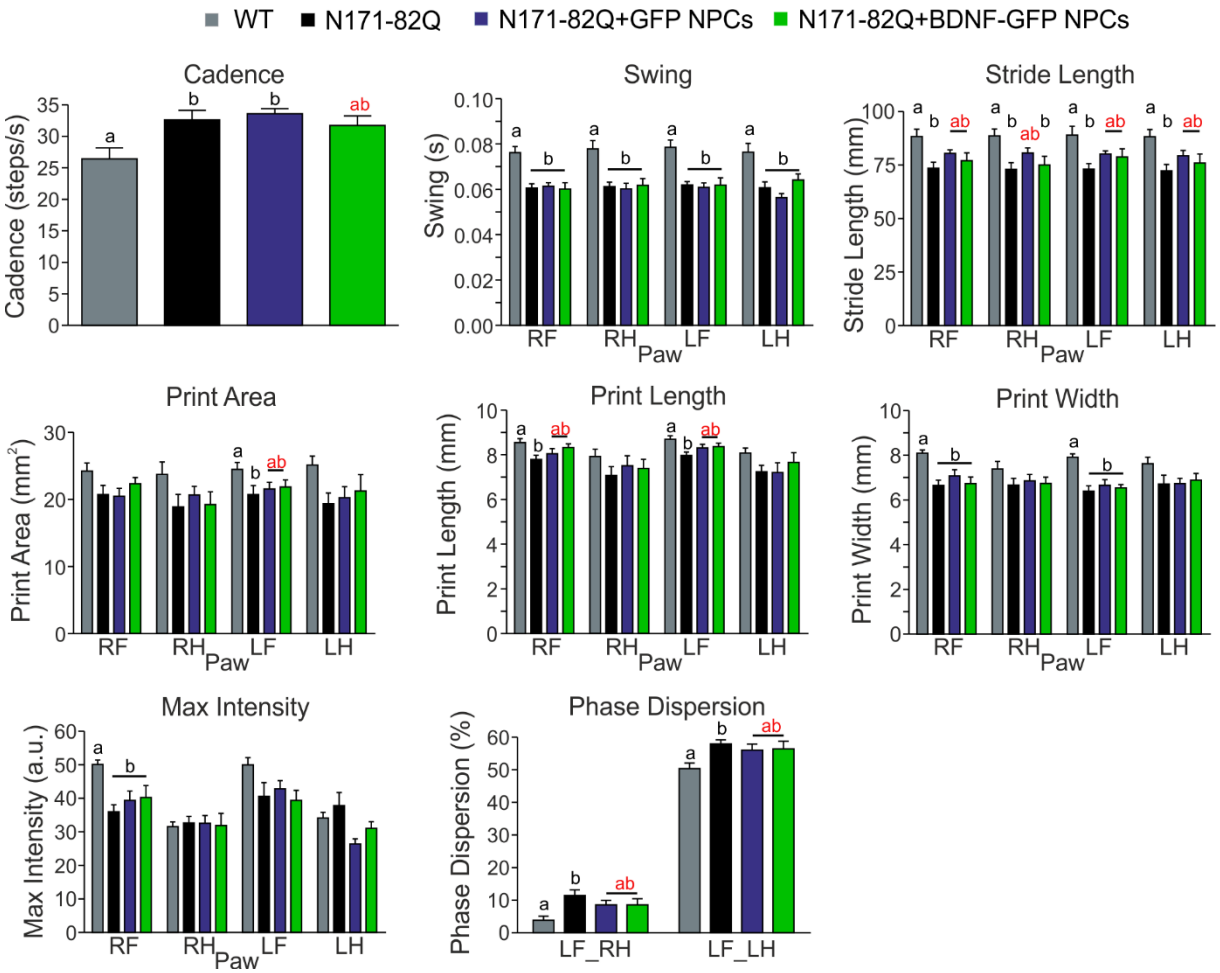

Figure 19. Affected CatWalk parameters in the N171-82Q mouse model. Detailed graphs for the table in Figure 14F. Transplanted NPCs had a lasting effect on transgenic compared to wildtype mice. One-way ANOVA with post-hoc Tukey's test between groups for each paw (n=10-12). Data represent mean ± SEM. Values of bars with a different letter (a or b) were significantly different ($p<0.05$) to each other. Values of bars with the same letter (a or b) were not significantly different from each other, hence values of bars marked with "ab" (marked in red) are not significantly different from either a or b, which indicates a partial/incomplete rescue of the phenotype. RF= right forepaw, RH= right hindpaw, LF= left forepaw, LH= left hindpaw.

Affected gait parameters were cadence (WT: 26.41 ± 1.75 steps/s, TG: 32.59 ± 1.50, p=0.031), swing (e.g. WT (RF): 0.0761 ± 0.0027 s, TG(RF): 0.0605 ± 0.0019 s, p=0.0001), stride length (e.g. WT(RF): 88.37 ± 3.39 mm, TG(RF): 73.54 ± 2.82 mm, p(RF)=0.01), print area (WT(LF): 24.85 ± 0.98 mm², TG(LF): 20.74 ± 1.32 mm², p=0.047), print length (e.g. WT(RF): 8.54 ± 0.18 mm, TG(RF): 7.79 ± 0.19 mm, p(RF)=0.028), print width (e.g. WT(RF): 8.09 ± 0.14 mm, TG(RF): 6.64 ± 0.24 mm, p(RF)=0.001), maximum (max) intensity (WT(RF): 50.14 ± 1.29 a.u., TG(RF): 35.95 ± 2.11 a.u., p(RF)=0.001), and phase dispersion (e.g. WT(LF_right hindpaw, RH): 3.89 ± 1.24%, TG(LF_RH): 11.43 ± 1.72%, p(LF_RH)=0.009). This demonstrates that the CatWalk can be used as a valid system to address motor function in the N171-82Q mouse line. With this method changes of defined motor parameters due to NPC transplantation were detected. These are summarized in tabular representation (Figure

18F). Most of the parameters (stride length (e.g. TG+GFP NPCs (RF): 80.46 ± 1.68 mm, p(RF) vs WT=0.359, TG+BDNF-GFP NPCs (RF): 77.02 ± 3.71 mm, p(RF) vs WT=0.058); print area (TG+GFP NPCs (LF): 22.16 ± 1.04 mm², p(LF) vs WT=0.359, TG+BDNF-GFP NPCs (LF): 22.26 ± 1.01 mm², p(LF) vs WT=0.304), print length (e.g. TG+GFP NPCs (RF): 8.04 ± 0.22 mm, p(RF) vs WT=0.286, TG+BDNF-GFP NPCs (RF): 8.32 ± 0.17 mm, p(RF) vs WT=0.816) ; phase dispersion (e.g. TG+GFP NPCs(LF_RH): 8.56 ± 1.39%, p(LF_RH) vs WT=0.222, TG+BDNF-GFP NPCs (LF_RH): 8.57 ± 1.92%, p(LF_RH) vs WT=0.151) were partially rescued by both NPC types, and no significant difference between transplantation with GFP and BDNF-GFP cells was measured. However, cadence was only positively affected after transplantation with BDNF-GFP NPCs (TG+BDNF-GFP NPCs: 31.70 ± 1.53 steps/s, p vs WT=0.069).

3.3.6 Cell survival is differentially altered in NPC transplanted groups in the three mouse models

Stereotaxic injection of QA into the striatum of C57BL/6J mice led to an almost complete depletion of medium spiny neurons positive for DARPP32 (Figure 20A).

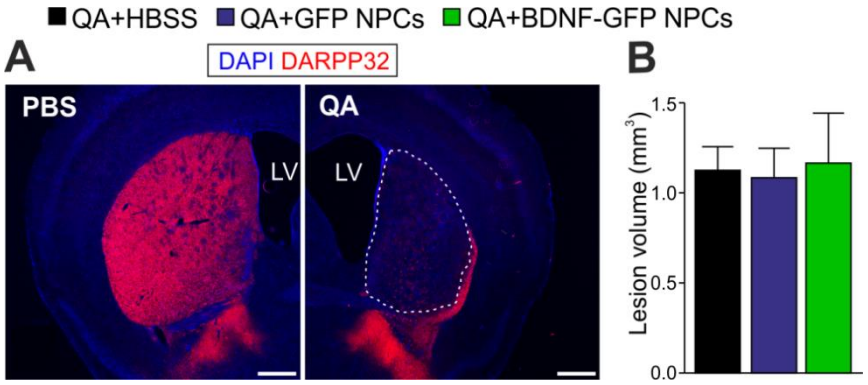

Figure 20. Representative photomicrographs of mouse brain sections from lesioned (QA) and non-lesioned (PBS) mice. Immunostaining for DARPP32 (red) showed that lesioning leads to a widespread loss of medium spiny neurons in the striatum. Scale bar, 500 µm. Dotted lines indicate lesioned area. (B) Quantitative analysis showed that lesion volume does not differ (p=0.97) between vehicle-treated and transplanted groups (n=4 animals). Values are expressed as mean ± SEM.

The lesion volume did not differ between the groups (QA+HBSS: 1.13 ± 0.13 mm3, QA+GFP NPCs: 1.09 ± 0.16 mm3 and QA+BDNF-GFP NPCs: 1.17 ± 0.28 mm3, Figure 20B, n=4/group). Differentiated ESCs injected into the lesion center one week after lesioning were detected by BrdU staining (Figure 21A), and most importantly showed no sign of tumor formation. The initial graft contained 100,000 cells, and stereological estimation (n=4/group) revealed 20.10 ± 4.51% BDNF-GFP and 21.65 ± 2.98% GFP NPCs survived 9 weeks after

transplantation in the striatum (Figure 21B). No significant differences were detected between both transplantation groups.

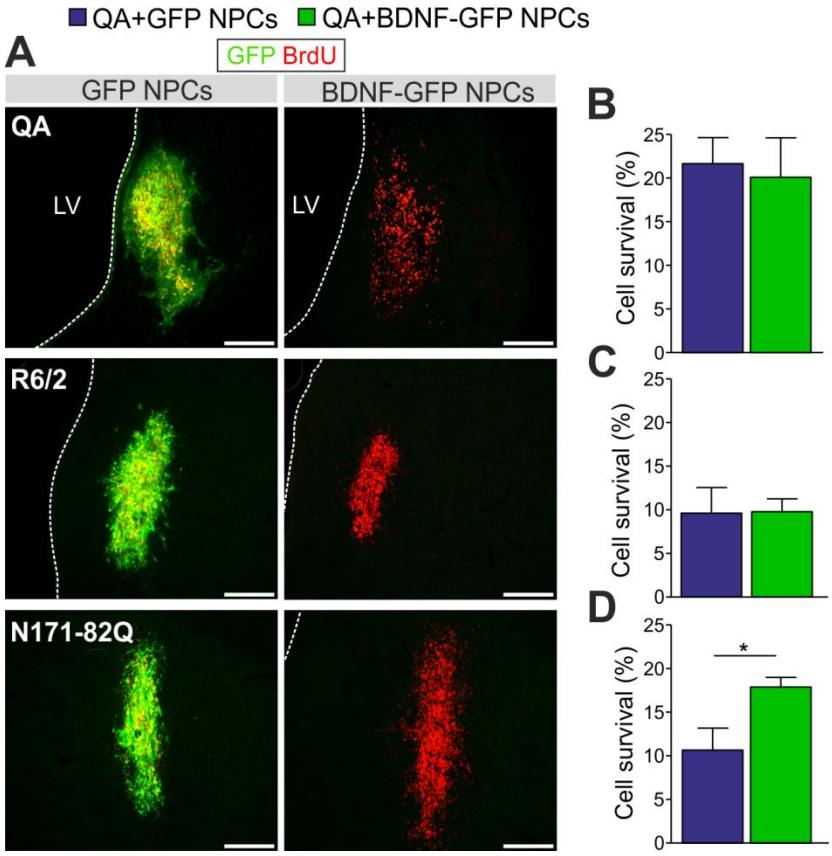

Figure 21. Representative micrographs for all three mouse models. (A) GFP cells are positive for BrdU and showed robust GFP expression. However, GFP signal of BDNF-GFP expressing cells is very weak and almost undetectable by confocal microscopy, but cells could be efficiently traced by BrdU. Scale bar, 250 µm. Dotted lines indicate the lateral ventricle (LV). Quantification of cell survival (n=4 animals) in the QA (B), the R6/2 (C) and N171-82Q (D) mouse model. Cell survival in the QA and R6/2 model is not different between BDNF-GFP and GFP transplanted cells, whereas in the N171-82Q model cell survival was significantly increased (p=0.039) by transplanting BDNF-GFP cells. Data represent mean ± SEM, *p<0.05.

Additionally, we investigated cellular survival for the two genetic mouse models. Cell survival in the transgenic R6/2 model (Figure 21C, n=4/group) was lower than in the QA model; 9.61 ± 2.96% BDNF-GFP and 9.78 ± 1.48% GFP cells survived after transplanting 100,000 cells/hemisphere. In contrast, quantification of transplanted cells in the transgenic N171-82Q model (Figure 21D, n=4/group) shows that 17.89 ± 1.09% BDNF-GFP cells and 10.65 ± 2.52% survive. Here, cell survival was increased when transplanting BDNF-GFP cells (p=0.039).

In both transgenic mouse lines, BDNF-GFP cells produce BDNF as detected by BDNF-antibody staining (Figure 22). In high magnification, BDNF-GFP can also be detected with

the GFP antibody, however at an almost undetectable level (Figure 22B). In contrast, GFP cells are only positive for GFP without showing BDNF expression (Figure 22A,B).

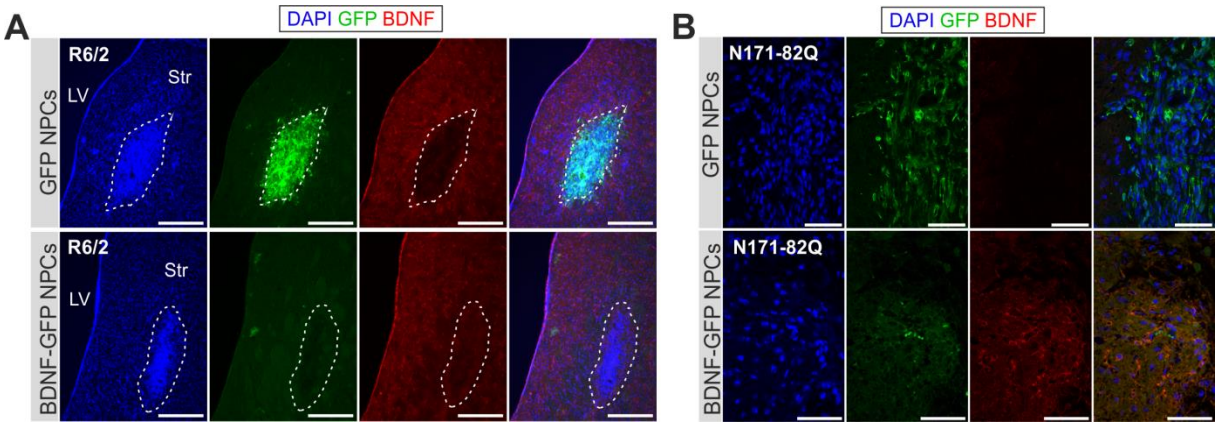

Figure 22. NPC transplants expressing GFP or BDNF. (A) Grafts (dotted lines) of GFP and BDNF-GFP expressing NPCs in the striatum of R6/2 mice seven weeks after cell transplantation in low magnification, Scale. 250 µm, or (B) in N171-82Q mice nine weeks after cell transplantation in higher magnification, Scale: 50 µm. Representative micrographs prove BDNF expression in BDNF-GFP NPCs with very weak detection of GFP signal in higher magnification (lower panels in A and B). In contrast, BDNF-signal was absent in GFP expressing cells (upper panels in A and B).

3.3.7 BDNF-GFP NPCs differentiate preferably towards a neuronal cell fate in the QA-lesioned striatum and influence endogenous neurogenesis

QA-induced lesion was the only HD mouse model that exhibited a robust functional improvement after injection of BDNF-GFP NPCs. For this reason, we analyzed positive NPC effects in detail in order to elucidate their mechanism of action. To determine the cell fate of transplanted cells, BrdU cells (n=8 animals/group) were double stained with antibodies against the three neural cell lineages (Figure 23A).

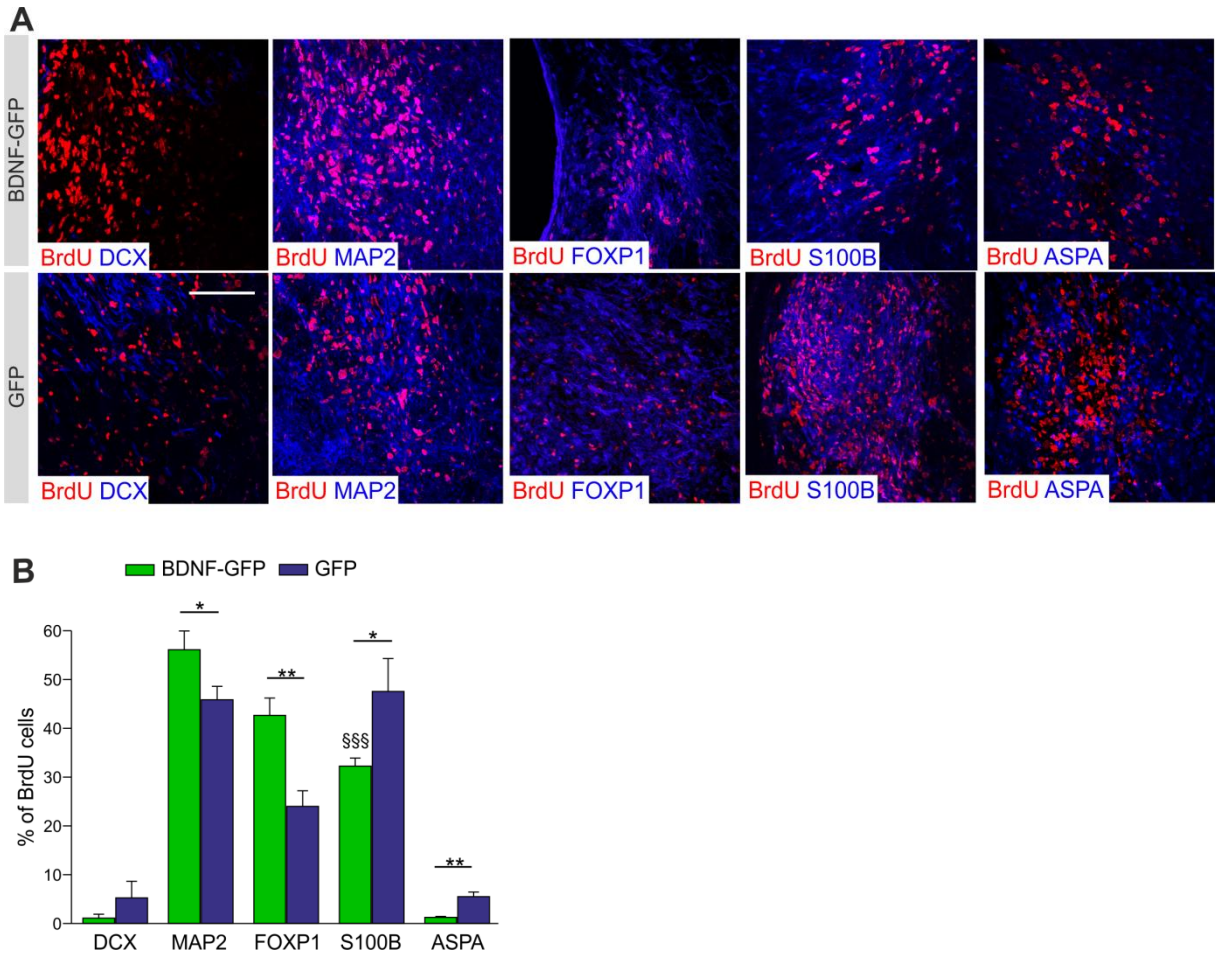

Figure 23. BDNF-GFP cells in the QA-lesioned striatum showed enhanced neuronal differentiation. (A) Maximum intensity projections of confocal micrographs of BDNF-GFP and GFP grafted cells. Transplanted cells were detected with BrdU staining (red) and were positive for DCX, MAP2, FOXP1, S100B and ASPA (all in blue). Scale bar, 100 µm. (B) Corresponding counts of double positive cells (n=8 animals). BDNF-GFP cells differentiated significantly more into a neuronal (MAP2+, p=0.0446) and striatal (FOXP1+, p=0.0022) lineage as compared to GFP cells, whereas GFP cells differentiated more into the glial (S100B+, p=0.0486 and ASPA+, p=0.0015) lineage as compared to BDNF-GFP cells. Additionally, BDNF-GFP cells favor highly significant neuronal (MAP2+) differentiation over astrocytic (S100B+) differentiation (§§§p=0.0001 vs BDNF-GFP MAP2).

Figure 23B shows that nine weeks after transplantation, the number of BrdU-positive neurons was significantly higher (p=0.0446) in BDNF-GFP grafts (MAP2, 56.14 ± 3.83%) than in GFP grafts (45.88 ± 2.74%). In contrast, the number of corresponding S100B+ astrocytes (BDNF-GFP: 32.29 ± 1.63%, GFP: 47.57 ± 6.77%) was decreased (p=0.0486). This means that BDNF-GFP NPCs favor neuronal (MAP2+) over astrocytic (S100B+) differentiation (p=0.0001). Only few aspartoacylase (ASPA)+ oligodendrocytes were observed in BDNF-GFP grafts (1.29 ± 0.18%), but less (p=0.0015) than in GFP grafts (5.50 ± 0.96%). BDNF-GFP NPCs differentiated strikingly (p=0.0022) into the striatal lineage, as assessed by staining for the striatal specific transcription factor forkhead box protein 1 (FOXP1) (BDNF-GFP graft: 42.67 ± 3.55%, GFP graft: 24.00 ± 3.22%). Analysis of DCX

immunolabeling showed no significant difference in the percentage of DCX-positive cells in BDNF-GFP (1.13 ± 0.79%) and GFP (5.25 ± 3.44%) grafts.

Endogenous neurogenesis in the dorsal SVZ was increased upon QA lesioning of the striatum, as evaluated by staining (n=4 animals/group) for the neuronal precursor marker DCX (Figure 24A).

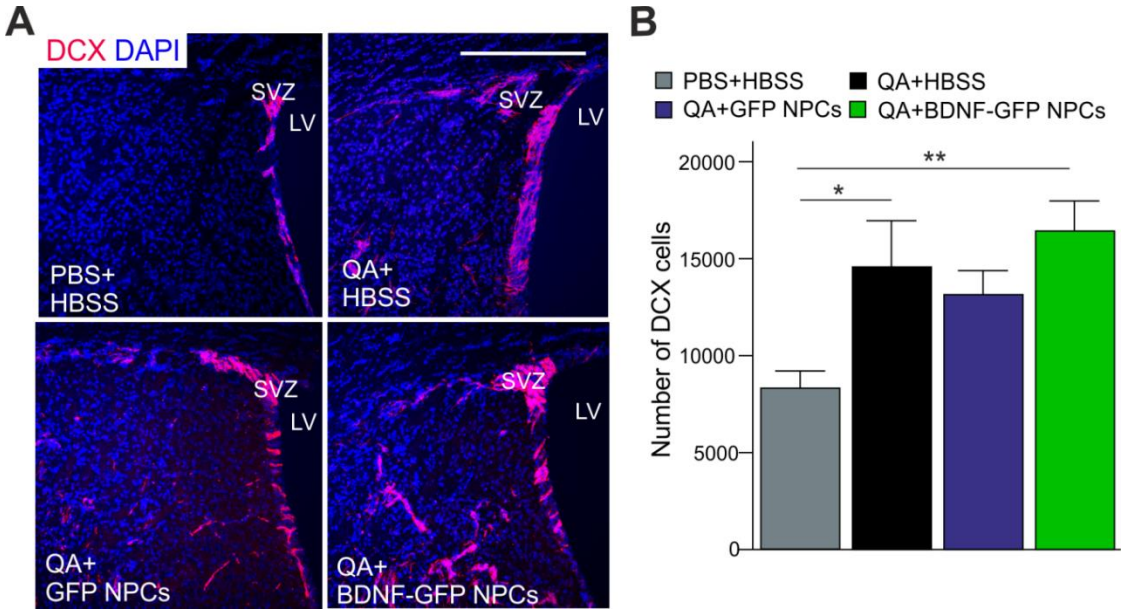

Figure 24. BDNF-GFP cells grafted into the QA-lesioned striatum showed preserved adult neurogenesis of the SVZ. (A) Representative sections through the SVZ of NPC transplanted, vehicle treated and non-lesioned animals immunostained for DCX (red) and DAPI (blue). Scale bar, 200 µm. (B) Stereological counts through the dorsolateral SVZ of BDNF-GFP NPC grafted, GFP NPC grafted, non-grafted lesioned and non-lesioned mice (n=4 animals). A significant increase in the number of DCX cells of BDNF-GFP NPC grafted (p=0.010) and non-grafted, lesioned animal (p=0.039) compared to non-lesioned mice was detected. Transplantation of GFP NPCs also led to an increase in number of DCX cells, but not significantly (p=0.124). Values represent mean ± SEM, *p<0.05 and **p<0.01, ***p<0.001.

Quantification of DCX numbers (Figure 24B) revealed a significant increase in the number of DCX cells of BDNF-GFP NPC grafted (16430 ± 1567 cells) and non-grafted, lesioned (14690 ± 2327 cells) animals compared to healthy (8335 ± 885 cells) animals. GFP NPC transplantation (13210 ± 1241 cells) did not significantly (p=0.124) affect endogenous neural precursor proliferation.

3.4 Discussion

Stem cell therapy and BDNF supply are two individual approaches for the treatment of HD. Given that a combination of both might be particularly promising, we tested the use of BDNF overexpressing NPCs, which had been derived from mouse embryonic stem cells. We compared the functional outcome after transplantation into three different HD mouse models and observed robust motor improvements only in the QA toxin-induced lesion model of HD. In contrast, transplantation into both transgenic HD mouse models R6/2 and N171-82Q resulted only in minor general NPC effects.

The standard behavioral paradigm to test motor function in the QA model is the apomorphine-induced rotation assay, which tests the unilateral dysfunction of the striatum (Bernreuther et al., 2006; Ramaswamy et al., 2007). Furthermore, the Rotarod as a test for motor coordination and motor learning, which is widely used for QA-lesioned rats, has been also described for mice with QA-lesion (Chiarlone et al., 2014). With both assays, we detected a functional improvement after transplantation of BDNF-GFP NPCs. Instead, GFP NPCs were only supportive when animals were tested in the Rotarod. Both types of NPCs exerted beneficial effects when looking at distinct CatWalk gait parameters. The CatWalk method is an automated, computerized gait analysis technique that allows objective analysis of very confined motor function. In HD research, it has so far only been described for the analysis of the R6/2 mouse model (Chiang et al., 2010) and of HD transgenic rats (Vandeputte et al., 2010). Our data show that the CatWalk assay is also a valuable behavioral paradigm for the analysis of the QA-lesioned mouse model. Specific gait characteristics (walk and swing speed; swing; cadence; stride length; duty cycle) were significantly different in QA-lesioned and non-lesioned mice. Furthermore, we established the CatWalk gait system for the N171-82Q mouse model and could show that multiple gait parameters were significantly changed when comparing wildtype and transgenic mice. With this tool, we further identified functional improvements after transplanting NPCs into N171-82Q mice, which we were not able to detect with the Rotarod and Grip Strength tests. Therefore, we assume that the CatWalk system is a more sensitive assay for detection of subtle, but profound, well-defined motor functions, which can be related to patients' symptoms. Besides chorea, HD patients display a more general progressive deterioration of skilled movements, which may also affect essential motor skills such as manual dexterity, locomotion and specific gait parameters (Folstein et al., 1983; Koller and Trimble, 1985). The CatWalk test is able to detect these gait impairments in mice. Other behavioral measures, such as the Rotarod test, detect general coordination, especially chorea. With our transplant

intervention, we were able to detect partial improvements in several gait parameters. However, due to small differences in absolute values between wildtype and transgenic animals, it was difficult to reveal intermediate improvements, such as those between BDNF-GFP and GFP transplants. In most gait parameters, both NPC types partially rescued the pathological phenotype, but effects were not different when comparing both transplant groups. However, cadence, as a single gait parameter, was only positively affected by BDNF-GFP cells in the N171-82Q mouse model. In contrast to N171-82Q mice, the R6/2 line behaved differently on the CatWalk, only stride length and lateral support were significantly changed, which is in agreement with published data (Chiang et al., 2010). Both gait parameters could be partially rescued either by GFP or BDNF-GFP cells, or by both NPC types. In general, we did not detect a considerable improvement of functional recovery in the R6/2 mouse line, as the two vigorous behavioral paradigms Rotarod and Paw Clasping were unchanged.

One possible explanation for the differential behavioral improvements in the three distinct HD mouse models could be the different cell survival rate with the highest survival rate in QA-lesioned animals. NPCs transplanted into transgenic animals generally displayed lower cell survival, a phenomenon which has already been demonstrated in other publications (Ebert et al., 2010; El-Akabawy et al., 2012; Snyder et al., 2010), possibly due to the progressive pathology in transgenic mice. Particularly after transplantation into R6/2 animals, approximately only half of the cells compared to QA-lesioned animals were detectable. Transplantation into the N171-82Q mice resulted in an intermediate cell survival rate compared to both other mouse models. Interestingly, only in the N171-82Q mouse model we detected a difference in the cell survival rate of both NPC types. Here, BDNF-GFP cells survived better than GFP cells, which might explain why more gait parameters were significantly changed by BDNF-GFP NPCs compared to the R6/2 line. Furthermore, the different degree of survival may be explained by the fact that in the transgenic lines, the absence of a lesion leads to a densely packed graft core, which might hinder survival, migration and integration of grafted cells (Behrstock et al., 2008). Although transgenic mouse models are genetically more accurate, and neurodegeneration is progressive, they still lack the feature of extensive neuronal cell death, which seems to be a prerequisite for survival and integration of transplanted cells (Labandeira-Garcia et al., 1991; Watts and Dunnett, 1998). Therefore, most of studies addressing cellular therapies for HD used QA-lesioned rodent models, which display massive and predictable cell loss (Aubry et al., 2008; Bernreuther et al., 2006; Ma et al., 2012b; Shin et al., 2012). Only few cell transplantation studies with different types of stem or progenitor cells used transgenic HD mouse models and obtained minor or no motor outcome. Especially with the R6/2 line, it was difficult to

obtain any kind of improvement (El-Akabawy et al., 2012; Fink et al., 2013), whereas N171-82Q seemed to be the more appropriate transgenic model for cell transplantation (Ebert et al., 2010; Snyder et al., 2010). We can affirm these observations with our CatWalk data, as more gait parameters were changed by NPC transplantation in N171-82Q mice than in the R6/2 line. Both mouse models differ in their extent of neuropathology, life span and most importantly in their disease progression. Compared to N171-82Q mice, R6/2 animals display a very drastic, accelerative phenotype with a very short life span of 12 weeks, which could hinder cellular survival, proper differentiation and functional integration after transplantation. In conclusion, toxin-induced lesions, causing massive cell death, serve as the most appropriate HD mouse model for cellular transplantation to date. Even if not optimal in terms of acute cell death, clear positive effects of BDNF NPCs were obtained in the present study. For this reason, we analyzed the mode of action of BDNF NPCs in the QA lesion model. NPCs either expressing GFP or BDNF-GFP similarly survived grafting and no differential effect of proliferation was observed. Furthermore, due to the use of MACS purification, no tumor formation was induced by either cell type. Instead, *in vivo* differentiation was affected in a cell type-specific manner. BDNF expressing progenitors mainly differentiated into neurons compared to GFP control cells, which favored glial, and specifically astrocytic lineage differentiation. Enhanced neuronal and GABAergic differentiation by BDNF has been already shown by us and others (Butenschon et al., 2016; Leschik et al., 2013; Ortega and Alcantara, 2010; Trzaska and Rameshwar, 2011). Furthermore, BDNF is known to be an important factor for the postnatal growth of the striatum (Rauskolb et al., 2010) and is essential for the *in vitro* and *in vivo* differentiation of striatal neurons (Gokce et al., 2009; Ivkovic and Ehrlich, 1999). Indeed, we found more neurons positive for the striatal marker FOXP1 in BDNF cell grafts than in GFP cell grafts, which underlines the HD-therapeutic potential of BDNF NPCs.

FOXP1 labels striatal precursors and differentiated MSNs (Delli Carri et al., 2013). Diverse studies so far attempted to pre-differentiate stem cells into transplantable striatal progenitors or MSNs by using various kinds of differentiation protocols. Human ESCs were demonstrated to terminally differentiate into GABAergic DARPP32 positive neurons *in vitro* and *in vivo* by the use of sonic hedgehog and BDNF as key molecules (Aubry et al., 2008; Ma et al., 2012b). Therefore, our approach with mouse ESCs was to analyze whether very early PSA-NCAM positive neural progenitors, which expressed one of the earliest telencephalic markers FOXG1, could differentiate *in vivo* into MSNs through continuous BDNF supply. To obtain NPCs, we used the differentiation protocol of (Bernreuther et al., 2006) with minor modifications. This study used mouse ESC-derived neuronal cell adhesion molecule L1 overexpressing NPCs in QA-lesioned mice, which led to short-term functional improvement.

Here, we show that functional improvement was accompanied by increased striatal differentiation of BDNF NPCs, meaning that BDNF as signaling molecule is sufficient to trigger *in vivo* differentiation into MSNs. Likewise for *in vitro* striatal differentiation of human ESCs, alternatively, the potent telencephalic morphogen sonic hedgehog could be used at early stages of differentiation to obtain MSNs after transplantation (Danjo et al., 2011).

In addition to the analysis of *in vivo* differentiation of transplanted cells, precursor proliferation of endogenous DCX positive cells was investigated as a potential mechanism leading to improved motor behavior. It is known that striatal QA-lesion by itself induces proliferation and migration of adult neuronal stem cells from the dorsal SVZ as an attempt to regenerate the lesioned striatum (Tattersfield et al., 2004). BDNF is known to be an important trigger of adult neurogenesis (Vilar and Mira, 2016). Therefore, transplantation of BDNF expressing cells could induce a higher migration rate, better survival, increased proliferation and/or differentiation of SVZ precursor cells. However, we found no difference in the number of DCX-positive cells in QA-lesioned animals with or without BDNF cell transplants, which implies that BDNF exerted no positive effect on endogenous progenitors. Interestingly, GFP transplants significantly reduced the number of DCX-cells. In conclusion, this would mean that NPC transplantation by itself induces negative changes in tissue homeostasis or endogenous regeneration, which might be overcome by BDNF. The differences in the motor outcome after transplantation of both cell types could be hence due to a combination of BDNFs positive effects on differentiation of transplanted cells and its preserving effects of lesion-induced SVZ neurogenesis.

Although incurable, Huntington disease is not untreatable. Clinical care of patients focuses on expert assessment and the multidisciplinary management of symptoms, through medical and non-medical means, to maximize function and quality of life. The results obtained in this study are of high impact for therapeutic interventions as they add knowledge to former and future cell replacement approaches in HD patients.

4 Functional role of CB1 receptor on adult neural stem cells *in vivo*

4.1 Introduction

Adult-born neurons are continuously generated in the SGZ of the DG of the mammalian brain throughout life (Altman and Das, 1965). Newborn neurons are then integrated in the hippocampal circuitry and regulate multiple physiological functions (Kee et al., 2007).

4.1.1 Adult neurogenesis in the subgranular zone

In the SGZ, the process of adult neurogenesis is comprised of slowly dividing radial glial cells (type 1 cells) and the rapidly amplifying NPCs (type 2 cells), the latter differentiating into neuroblasts. Immature neurons migrate into the inner granule cell layer and differentiate into dentate granule cells (Figure 25). They extend dendrites towards the molecular layer, receiving input from the entorhinal cortex and project axons through the hilus toward the Cornu Ammonis region (CA) 3 (Aimone et al., 2014). Finally, they become integrated into the hippocampal network (Figure 26), which involves the trisynaptic circuit of neurons. It connects neurons from the entorhinal cortex via the medial perforant path, dentate gyrus, CA3, and via the Schaffer collateral pathway CA1.

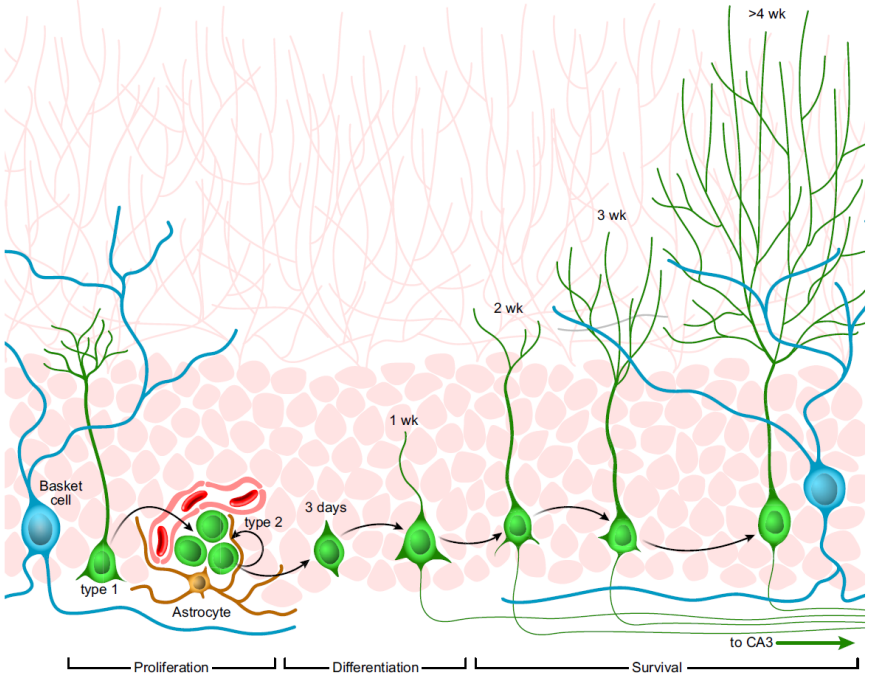

Figure 25. Development of dentate gyrus granule cells from stem cells to mature neurons. Slowly dividing type 1 cells (radial glial cells) and rapidly amplifying type 2 cells give rise to new neurons over the course of few weeks, developing dendritic arborizations and axonal projections (Aimone et al., 2014).

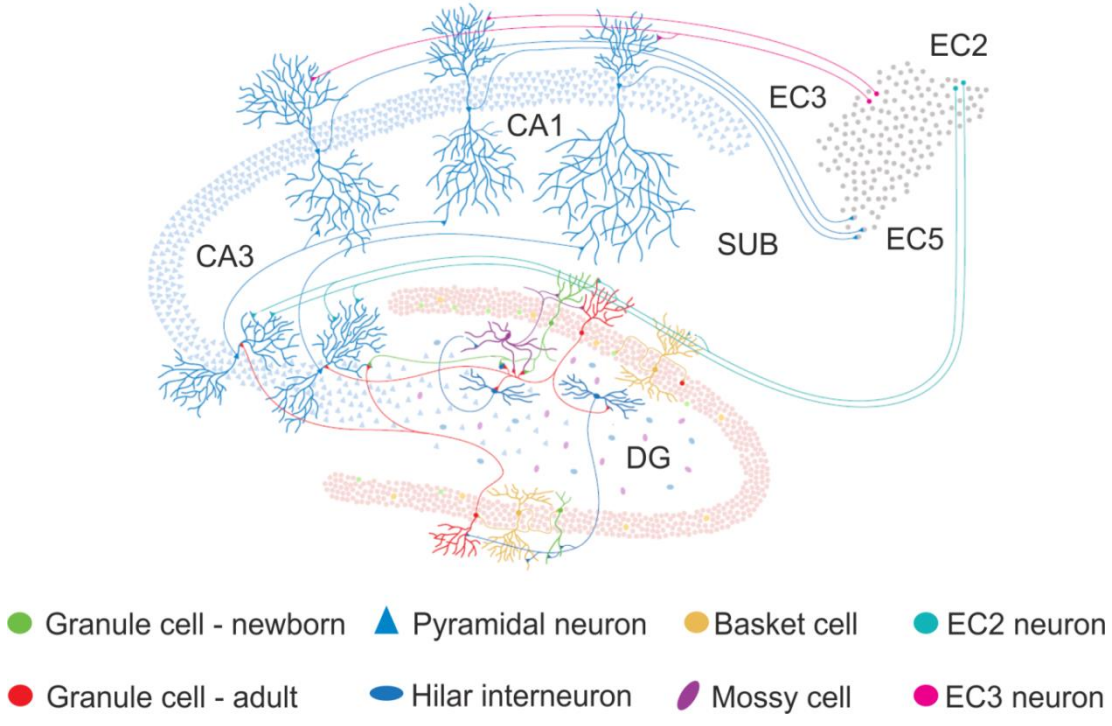

Figure 26. Adult-born neurons integrate into the hippocampal network. Adult-born neurons extend their dendrites towards the molecular layer and receive input from the entorhinal cortex layer 2 and from GABAergic interneurons. Axonal projections are found in the CA3 region on pyramidal neurons, which project to the CA1 region. CA1 pyramidal neurons send their projections back to the entorhinal cortex layer 5 (Aimone et al., 2014).

In the SGZ, type 1 cells are radial-glia like precursor cells, have astrocytic properties and express the marker GFAP (Filippov et al., 2003; Seri et al., 2001). They have a triangular-shaped soma with long apical processes reaching into and branching out of the granular cell layer (Filippov et al., 2003), appearing with a tree-like structure. In contrast to fully mature astrocytes, they do not express the astrocytic marker S100B (Seri et al., 2004; Steiner et al., 2004). However, they are positive for nestin, a class IV intermediate filament protein (Palmer et al., 2000), and the transcription factor Sox2 (Garcia et al., 2004; Suh et al., 2007). Type 1 cells are rarely dividing (Kronenberg et al., 2003) and can divide asymmetrically, giving rise to a daughter cell, which lacks radial morphology and is named type 2 cell (Filippov et al., 2003; Goncalves et al., 2016). In contrast to type 1 cells, they are highly proliferative, and have a plump morphology with short processes (Steiner et al., 2006). They express the markers nestin and Sox2, but not GFAP. The prevalent view is that the fate choice between glial and neuronal phenotype occurs at the level of type 1 cells, since at no later stage an overlap between glial or neuronal properties has been found. Type 2 cells are divided in two populations (Kronenberg et al., 2003). Type 2a cells are negative for DCX, whereas type 2b cells are positive for DCX. The expression of DCX is associated with the expression of PSA-NCAM, which creates a starting point for neuronal differentiation and migration (Seki and Arai, 1993). In the course of development, type 2 cells differentiate into type 3 cells, which are the migratory neuroblasts in the SGZ. They are negative for all glial markers as well as Sox2 and nestin. Many cells show a first apical dendrite (Plumpe et al., 2006) and have a horizontal orientation. Once they exit the cell cycle, they start the terminal differentiation into postmitotic granule cells. These young neurons express the neuronal marker neuronal nuclei (NeuN) and start to integrate into the hippocampal network, establishing dendritic trees, spines, and axonal projections to the CA3 region (Zhao et al., 2006).

The unique microenvironment in the SGZ regulates activation, development and maintenance of adult neural precursor cells by a number of signaling molecules (Mu et al., 2010). These include the endocannabinoids, their receptors, and the endocannabinoid synthesizing and degrading enzymes (Aguado et al., 2005).

4.1.2 The endocannabinoid system

Marijuana has been used for therapeutic and recreational purposes for many centuries (Lemberger, 1980; Li, 1973). The cannabis plant *Cannabis sativa* contains among others, the cannabinoids Δ^9-tetrahydrocannabinol (THC) and cannabidiol (CBD). THC, the psychoactive constituent of marijuana, has been isolated in 1964 (Gaoni and Mechoulam, 1964) and the

structure has been solved in the same year. It was then synthesized in 1967 (Mechoulam et al., 1967) and became available for research. The structure of CBD was elucidated in 1963 (Michoulam and Shvo, 1963).

Cannabinoids act through endogenous receptors (Devane et al., 1988; Herkenham et al., 1990; Howlett et al., 1986) called cannabinoid receptors. The CB1 receptor is one of the most abundant G-protein coupled receptors (GPCR) in the brain with high expression levels in multiple neuronal subtypes (Marsicano and Kuner, 2008), whereas the CB2 receptor, another member of the GPCR superfamily, has been found in peripheral tissue, but has also been identified in the CNS, mainly on microglia (Nunez et al., 2004; Stella, 2004). CB1 and CB2 share 48% of their amino acid sequence identity, signal through inhibitory Gi/o heterotrimeric G proteins (Howlett, 1985), interact with β-arrestins (Jin et al., 1999) and elicit distinct intracellular signaling cascades (Katona and Freund, 2012). Just recently, the crystal structure of human CB1 in complex with the agonist AM6538 has been reported (Hua et al., 2016).

Endogenous compounds synthesized in the body to activate cannabinoid receptors are called endocannabinoids. The predominant endocannabinoids are 2-arachidonoylglycerol (2-AG) (Mechoulam et al., 1995) and anandamide (N-arachidonoylethanolamine, AEA) (Devane et al., 1992), which are endogenous lipids. They are synthesized on-demand by the synthesizing enzymes diacyl glycerol lipase-α (DAGL) and N-acyl phosphatidylethanolamine phospholipase D (NAPE-PLD), respectively, and act as retrograde synaptic messengers. The synthesis is triggered by a postsynaptic depolarization-induced rise in intracellular calcium concentrations (Di et al., 2005; Kim et al., 2002) and by stimulation of metabotropic glutamate receptors (Maejima et al., 2001; Varma et al., 2001). By binding to presynaptic CB1, they inhibit the active neurotransmitter release. They are then removed by the endocannabinoid degradading enzymes. AEA is degraded by fatty acid amide hydrolase (FAAH) in the postsynaptic terminal. Monoacyl-glycerol lipase (MAGL) degrades 2-AG in the presynaptic terminal, while α/β-hydrolase domain containing 6 (ABHD6) limits 2-AG availability at the site of production. Activity of endocannabinoids can be prolonged by suppression of these enzymes (Gaetani et al., 2009).

As mentioned above, CB1 is one of the most abundant GPCRs in the brain (Herkenham et al., 1990) (Figure 27).

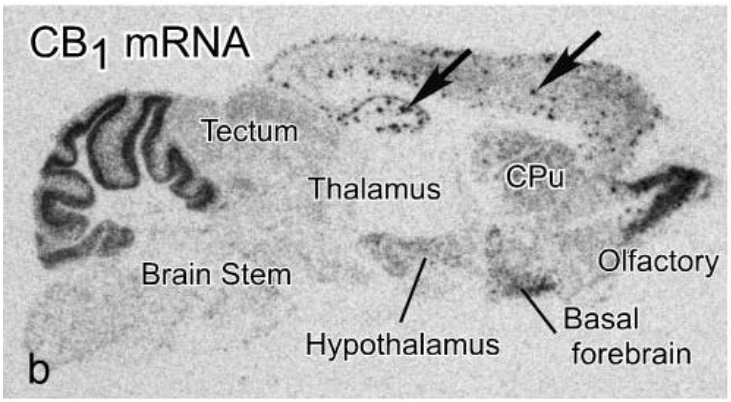

Figure 27. Autoradiography of mRNA expression in a sagittal mouse section. Cells expressing CB1 are found in the basal ganglia, cerebellum, hippocampus (arrow), and cerebral cortex (arrow) (Howlett et al., 2002).

Highest densities of CB1 are in the basal ganglia, substantia nigra, globus pallidus, cerebellum, hippocampus, cerebral cortex, but CB1 is almost not detected in the brainstem (Howlett et al., 2002; Mackie, 2005; Marsicano and Lutz, 1999). CB1 is localized on GABAergic and glutamatergic neurons, on central and peripheral neurons in the presynapse. After activation, it induces the inhibition of excitatory (glutamate) neurotransmitter release (Figure 28). The process is called transient eCB-mediated short-term depression (eCB-STD) or eCB-mediated long-term depression (eCB-LTD) of synaptic transmission or depolarization induced suppression of excitation (DSE) for the suppression of glutamate release. Inhibition of inhibitory GABA release is named depolarization-induced suppression of inhibition (DSI) (Kano et al., 2009).

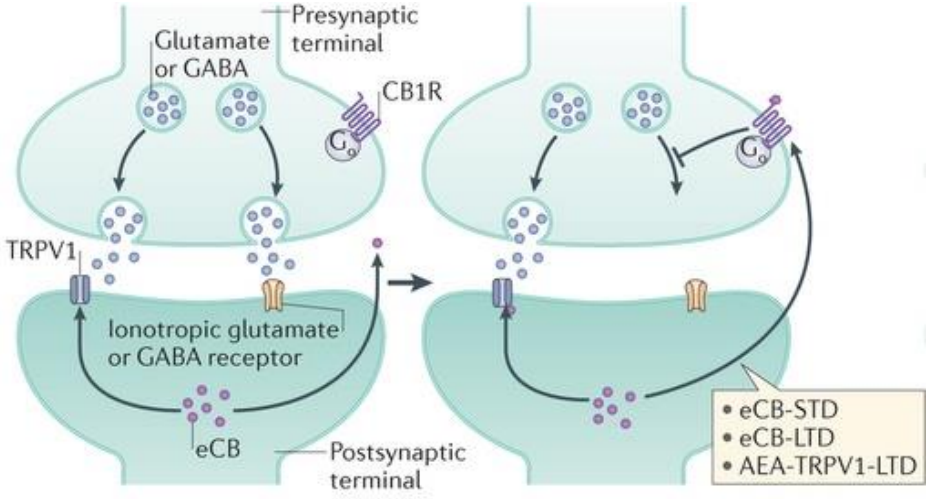

Figure 28. Signaling of endocannabinoids suppresses synaptic excitatory and inhibitory transmission (Lutz et al., 2015). Depolarization of the presynaptic terminal leads to glutamate or GABA release and subsequent activation of the postsynaptic neuron. This stimulates production and release of endocannabinoids (eCB) AEA and 2-AG to the synaptic cleft to activate CB1 receptors (CB1R) in the presynaptic terminal. Glutamate (eCB-STD, eCB-LTD) and GABA release are suppressed. AEA acts also through the transient receptor potential vanilloid type 1 (TRPV1) cation channel and produces AEA-TRPV1-LTD.

Other types of receptors have also been related to endocannabinoid signaling; e.g. the transient receptor potential vanilloid type 1 (TRPV1) cation channel (Toth et al., 2009), GTP-binding protein-coupled receptor GPR55 (Ross, 2009), and the peroxisome-proliferator-activated receptor PPAR family (O'Sullivan, 2007). AEA acts through both cannabinoid receptors, which leads to eCB-LTD, but also activates TRPV1, which results in a specific AEA-TRPV1-LTD.

Intracellularly, activation of CB1 leads to a decrease in cAMP accumulation and to the inhibition of protein kinase A (PKA) and a stimulation of the MAP kinase activity. One immediate early gene of CB1 signaling includes BDNF (Khaspekov et al., 2004; Marsicano et al., 2003). Thereby, synaptic plasticity, cell migration, and neuronal growth are affected. CB1 is also coupled to different types of calcium and potassium channels.

Furthermore, recent studies showed that the CB1 receptor is expressed on astroglial cells and oligodendrocytes (Benito et al., 2007; Navarrete and Araque, 2010). In astrocytes, CB1 is coupled to Gq signaling. Upon agonist stimulation of the receptor, intracellular Ca^{2+} concentration rises, and then so-called 'gliotransmitter' (e.g. glutamate, GABA, ATP) are released, modulating synaptic transmission (Metna-Laurent and Marsicano, 2015; Navarrete et al., 2014). The astroglial CB1 seems to potentiate synaptic glutamate signaling (Navarrete and Araque, 2010), whereas CB1 at the presynapse is reducing neurotransmitter release. Both cannabinoid receptors CB1 and CB2 are also localized on microglial cells and are involved in immune reactions (Stella, 2009).

The endocannabinoid system has been implicated in multiple physiological functions in the nervous system, such as locomotion, appetite, fear, anxiety, depression, and cognition. Many of the pharmacological effects of cannabis are biphasic (Moreira and Lutz, 2008; Rey et al., 2012), probably originating from the differential expression of CB1 in multiple brain regions and its localization on distinct neuronal populations. Mostly, psychotropic effects depend mainly on the dose and on the personality of the user (Bortolato et al., 2010).

To study the role of CB1 in the nervous system and to dissect cell-type specific CB1 functions, conditional CB1 knockout mice have been generated. In the hippocampus, CB1 is expressed on glutamatergic principal neurons, but not on glutamatergic granule cells in the dentate gyrus. It is also expressed on GABAergic interneurons. Together, they exert opposing effects on the neuronal circuitry (Lutz et al., 2015). Even though CB1 density is lower in glutamatergic than in GABAergic neurons, G protein signaling is stronger in glutamatergic neurons (Steindel et al., 2013). Consequently, glutamatergic CB1 is engaged in the majority of CB1-mediated physiological effects such as behavioral studies. Low doses

of cannabinoids activate glutamatergic CB1 and high doses activate CB1 on GABAergic terminals (Rey et al., 2012).

The endocannabinoid system modulates synaptic transmission, and thereby regulates behavioral outputs. Cognition involves acquisition, storage, and retrieval of new information. Learning and memory impairments are among the most commonly reported behavioral effects of cannabinoids (Lichtman et al., 1995). By using the most widely used spatial learning task, the Morris water maze, systemic administration of cannabinoid agonists has been shown to impair the learning in the hidden platform task (Ferrari et al., 1999). However, the learning performance was intact in CB1 knockout (KO) mice (Varvel and Lichtman, 2002), but was impaired in the extinction process. Fear conditioning is another behavioral test to study memory acquisition, particularly aversive memory. The endocannabinoid system has been revealed to be involved in contextual and auditory cued fear conditioning (Marsicano et al., 2002; Pamplona and Takahashi, 2006). Furthermore, a hypo- or hyperfunctional endocannabinoid system has been implicated in depression (Hill et al., 2008). Additionally, an enhanced endocannabinoid signaling is associated with antidepressant efficacy (Bambico et al., 2007; Haring et al., 2013; Hill et al., 2005). One hypothesis of the development of depression is that it is linked to neurogenesis (Yun et al., 2016). It is based on the downregulation of neurogenesis in depressive-like behaviors in animals and its upregulation by antidepressants. Over the last years, studies have shown that the endocannabinoid system plays a central role in neurogenesis (Galve-Roperh et al., 2009; Oudin et al., 2011).

4.1.3 Impact of cannabinoids on adult neurogenesis

Neural stem cells and neural progenitors are very sensitive to their microenvironment, the stem cell niche. Extrinsic signaling molecules direct the proliferative activity and differentiation potential of these cells.

Mature granule neurons in the dentate gyrus do not express CB1 (Monory et al., 2006), implicating that CB1 serves as an important regulator of adult neural progenitor cells. In the developing rodent brain, the endocannabinoid system is expressed from early stages of brain development (Harkany et al., 2007) and is essential for neural cell lineage commitment (Bertrand et al., 2002), migration (Mulder et al., 2008), survival, and maintenance (Galve-Roperh et al., 2008) of neural cells. It has been shown to be involved in dendrite arborization and synaptic maturation in a CB1-dependent manner (Berghuis et al., 2007).

Cannabinoids stimulate neurogenesis during development (Berghuis et al., 2007). In the past years, growing evidence has evolved that both exogenous and endogenous cannabinoids affect the process of adult neurogenesis (Figure 29).

Treatment	Measurement	Observation	Reference
HU-210	Cell proliferation in the dentate gyrus in adult rats	Enhanced	Jiang *et al.* (2005)
HU-308	Hippocampal progenitor proliferation in adult mice	Enhanced	Palazuelos *et al.* (2012)
WIN55,212-2	Dorsal hippocampal neurogenesis during adolescence	Reduced	Abboussi *et al.* (2014)
WIN55,212-2	Age-related deficits in hippocampal neurogenesis	Partial restoration	Marchalant *et al.* (2009)
Δ^9-THC/CBD	Precursor cell proliferation in the dentate gyrus	Reduced	Wolf *et al.* (2010)
CBD	Cell survival in the dentate gyrus	Enhanced	Wolf *et al.* (2010)
CBD	Number of $BrdU^+$ cells colocalized with $NeuN^+$ cells in hippocampus	Enhanced	Campos *et al.* (2013)
DAGL inhibitor	Cell proliferation in the adult SVZ	Reduced	Goncalves *et al.* (2008)
URB597/AEA/ WIN55,212-2	Adult hippocampal NPC proliferation	Enhanced	Aguado *et al.* (2005)
WIN55,212-2/ JWH-133/URB597	Progenitor cell proliferation in the SVZ	Enhanced	Goncalves *et al.* (2008)
AM251	Cell proliferation in the SGZ	Enhanced	Hill *et al.* (2006)
AM251	Cell proliferation in the SGZ	Enhanced at 24 h/ reduced at 48 h	Wolf *et al.* (2010)
$FAAH^{-/-}$	Cell proliferation in the dentate gyrus of adult mice	Enhanced	Aguado *et al.* (2005)
$DAGL\alpha^{-/-}$	Cell proliferation and number of DCX^+ neurons in the hippocampus	Reduced	Gao *et al.* (2010)
$DAGL\beta^{-/-}$	Cell proliferation in the hippocampus	Reduced	Gao *et al.* (2010)
$CB_1^{-/-}$	Cell proliferation in the dentate gyrus and SVZ	Reduced	Jin *et al.* (2004) Kim *et al.* (2006)
$CB_1^{-/-}$	Number of $BrdU^+$ cells colocalized with $S100\beta^+$ cells in the SGZ and granule cell layer of the dentate gyrus	Reduced	Aguado *et al.* (2006)
$CB_1^{-/-}$	Number of $BrdU^+$ cells colocalized with $NeuN^+$ cells in the SGZ and granule cell layer of the dentate gyrus	Enhanced	Aguado *et al.* (2006)
$CB_1^{-/-}$	Kainic acid-induced hippocampal NPC proliferation	Reduced	Aguado *et al.* (2007)
$CB_1^{-/-}$	Cortical thickness	Reduced at P2	Diaz-Alonso *et al.* (2012)
SR141716A	Cell proliferation in the SVZ	Enhanced	Jin *et al.* (2004)
JTE-907/AM630	Cell proliferation in the SVZ	Reduced	Goncalves *et al.* (2008)
$CB_2^{-/-}$	Number of $BrdU^+$ cells in dentate gyrus	Reduced	Palazuelos *et al.* (2006)

JTE-907 and AM630 are CB_2 receptor antagonists. NeuN, neuronal nuclei.

Figure 29. *In vivo* effects of cannabinoids on adult neurogenesis in rodent models (Prenderville et al., 2015).

A shared feature of synthetic and plant-derived cannabinoids is that acute administration has no effect on cell proliferation or overall neurogenesis, whereas chronic treatment has. Chronic treatment for example with the synthetic cannabinoid HU-210 enhances proliferation in the adult dentate gyrus (Jiang et al., 2005). A positive effect has also been shown in the aged brain, where the synthetic CB1/CB2 agonist WIN55,212-2 partially restored age-related deficits in hippocampal neurogenesis (Marchalant et al., 2009). The impact of chronic administration of the phytocannabinoid Δ^9-THC has been shown to be dose- and time-dependent, either having no effect on cell proliferation (Kochman et al., 2006) or decreasing the rate of cell proliferation (Wolf et al., 2010). However, repeated administration of the phytocannabinoid cannabidiol (CBD) increases cell proliferation in the dentate gyrus, presumably explaining the anxiolytic effect of CBD in chronic stressed animals (Campos et al., 2013). In contrast, acute administration of the inverse agonist AM251 increases

proliferation for 24 h (Hill et al., 2006), but decreases it after 48 h (Wolf et al., 2010). Chronic administration of AM251 has no effect on adult neurogenesis (Rivera et al., 2011). Since the endocannabinoid anandamide also activates TRPV1, the antagonist SR141716A has been shown to increase cell proliferation in both neurogenic regions the dentate gyrus and the lateral ventricles. However, this effect has not been detected in TRPV1 KO mice, but in wildtype and CB1 KO mice (Jin et al., 2004). This suggests that cannabinoid signaling plays a complex temporal role in adult neurogenesis and multiple receptors are responsible for the effect of administered cannabinoids, leading to an intricacy of previous studies.

To study fundamental processes of the endocannabinoid system in adult neural stem cells, gene knockdown technologies have been developed, which have linked cannabinoids and adult neurogenesis. Loss of CB1 signaling in complete CB1 KO mice inhibits neural precursor proliferation (Aguado et al., 2005; Jin et al., 2004) and decreases astroglial differentiation *in vitro* and *in vivo* (Aguado et al., 2006). Until now, it is not known, whether this phenomenon is regulated through a direct or an indirect mechanism of CB1 signaling.

In the DG, CB1 is localized on GABAergic interneuron output, on radial glia cell membranes, and on early progenitor membranes. Mature glutamatergic granule cells do not contain CB1 (Monory et al., 2006), placing the cannabinoid receptor as a key player in processes underlying adult neurogenesis.

4.1.4 Functional and physiological role of adult neurogenesis

In the past two decades, the neurogenesis field has made remarkable progress. Multiple extrinsic and intrinsic signals have been shown to mediate the complex process of adult neurogenesis (Suh et al., 2009). But to what extent is the importance of adult hippocampal neurogenesis reflected on the physiological level? Does integration of adult-born neurons into the existing circuit affect hippocampus-related behaviors?

Newborn neurons have been shown to contribute to adult brain function at the cellular, network and systemic level. At the cellular level, newborn neurons differ from existing neurons transiently in their cellular function. Young neurons show a greater tendency for synaptic plasticity compared with older counterparts (Schmidt-Hieber et al., 2004). Maturation of adult-born granule cells includes synaptic integration into the hippocampal network (Esposito et al., 2005; Zhao et al., 2006). During the first week after birth, cells are tonically activated by GABA, but are not yet synaptically incorporated. During the second week after birth, cells become more neuron-like and start growing their dendrites toward the

molecular layer and extending their axons to CA3 region. These immature granule cells are characterized by their high membrane resistance and different firing properties. They lack glutamatergic input and do not have develop spines yet. However, they receive synaptic GABAergic input from local interneurons, which causes depolarization in these cells and promotes their differentiation (Tozuka et al., 2005; Zhao et al., 2008). During the third week after birth, immature granule cells form afferent and efferent connections with the local network. At day 16, spines appear on the dendrites and form synapses with afferent axonal fibers from the medial performant pathway coming from the entorhinal cortex. Furthermore, mossy fiber boutons of newborn granule cells form synapses with the dendritic shaft of CA3 pyramidal neurons. At the time of synaptic integration, the GABAergic input switches from being excitatory to being inhibitory and cells receive glutamatergic input (Ge et al., 2006). Around 4-6 weeks after birth, maturing granule cells display an increase in synaptic plasticity compared to the existing granule cells, as suggested by the lower threshold for induction of long-term potentiation (LTP) and the higher LTP amplitude. This is controlled by the NMDA receptor subunit NR2B (Ge et al., 2007). Adult-born granule cells continue to structurally modify the dendritic and axonal synaptic output, and finally at 8 weeks of age basic physiological properties and synaptic plasticity are indistinguishable from mature granule cells.

At the network level, adult-born neurons contribute to characteristics that are created by the joint activity of a group of cells. Oscillations and synchrony of neuronal activity are two properties that can be influenced by adding new neurons to the network. Individual networks can store or encode distinct information, and models of adult neurogenesis suggest that newborn neurons can be necessary for this function. The question related to memory formation is whether adult-born neurons replace existing neurons, or whether they are added to the network. In replacement models, old granule cells are removed and replaced by new granule cells with random or naïve synapses. This could facilitate the learning process, because new neurons can form new synapses at flexible networks. However, this accelerated learning process must be accompanied by a loss of neurons, the stored information and subsequently to forgetting of older memories. However neuronal loss has not been demonstrated so far, instead the DG granule cell layer has been shown to increase in cellular density over time (Imayoshi et al., 2008). Therefore, another more recent model of adding more cells to the network has evolved. Existing neurons in the network would remain specialized for the same memories. By using computational models (Aimone et al., 2009; Crick and Miranker, 2006) researchers showed that if all granule cells grow into the network through neurogenesis, thus move from a highly plastic, immature state to a lower plastic,

mature state, it would result in a network where granule cells mostly encode past experiences.

Nevertheless, most work into functions of adult neurogenesis occurs at the systems level. The first study to characterize radial glia cells as the putative stem cells ablated dividing neural precursor cells *in vivo* by infusing the anti-mitotic drug cytosine-β-D-arabinofuranoside (AraC) (Seri et al., 2001). Despite anti-mitotoc drugs, irradiation or genetic ablation serve as tools to disrupt neurogenesis (Imayoshi et al., 2008). Furthermore, strategies exist to augment neurogenesis, such as wheel running or the enriched environment paradigm. Pharmacological treatment with the NMDA-receptor antagonist memantine or the antidepressant drug fluoxetine also efficiently increase neurogenesis in rodent models (Akers et al., 2014; Malberg et al., 2000).

Intriguingly, inconsistent results regarding learning and memory have been reported over the past years. Neurogenesis is required for some, but not other hippocampus-dependent tasks. Ablation of neurogenesis in rats by the anti-mitotic methylazoxymethanol acetate (MAM) treatment resulted in deficits in the hippocampus-dependent trace-conditioning task, but not in the hippocampus-independent delay conditioning task (Shors et al., 2001). It prevented the improvement of long-term recognition memory by environmental enrichment, but it did not affect contextual fear conditioning nor spatial navigation learning in the Morris water maze. However, an apparent deficit in spatial navigation-learning (latency/distance to the hidden platform) has been detected in studies using genetic ablation of adult neurogenesis (Dupret et al., 2008; Zhang et al., 2008). Many studies showed impairments of long-term, but not short-term formation of spatial memory as a consequence of reduced adult neurogenesis (Deng et al., 2009; Jessberger et al., 2009; Snyder et al., 2005). In another commonly used hippocampus-dependent learning and memory task, contextual fear conditioning, discrepancies also exist between studies. Deficits have been observed in rodents, where adult neurogenesis was eliminated by irradiation (Saxe et al., 2006). However, when different methods were used to suppress neurogenesis, such deficits were not detected (Deng et al., 2009; Dupret et al., 2008; Shors et al., 2002; Zhang et al., 2008). Irradiation also produces deficits in spatial memory retention in the water maze (Snyder et al., 2005) and on spatial learning in the Barnes maze (Raber et al., 2004) without affecting water maze learning. The specificity of the effects of MAM treatment and irradiation has to be questioned, since not only specific effects on diving cells have been investigated, but rather effects on the SGZ microenvironment (Monje et al., 2002). Both treatments have also been shown to produce severe side effects, such as general health deterioration and inflammation (Dupret et al., 2005; Monje et al., 2003).

More specific approaches with less off-target side effects to manipulate neurogenesis include genetic approaches, such as transgenic expression of lethal genes including diphtheria toxin (Imayoshi et al., 2008), thymidine kinase (TK) (Deng et al., 2009; Saxe et al., 2006), or the pro-apoptotic protein Bax (Dupret et al., 2008) to selectively kill adult-born cells in the brain. Still, contradictory results persist. Expression of thymidine kinase under the control of either nestin (Deng et al., 2009) or GFAP (Saxe et al., 2006) and subsequent treatment with the antiviral prodrug ganciclovir killed TK-expressing, dividing cells. Behavioral analysis in contextual fear conditioning showed GFAP-TK mice were impaired in the contextual fear conditioning, when tested 24 h after a foot shock, while the nestin-TK transgenic mice were not.

Both prominent hippocampus-dependent memory tests, Morris water maze and context fear conditioning, are different: fear conditioning has a strong emotional component and is not dependent on navigation, meaning they connect cognitive and affective functions of the hippocampus (Mizuno and Giese, 2005). Inconsistent results can be due to differences in the strain or genetic background of mice used, the age of the animal, the neurogenesis-ablation protocol (where different populations are targeted), the functional readout, and behavioral protocols used. However, across multiple studies it does not remain disputable that adult-generated neurons contribute to hippocampal memory function.

In addition to its role in learning and memory, adult neurogenesis has been shown to regulate emotional function. The hippocampus varies along its dorsoventral axis; while the dorsal part is involved in cognitive function, the ventral part is regulating emotional behavior (Fanselow and Dong, 2010; Kheirbek et al., 2013). One main hypothesis is that a reduced rate of adult neurogenesis leads to anxiety and depression. One of the initial studies ablated neurogenesis by irradiation and showed that it is required for the effectiveness of fluoxetine, an antidepressant of the selective serotonin reuptake inhibitor (SSRI) class, in distinct tests for anxiety-like and depressive-like behavior (Santarelli et al., 2003). A further study demonstrated that by reducing adult neurogenesis through deletion of the BDNF receptor TrKB on adult-born neurons, animals displayed an increase in anxiety-like behavior (Bergami et al., 2008). This idea was supported by using another genetic model with the pro-apoptotic protein Bax (Revest et al., 2009). On the other side, physical activity has been shown to have anxiolytic and antidepressant effects (Bjornebekk et al., 2005). Depression is a disorder that also includes cognitive symptoms of hippocampal origin. The link between both functions still needs to be elucidated.

In humans, the role of new neurons in cognitive disorders remains unknown, since methods to study human neurogenesis are not as easily feasible as in rodents (Knoth et al., 2010;

Sanai et al., 2011). However, human neurogenesis might be potentially lower in psychiatric and neurological conditions. Both stress and aging are associated with memory impairments in the clinical human population (Lupien et al., 2007). Furthermore, cancer patients who underwent irradiation for brain tumors experience cognitive and memory deficits (Lee et al., 2012). Altogether, studies from mice and observations in humans provide a basis to suggest that activities and interventions improving neurogenesis may ameliorate cognitive and emotional deficits in humans.

To understand underlying mechanisms of the role of the endocannabinoid system in a proper function of adult neurogenesis, we deleted CB1 specifically in adult neural stem cells and assessed the impact on proliferation and differentiation of targeted cells, long-term potentiation, and behavior mediated by the hippocampus. We generated a triple-transgenic nestin-CreERT2/R26R-YFP/CB1flox/flox mouse line by crossbreeding CB1flox/flox mice (Marsicano et al., 2003) with homozygous ROSA-stop-YFP mice (Srinivas et al., 2001) to visualize targeted cells and their progeny. To further restrict CB1 deletion to adult neural stem cells we took advantage of the nestin-CreERT2 mouse line, in which a tamoxifen (TAM)-inducible Cre recombinase is expressed under the control of the nestin promoter and enhancer. We found that neural stem cell-specific deletion of CB1 led to a reduced number of YFP positive cells in the DG due to a decreased proliferation rate of targeted cells, suggesting that signaling of CB1 is required in early NPCs. Additionally, we demonstrate that CB1-deficient newborn neurons display impaired long-term potentiation in the DG. Consistent with this, animals lacking functional CB1 in newborn neurons reveal a decrease in spatial memory function and an increase in behavioral despair. The present study shows that proliferation of adult neural stem cells critically depends on the cell autonomous activation of CB1 *in vivo* and reveals the consequent remarkable impact on functional connectivity and involvement on the behavioral level.

4.2 Materials and Methods

4.2.1 Animals

Homozygous CB1flox/flox mice (Marsicano et al., 2003) were bred with homozygous ROSA-stop-YFP mice (Srinivas et al., 2001) and heterozygous nestin-CreERT2 (generated in the lab of Prof. Dr. Schütz, DKFZ Heidelberg) mice, all on a C57BL/6 background to generate nes-CB1ko/ko mice. Transgenic mice used for the study were 8 weeks old and littermates were used as controls. Animals were single housed in a temperature- and humidity-controlled room with a 12 h light dark cycle (lights on 5 am - 5 pm) and had access to food and water *ad libitum*. All experiments were carried out in accordance with the European Communities Council Directive of 24 November 1986 (86/609/EEC) and were approved by the local animal care committee (Landesuntersuchungsamt Koblenz, permit number G 13-1-093 and G 16-1-018). Experimenters were blind to the genotype of mice and to the treatment.

4.2.2 Tamoxifen and BrdU administration

Eight weeks old nes-CB1ko/ko and CB1wt/wt mice were administered TAM at 60 mg/kg/d for 5 days (intraperitoneal (i.p.); dissolved in 10% EtOH/90% sunflower oil). To examine the survival, proliferation, and differentiation of targeted cells, mice were injected for 5 days with BrdU (50 mg/kg/d) 23 days after TAM treatment. Mice were killed either 1 or 28 days after BrdU injections.

4.2.3 Production of recombinant lentivirus

The lentiviral vector (Figure 30) has been produced by (Suh et al., 2007) and has been modified by Christin Lehmbrock in the laboratory of Prof. Lutz (Lehmbrock, 2011).

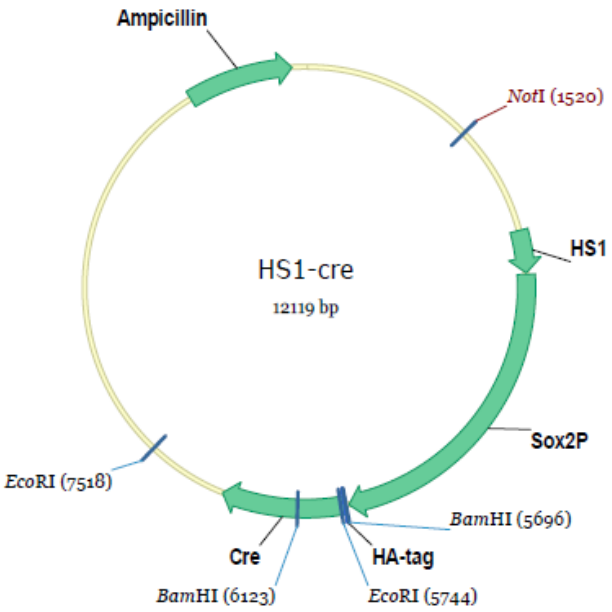

Figure 30. Plasmid map of HS1-Cre. HS1, hypersensitive site 1, Sox2P, (sex determining region Y)-box 2 promoter, HA-tag, human influenza hemagglutinin tag, Cre recombinase. Vector backbone, pRRLSIN.cPPT.PGK-GFP.WPRE (Consiglio et al., 2004). Generated by Christin Lehmbrock.

High titer lentiviral particles were produced in HEK 293LTV cells by transient transfection (standard calcium phosphate transfection) of transfer vector HS1-Cre, second-generation packaging construct pCMV-deltaR8.91, and vesicular stomatitis virus envelope-expressing construct pMD2.G. 72 h after transfection the supernatant was collected and purified by ultracentrifugation (2 h, 27000 rpm and 4°C). The pellet was resuspended in PBS and aliquots stored at -80°C until use.

The amount of transducing units was determined by diluting serially concentrated lentivirus into cell suspensions, plating cells and growing for 3 d. Cells were immunocytochemically stained and clones per sample were counted on a microscope. Measurement of p24 concentration was carried out with the HIV-1 p24 ELISA assay (BioCat, Heidelberg, Germany). The titer was 1.4 x 10^{13} transducing units/ml.

4.2.4 Lentivirus vector administration

Adult mice were anesthetized by an i.p. injection of a combination of fentanyl (0.05 mg/kg), midazolam (5 mg/kg) and medetomidin (0.5 mg/kg). Mice were positioned in a stereotactic apparatus and kept on an animal heating pad to control body temperature during surgery. The scalp was cut open in rostrocaudal direction and lidocaine spray was applied on the skull and the surrounding skin to reduce pain. 1 µl of lentiviral solution was injected bilaterally into

the DG at the following coordinates from bregma: -2.0 mm anteriorposterior, +/-2.0 mm mediolateral, -2.0 dorsoventral. The virus was applied using a microprocessor controlled mini-pump with a 34G beveled NanoFil needle at a flow rate of 200 nl/min. The injection needle was left in place for additional 5 min and then slowly removed. After sewing the scalp, anesthesia was antagonized by intraperitoneal injection of flumazenil (0.5 mg/kg), naloxon (1.2 mg/kg) and atipamezol (2.5 mg/kg). Additionally, mice received a subcutaneous injection of buprenorphine (0.05 mg/kg) to reduce pain and 1 ml of 0.9% saline to compensate fluid loss during and after surgery. The mice were returned to their home cages, but kept on a heating plate at 37°C overnight.

4.2.5 Electrophysiology

The experiments involving DG recordings were performed in the lab of Prof. Ivan Soltesz by Mattia Maroso at the Department of Neurosurgery (Standford University, USA).

Recordings in the CA1 region were carried out in the lab of Prof. Martin Korte by Susann Ludewig at the Zoological Institute, Division Cellular Neurobiology (Technische Universität Braunschweig, Germany).

In vitro extracellular recordings were performed on acute hippocampal slices of wildtype littermates (CB1wt/wt) and CB1 KO animals (nes-CB1ko/ko). Mice were injected with Tamoxifen for 5 consecutive days at an age of 8 weeks. Electrophysiological recordings were performed 4-6 weeks later. In-between animals were housed in a temperature- and humidity-controlled room with a 12 h light-dark cycle and had access to food and water *ad libitum*.

4.2.6.1 Electrophysiology medial perforant path – DG

Transverse hippocampal slices (300 µm) were prepared from the dorsal hippocampus of 12-14 week old mice. Slices were incubated in oxygenated sucrose-containing artificial cerebrospinal fluid (ACSF) for 2 to 3 h, then transferred into oxygenated ACSF used for recordings. Composition of sucrose-containing ACSF: 85 mM NaCl, 75 mM sucrose, 2.5 mM KCl, 25 mM glucose, 1.25 NaH_2PO_4, 4 $MgCl_2$, 0.5 $CaCl_2$, and 24 $NaHCO_3$; composition of recording ACSF: 126 mM NaCl, 2.5 mM KCl, 26 mM $NaHCO_3$, 2 mM $CaCl_2$, 2 mM $MgCl_2$, 1.25 mM NaH_2PO_4, and 10 mM glucose. As specified in the results, in a subset of experiments, ifenprodil (3 µM; Tocris Bioscience, Bristol, UK) or picrotoxin (50 µM, Sigma-Aldrich, Saint Louis, MO, USA) were added to the recording ACSF 20 min before to start the recordings and maintained throughout the recording time.

To elicit field excitatory postsynaptic potentials (fEPSPs) in the DG, a concentric bipolar stimulating electrode was placed in in the medial molecular layer of the upper blade of the DG to stimulate the afferent fibers of the medial perforant path (MPP). Input/output curves were obtained and the stimulation intensity producing ~50% of maximal response was used for test pulses and LTP induction. Baseline fEPSP were recorded for 20 min with a frequency of one test stimulus every 30 s. LTP was induced by tetanic stimulation that consisted of four trains of 100 Hz lasting 500 ms each, repeated every 20 s. After LTP induction, fEPSP were recorded every 30 s for additional 60 min. Slices were visualized with an upright microscope (Olympus; BX61WI) with infrared–differential interference contrast (IR-DIC) optics. All electrophysiological recordings were done at 33°C. MultiClamp700B amplifier (Molecular Devices) was used for recordings. Signals were filtered at 3 kHz using a Bessel filter and digitized at 10 kHz with a Digidata 1440A analog–digital interface (Molecular Devices). The recorded traces were analyzed using Clampfit 10.2 (Molecular Devices).

4.2.6.2 Electrophysiology Schaffer collaterals – CA1

Acute hippocampal transversal slices were prepared from individuals at an age of 12 weeks, 4 weeks after Tamoxifen treatment. Mice were anesthetized with isoflurane and decapitated. The brain was removed and quickly transferred into ice-cold carbogenated (95% O2, 5% CO2) ACSF containing 125.0 mM NaCl, 2.0 mM KCl, 1.25 mM NaH2PO4, 2.0 mM MgCl2, 26.0 mM NaHCO3, 2.0 mM CaCl2, 25.0 mM glucose. After dissection of the two hemispheres one was used for Golgi-Cox staining and the other for electrophysiology. The hippocampus was sectioned into 400 µm thick transversal slices with a vibrating microtome (Leica, VT1200S). Slices were maintained in carbogenated ACSF at room temperature for at least 1.5 h before being transferred into a submerged recording chamber.

Slices were placed in a submerged recording chamber and perfused with carbogenated ACSF (32°C; (125.0 mM NaCl, 2.0 mM KCl, 1.25 mM NaH2PO4, 1.0 mM MgCl2, 26.0 mM NaHCO3, 2.0 mM CaCl2, 25.0 mM glucose) at a rate of 1.2 to 1.5 ml/min. fEPSPs were recorded in stratum radiatum of the CA1 region with a borosilicate glass micropipette (resistance 2-5 Ω) filled with 3 M NaCl at a depth of 150-200 µm. Monopolar tungsten electrodes were used for stimulating the Schaffer collaterals at a frequency of 0.1 Hz. Stimulation intensity was adjusted to 40% of maximum fEPSP slope for 20 min baseline recording. LTP was induced by applying theta-burst stimulation (TBS: 10 trains of 4 pulses at 100 Hz in a 200 ms interval, repeated 3 times).

Basal synaptic transmission properties were analyzed via input-output measurements and short-term plasticity was examined via paired pulse facilitation . The IO- measurements were performed either by application of a defined current values (25 - 175 µA) or by adjusting the stimulus intensity to certain fiber volley amplitudes (0.1 – 0.7 mV). PPF was performed by applying a pair of two closely spaced stimuli in different inter-stimulus-intervals (ISI) ranging from 10 to 160 ms.

4.2.6 Behavioral assays

Bodyweight was measured once per week to observe any effect of TAM treatment on the overall health of animals. Animals were separated and single-housed one week before the start of behavioral assays. All behavioral tests were performed during the light phase of the cycle, starting at 8 am.

4.2.7.1 Open Field

Mice were placed in the center of a white box (40 x 40 x 40 cm^3) at 90 lux and their behavior was video recorded for 15 min and tracked using EthoVision XT (Cryan and Holmes, 2005). The distance moved was analyzed.

4.2.7.2 Light/Dark Box Test

The experimental setup comprises an open, white, brightly-illuminated (100 lux at entry site) compartment (40 x 27 x 40 cm^3) and a closed, black, dark compartment (40 x 13 x 40 cm^3). Mice were placed in the dark compartment and allowed to explore the arena freely for 5 min. The entries and the time spent in the lit compartment were used as parameters to assess aversive behavior (Cryan and Holmes, 2005).

4.2.7.3 Spatial Object Recognition Test (SORT)

The test was performed in a Y-maze (three arms (30 x 10 cm) at 120° from each other made of grey PVC) at 10 lux in the center of the maze (similar to (Masana et al., 2014; Zlomuzica et al., 2012)). The mazes were surrounded by spatial extra-maze cues (white paper with black shapes) and intra-maze cues with tape. Mice were placed in the center of the Y-maze. Animals were habituated to the empty Y-mazes for 10 min on two consecutive days before

testing. Testing consisted of acquisition, an inter-trial interval and a retrieval trial. During the acquisition trial, mice were allowed to explore two identical copies of an object for 10 min. The objects were glass salt shakers (10 cm height) and were placed 5 cm apart from the walls at the end of two arms. The retrieval trial started after the 30 min inter-trial interval. During the 10 min retrieval trial, one object was placed in the empty arm of the maze (relocated object). The position of the relocated object was counterbalanced among animals. The acquisition and retrieval trials were video recorded and the total distance measured with EthoVision. For each mouse, the time spent exploring either object was manually scored during the retrieval trial and the index of recognition was calculated:

Index of recognition (%) = (new position time/ total exploration time) *100

Mice that remembered the original spatial location of the objects were expected to explore more the relocated object, having an index of recognition higher than 50%.

4.2.7.4 Forced Swim Test

The forced swim test has been shown to be a measure of behavioral despair (Porsolt et al., 1977). Mice were place in a beaker filled with water (23°C) and were video recorded for 5 min. The behavior was analyzed manually. The immobility time was defined as the duration a mouse floating in the water without struggling and making only small movements to keep its head above the water.

4.2.7.5 Morris Water Maze

The Morris water maze is a spatial learning task originally developed for rats (Morris et al., 1982). A large circular tank (diameter 1.20 m) was filled with water (25 ± 1°C) and the escape platform (diameter 10 cm) was submerged 1 cm below the surface. The animals were tracked with the Video Tracking System EthoVision XT.

During the first 2 days, mice were trained to swim to a visible platform (visible platform task) that was marked with a 15 cm high black flag and placed pseudo-randomly in different locations across trials (non-spatial training). The extra-maze cues were hidden during these trials. After 2 days of visible platform training, hidden platform training (spatial training) was performed.

The next following 8 days, mice had to navigate using extra-maze cues which were placed on the walls of the testing room. Mice were trained to find a hidden platform which was

located at the center of the southwest quadrant of the pool. The location of the platform was fixed throughout testing. Every day, mice performed four trials with an intertrial interval of 5 min. The animals were released into the water facing the pool wall randomly at one of four start locations and allowed to swim until they find the platform, or for a maximum of 90 s. Any mouse that failed to find the platform within 90 s was guided to the platform. The animal then remained on the platform for 20 s before being removed from the pool. The day after completion of the hidden platform training, a probe trial was conducted in order to determine whether the mice had developed a spatial bias for the former platform quadrant. The platform was removed from the pool and the mice were allowed to swim freely for 90 s.

4.2.7.6 Tail Suspension

Behavioral despair was measured by suspending the mouse by the tail for 6 min (Steru et al., 1985). The tail was attached to the top of a light panel by adhesive tape. The distance between the tip of the nose of the mouse and the floor was approximately 40 cm. The animals were video recorded and the time spent immobile was analyzed by the video tracking system EthoVision XT.

4.2.7.7 Sucrose Preference

This test is a measurement for anhedonia (lack of interest in rewarding stimuli (Papp et al., 1991)). In this task, the animal is assessed for its interest in seeking out a sweet rewarding drink relative to plain drinking water. A bias towards the sweetened drink is typical, failure to do so is indicative of anhedonia/depression. Sucrose preference testing is carried out in the home cage, which is equipped with 2 drinking bottles. One bottle contains plain drinking water, and the second contains a 2% sucrose solution. The mice are habituated to the presence of the two drinking bottles for 48 h, and the positions of the two bottles is switched every 12 h to reduce any confound produced by a side bias. Following this habituation, mice can choose either drinking 2% sucrose solution or plain water for 24 h. Water and sucrose solution intake is measured, and sucrose preference is calculated as a percentage of the volume of sucrose intake over the total volume of fluid intake.

4.2.7.8 Fear Conditioning

Fear conditioning and learning has been performed as previously described (Radyushkin et al., 2005). For conditioning, animals were placed into the conditioning chamber, which

consisted of a transparent plexiglass box (15 x 20 x 20 cm^3) with a stainless steel shock-grid floor (Context A). After 2 min, a 28 s tone (85 dB, 10 kHz, pulsating every 200 ms) was presented, followed by an electric foot-shock (0.4 mA, 2 s). Tone and shock were repeated after a 20 s break. Afterwards, animals were returned to their home cages. To measure contextual fear extinction, freezing (defined as the absence of all movements except for respiration) was assessed 24 h later in the training context (Context A) for 3 min. To measure cued fear extinction animals were placed in a new box (Context B) and after 3 min presented with a 28 sec tone without a shock. Freezing was assessed for 3 min. The boxes were monitored via overhead cameras and the amount of freezing was evaluated with EthoVisionXT.

4.2.7 Immunohistochemistry

For immunohistochemistry, mice were perfused transcardially with 4% PFA, brains were removed, post-fixed overnight in 4% PFA and treated with 30% sucrose for 48 h. Then brains were sectioned 30 µm thick in coronal plane and stored at 4°C in cryoprotection solution until use.

Sections were blocked in PBS containing 5% NDS, 2.5% BSA and 0.3% TX for 90 min and incubated with the respective primary antibody (Table 4) in PBS containing 1% NDS, 0.1% BSA and 0.3% TX overnight. To double-stain with an anti-BrdU antibody, slides were fixed again for 15 min in 4% PFA to stabilize antigen-first primary antibody complexes. Sections were then incubated in 1 N HCl for 1 h at 37°C to denature DNA, followed by 3 x 5 min washes with TBS. Brain slices were then blocked in TBS with 1% NDS, 0.1% BSA and 0.3% TX for 90 min and incubated with primary antibodies in blocking buffer overnight at 4°C. On the next day, appropriate secondary antibodies were applied for 2 h. To visualize cell nuclei in non-BrdU treated sections, brain slices were incubated with DAPI for 5 min, washed with PBS and mounted with Mowiol onto slides.

Table 4. List of primary antibodies.

Antibody, anti-	Species	Dilution	Company	Catalog number
GFP	rabbit chicken	1:500 1:1000	Aves Labs	GFP-1020
RFP	rabbit	1:500	Rockland	600-401-379
DCX	guinea pig	1:500	Abcam	ab2253
NeuN	rabbit	1:500	Abcam	ab177487
S100b	rabbit	1:500	Abcam	ab41548
BrdU	rat	1:100	Abcam	ab6326

The respective secondary antibodies were applied: anti-rabbit IgG AlexaFluor488, goat anti-rabbit, goat anti-guinea pig, goat anti-rat AlexaFluor546 and goat anti-rabbit or anti-rat AlexaFluor647 (all 1:1000; Invitrogen).

4.2.8 Microscopic analysis of histology

Slides were observed under a Leica DM5500 (Leica Camera, Wetzlar, Germany) fluorescence microscope or a Zeiss Axiovert LSM 710 (Carl Zeiss, Oberkochen, Germany) laser scanning confocal microscope. For laser scanning confocal microscopy, z-stacks with optical sections of 1 µm were recorded.

YFP positive cell numbers and colocalization with specific markers were counted in every 6th section (180 µm apart) and calculated based on the Cavalieri principle of stereology for the DG. For each marker four to six animals were analyzed.

4.2.9 Quantitative polymerase chain reaction (qPCR)

Animals were killed by decapitation under deep isoflurane anesthesia. Brains were removed, the hippocampus or the DG isolated, and snap frozen on dry ice. Isolated samples were stored at -80 °C until further use.

Samples were homogenized using the TissueLyser (QIAGEN) according to the manufacturer guidelines. Then, RNA was isolated with the RNeasy Mini Kit (QIAGEN) with the on-colum DNA digestion (RNase-Free DNase Set, QIAGEN) and eluted in 20 µl of RNase free water. Total RNA was reverse transcribed using the High Capacity cDNA Reverse Transcription Kit with random primer hexamers (Life Technologies). cDNA was diluted 1:3 in RNase free water. Finally, cDNA was amplified using the commercial TaqMan assays (Applied Biosystems, Table 5) with an ABI7300 real-time PCR cycler (Applied Biosystems). For BDNF-3'UTR a custom Taqman gene expression assay was generated (Leschik et al., 2013):

Forward primer, 5'-GCTGGCGATTCATAAGGATAGAC-3';
reverse primer, 5'-TATACAACATAAATCCACTATCTTCCCCT-3';
probe sequence, 5'-TATGTACACTGACCATTAAA-3'.

All reactions were performed in duplicates using either Glucoronidase beta (Gusb) or Glyceraldehyde 3-phosphate dehydrogenase (GAPDH) as reference gene. Thermal cycler

conditions were: 1 x 2 min 50 °C, 1x 15 min 95 °C, 40 x 15 s 95 °C, and 1 min 60 °C. Data analysis was done using the 7300 system SDS software (Applied Biosystems).

Table 5. List of TaqMan assays used for qPCR.

Target gene	Assay name
Cnr1 (CB1)	Mm00432621_s1
BDNF-3'UTR	Custom made
GusB	Mm01197698_m1
GAPDH	Mm99999915_g1

Analysis of the relative gene expression was done using the $2^{-\Delta\Delta CT}$ method. Target genes were normalized to the reference gene. The normalized levels of the target genes were then normalized to the mean expression level of the wildtype group (Livak and Schmittgen, 2001).

4.2.10 Isolation of adult neural stem cells by fluorescence-activated cell sorting (FACS)

Mice (n=10/group) were killed by decapitation under deep isoflurane anesthesia. The brain was removed, the hippocampus isolated and immediately dissociated as described previously (Fischer et al., 2011). Briefly, hippocampi (n=5/falcon tube) were isolated in HBSS with $CaCl_2$ and $MgCl_2$, minced with a razor blade and enzymatically dissociated in 5 ml with 0.05% Trypsin/EDTA (Gibco) in HBSS containing 2 mM glucose at 37°C for 30 min. After 15 min and 30 min the tissue was triturated with a fire polished Pasteur pipette. Enzyme activity was stopped by adding 5 ml of 4% BSA in Earle's balanced salt solution (EBSS, Gibco). Subsequently the cell suspension was filtered through a 70 µm cell strainer (Miltenyi Biotec) and centrifuged for 5 min, 180 g at 4°C. The pellet was resuspended in 10 ml 0.9 M saccharose in HBSS. After further centrifugation for 20 min, 510 g at 4°C the pellet was resuspended in 2 ml 4% BSA in EBSS, placed on top of 12 ml 4% BSA in EBSS and centrifuged for 12 min, 290 g at 4°C. Finally, the resulting pellet was resuspended in staining solution (PBS/10%FCS/0.02%NaN_3) containing primary antibodies and respective Isotype controls. Phycoerythrin (PE)-conjugated Cluster of differentiation 133 (CD133) (1:100, BD Biosciences) was incubated for 30 min at 4°C, allophycocyanin (APC)-conjugated PSA-NCAM (1:10, Miltenyi Biotec) for 10 min at 4°C in the dark. Respective Isotype controls included rat IgG-PE (1:100, BD Biosciences) and mouse IgM-APC (1:10, Miltenyi Biotec). After a wash in FCS-containing PBS, samples were resuspended in 500 µl FCS-containing PBS and transferred through a 70 µm cell strainer into FACS tubes.

Cell analysis and sorting was performed at the Core Facility Flow Cytometry at the Institute of Molecular Biology (IMB) in Mainz. Prior to sorting, stained cells were incubated with DAPI (1:100) to exclude dead cells. Cells were sorted on a fluorescence-activated cell sorter BD FACS Aria™ III using FACSDiva™ software (BD Biosciences) with a sheath pressure of 70 psi and a nozzle diameter of 70 µm. Forward (FSC) and side-scattering (SSC) excluded debris. Single cells were gated out by SSC-A and SSC-W. Dead cells were excluded by being positive for DAPI (405 nm laser, 450/50 filter). Fluorophores were detected with a 488 nm laser and emission filters 530/30 (YFP), with a 561 nm laser and emission filters 586/15 (PE), and with a 640 nm laser and emission filters 670/30 (APC). Gating was done based on pure wildtype C57BL/6J animals (no YFP) and isotype-matched controls. Four fractions of the cells were isolated: CD133- PSA-NCAM+, CD133- PSA-NCAM-, CD133+ PSA-NCAM+, and CD133+ PSA-NCAM-. Cells were directly sorted into the RLT buffer of the RNeasy micro kit (QIAGEN) containing β-mercaptoethanol. In one experiment ExpressArt® N-Carrier (AmpTec GmbH) were added to stabilize RNA.

Total RNA was isolated using the RNeasy micro kit (QIAGEN). The quality (RNA integrity number (RIN)) and concentration of the RNA was determined at the Genomics Core Facility at the IMB Mainz using the NanoDrop3000 (Thermo Scientific) and the Agilent RNA 6000 Pico Kit (Agilent Technologies) including analysis on the Agilent 2100 Bioanalyzer (Agilent Technologies). cDNA of isolated RNA from the fraction of interest (CD133+ PSA-NCAM-) was synthesized and amplified using the SMART-Seq® v4 Ultra® Low Input RNA Kit for sequencing (Clontech Laboratories). cDNA was validated using the Agilent 2100 Bioanalyzer and Agilent's High Sensitivity DNA Kit (Agilent Technologies) and quantified using Qubit (Thermo Scientific). 0.5 ng cDNA/replicate of samples were then subjected to qPCR to verify CB1 knock out in targeted cells.

4.2.11 Statistical analysis

Data are represented as the mean ± standard error of the mean (SEM). Statistical analysis was done using GraphPad Prism 4 (GraphPad Software Inc, La Jolla, CA, USA) and IBM SPSS Statistics 22v software (IBM Corporation, Armonk, NY, USA). Unless otherwise specified, data were analyzed using the unpaired Student's t-test. The alpha-level to determine significance was set to $p<0.05$.

4.3 Results

4.3.1 Conditional deletion of CB1 from adult neural stem cells

To assess the direct influence of CB1 on regulating adult neurogenesis *in vivo*, we generated a triple transgenic mouse line (Figure 31A) by crossbreeding mice expressing a TAM-inducible Cre-recombinase under the neural stem cell specific nestin promoter and enhancer with floxed CB1 mice. To visualize recombined cells, the offspring was additionally crossed with with the reporter mouse line ROSA26-floxed-stop-YFP. TAM treatment led to excision of the floxed-stop cassette by Cre, expression of YFP, and deletion of CB1.

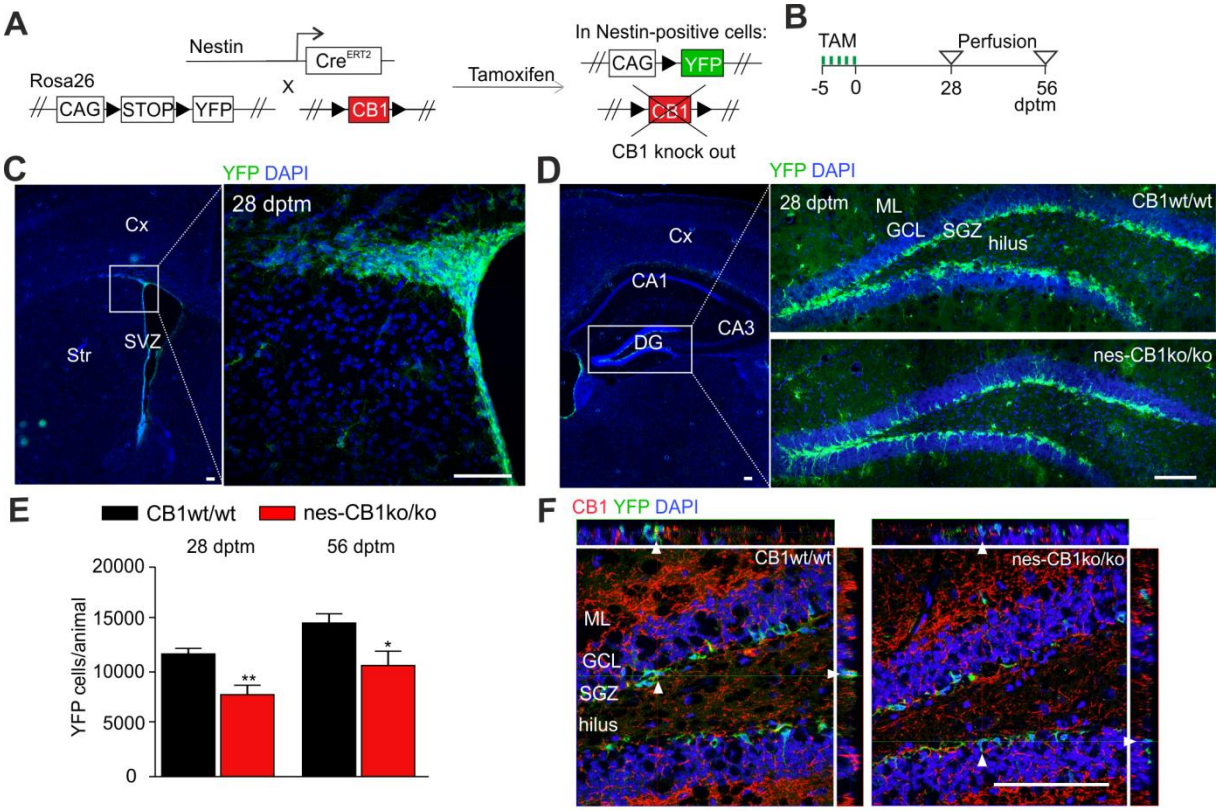

Figure 31. Tamoxifen (TAM) injections induce deletion of CB1 and expression of yellow fluorescent protein (YFP) specifically in adult nestin-expressing stem cells and their progeny. (A) Schematic of the strategy for conditional deletion of CB1 from neural stem cells *in vivo*. (B) Time course of experiment. Mice were perfused 28 days post tamoxifen (dptm) or 56 dptm. (C) Recombined cells express YFP (green) and are found in the subventricular zone (SVZ) and (D) in the subgranular zone (SGZ) of the dentate gyrus (DG). (E) Quantification of YFP positive cells in the DG reveals a significant decrease in nes-CB1ko/ko animals at 28 dptm and 56 dptm. (F) Representative confocal images display co-localization of recombined YFP cells (green) and CB1 expression (red) in CB1 wt/wt mice, whereas nes-CB1ko/ko mice show a lack of CB1 expression in recombined cells. DAPI, blue. n=4 animals/group, **p<0.01, *p<0.05, Student's t-test. Data are represented as mean ± SEM. Scale bar, 100 µm. Cortex (Cx); Striatum (Str); granule cell layer (GCL), molecular layer (ML).

Animals were injected with tamoxifen at 8 weeks of age and perfused 28 and 56 days post tamoxifen (dptm) (Figure 31B). Recombination and expression of YFP occurred specifically in both neurogenic regions, in the SVZ (Figure 31C) and the SGZ of the DG (Figure 31D). Quantification of reporter-positive cells in the SGZ (Figure 31E) showed 28 dptm in CB1wt/wt mice 11700 ± 534 cells were YFP+ and significantly less (p=0.007) in nes-CB1ko/ko mice (7823 ± 903). At 56 dptm the number of YFP+ cells was still reduced (p=0.048) in nes-CB1ko/ko mice (10600 ± 1375) compared to CB1wt/wt mice (14660 ± 887). To confirm that CB1 was deleted from YFP positive cells, we immunostained sections from CB1wt/wt and nes-CB1ko/ko with YFP and CB1 specific antibodies (Figure 31F). CB1 was not detected anymore in recombined cells of nes-CB1ko/ko mice.

4.3.2 Deletion of CB1 reduces proliferation capacity of newborn cells

Since nes-CB1ko/ko animals displayed a decreased number of YFP positive cells, we investigated the maturation stage of the cells by quantifying reporter positive cells co-expressing cell type specific antigens 28 and 56 dptm. At 23 dptm we injected BrdU for five consecutive days to follow the fate of recombined cells (Figure 32A).

At 28 dptm, recombined YFP cells were positive for BrdU, DCX and NeuN, as assessed by immunostaining (Figure 32B) in both genotypes. 4 weeks later, YFP cells were still positive for all the aforementioned markers (Figure 32C). When we quantified the co-localizing cells (Figure 32D), we found at 28 dptm 6424 ± 427 cells in CB1 wt/wt mice expressing the marker DCX, whereas 4388 ± 620 cells in nes-CB1ko/ko were positive for DCX, representing a decreased (p=0.035) pool of neuroblasts. At this stage 2178 ± 450 cells in CB1wt/wt mice were positive for the marker NeuN, but only 716 ± 250 cells in nes-CB1ko/ko mice, demonstrating additionally a decreased (p=0.047) number of mature neurons. The pool of both populations increased at 56 dptm, when 6992 ± 681 YFP cells were positive for DCX in the CB1wt/wt animals, while only 4358 ± 587 cells were positive for DCX in nes-CB1ko/ko mice (p=0.026). Again, nes-CB1ko/ko animals showed a decreased (p=0.029) number of YFP/NeuN double positive cells (3773 ± 84) compared to CB1wt/wt mice (6828 ± 851).

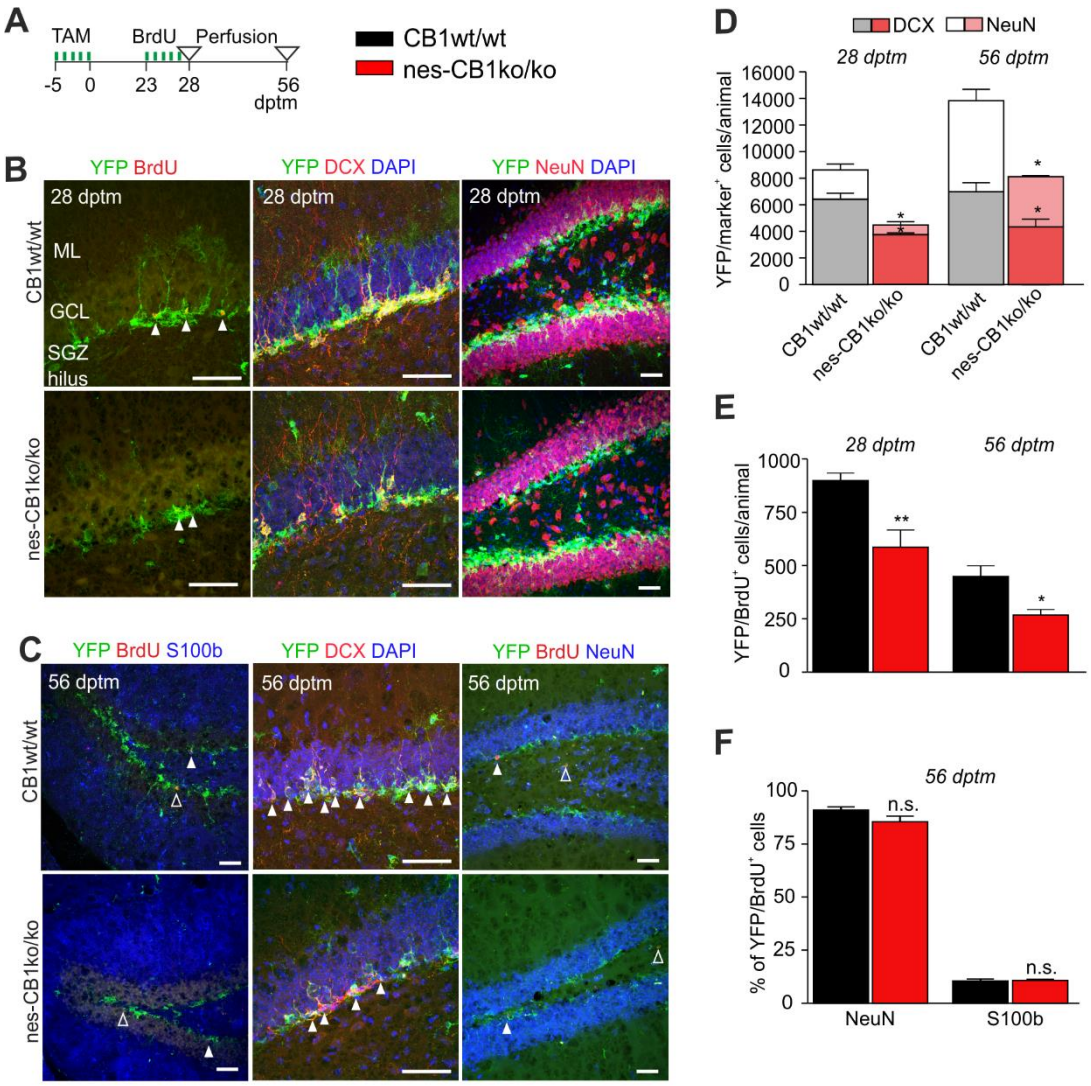

Figure 32. Conditional deletion of CB1 impairs proliferation of adult neural stem cells in the dentate gyrus. (A) Schedule of experiment. Mice were injected with BrdU for 5 d at 23 dptm and analyzed 28 dptm and 56 dptm. (B) Maximum intensity projections of z-stacks show YFP positive cells expressing BrdU, DCX, and NeuN 28 dptm and (C) 56 dptm. Filled arrow: colocalizing cell, empty arrow: non-colocalizing cell. (D) Quantification of YFP cells and co-localization with neuronal markers. Deletion of CB1 reduces the YFP/DCX and YFP/NeuN population 28 dptm and 56 dptm. (E) Nes-CB1ko/ko animals display a reduced number of newborn cells, as assessed by co-expression of YFP and BrdU. (F) Differentiation of BrdU labeled cells into the neuronal (NeuN) or astroglial (S100b) lineage is not affected 56 dptm. n=4-6 animals/group, *p<0.05, **p<0.01, Student's t-test, n.s. not significant. Data represent mean ± SEM. Scale bar, 50 µm. Subgranular zone (SGZ), granule cell layer (GCL), molecular layer (ML).

Since the deletion of CB1 from neural stem cells led to a decreased pool of neuroblasts and neurons, we assessed the proliferation rate of the recombined cells (Figure 32E). Indeed, we found in CB1wt/wt mice 900 ± 34 cells were YFP/BrdU positive and only 586 ± 81 in nes-CB1ko/ko, representing a significant smaller (p=0.009) pool of proliferating cells. BrdU positive cells were also counted 4 weeks after BrdU injection to measure their differentiation potential. 56 dptm, 449 ± 51 cells expressed YFP/BrdU in CB1wt/wt mice, but only 269 ± 26 cells in nes-CB1ko/ko mice, demonstrating a significant (p=0.020) smaller amount of

YFP/BrdU cells. Next, we determined the phenotype of YFP/BrdU cells by co-immunostaining with either the neuronal marker NeuN or the astroglial marker S100b (Figure 32F). 91.0 ± 1.5% of YFP/BrdU cells in CB1wt/wt mice were positive for NeuN and 85.5 ± 2.7% in nes-CB1ko/ko mice. In contrast, 10.6 ± 0.9% of YFP/BrdU cells in CB1wt/wt mice were positive for S100b and 10.8 ± 0.6% in nes-CB1ko/ko mice. Here, we found no difference between the two groups in differentiation into the neuronal or astroglial lineage. Taken together, our results indicate that CB1 regulates the proliferation capacity, leading to a reduced number of neuroblasts and neurons. CB1 itself does not alter directly the differentiation potential of adult neural stem cells.

These results are supported by an alternative approach in an additional mouse model, in which we injected a lentivirus containing a Sox-2 promoter-driven Cre recombinase (Sox2-Cre) into the DG of ROSA26-floxed-stop-YFP mice crossed with floxed CB1 animals (Figure 33A). Due to the active Sox-2 promoter, CB1 will be knocked-out in neural stem cells and YFP expressed. At 23 days post infection (dpi), BrdU was injected to quantify the proliferation at 28 dpi and the differentiation at 56 dpi (Figure 33B). Injection of Sox2-Cre-lentivirus led to expression of YFP in adult neural stem cells and their progeny in the SGZ of the DG in both CB1wt/wt and Sox2-CB1ko/ko mice and BrdU labeled dividing cells (Figure 33C). Quantification of YFP cells (Figure 33D) revealed that 28 dpi 22540 ± 2701cells were positive for YFP in CB1wt/wt mice and 15150 ± 1192 cells in Sox2-CB1ko/ko mice, a non-significant (p=0.066) decrease. At 56 dpi, the number of YFP cells in CB1wt/wt was 18780 ± 3493 cells and in Sox2-CB1ko/ko mice 16690 ± 1162 cells, presenting no change. However, the lentivirus-mediated fate-tracing study and subsequent BrdU labeling (Figure 33E) showed that YFP/BrdU positive cells were reduced (p=0.039) in Sox2-CB1ko/ko mice (289 ± 82 cells) 28 dpi compared to CB1wt/wt mice (686 ± 103 cells). At 56 dpi YFP/BrdU cells were also decreased in Sox2-CB1ko/ko mice (53 ± 10 cells) compared to CB1wt/wt mice (108 ± 18 cells), but not significantly (p=0.06). Furthermore, we were interested in investigating the differentiation potential of targeted cells, using colocalization analysis of YFP cells with either the astrocytic marker S100b or the neuronal marker NeuN (Figure 33F). Quantification of triple positive cells showed 81.0 ± 4.8% being positive for NeuN in CB1wt/wt and 73.5 ± 7.1% in Sox2-CB1ko/ko mice, revealing no difference between both groups (Figure 33G). In CB1wt/wt 12.2 ± 1.3% were triple positive for S100b and in Sox2-CB1ko/ko mice 14.7 ± 2.8%, indicating differentiation into the astroglial lineage was not affected.

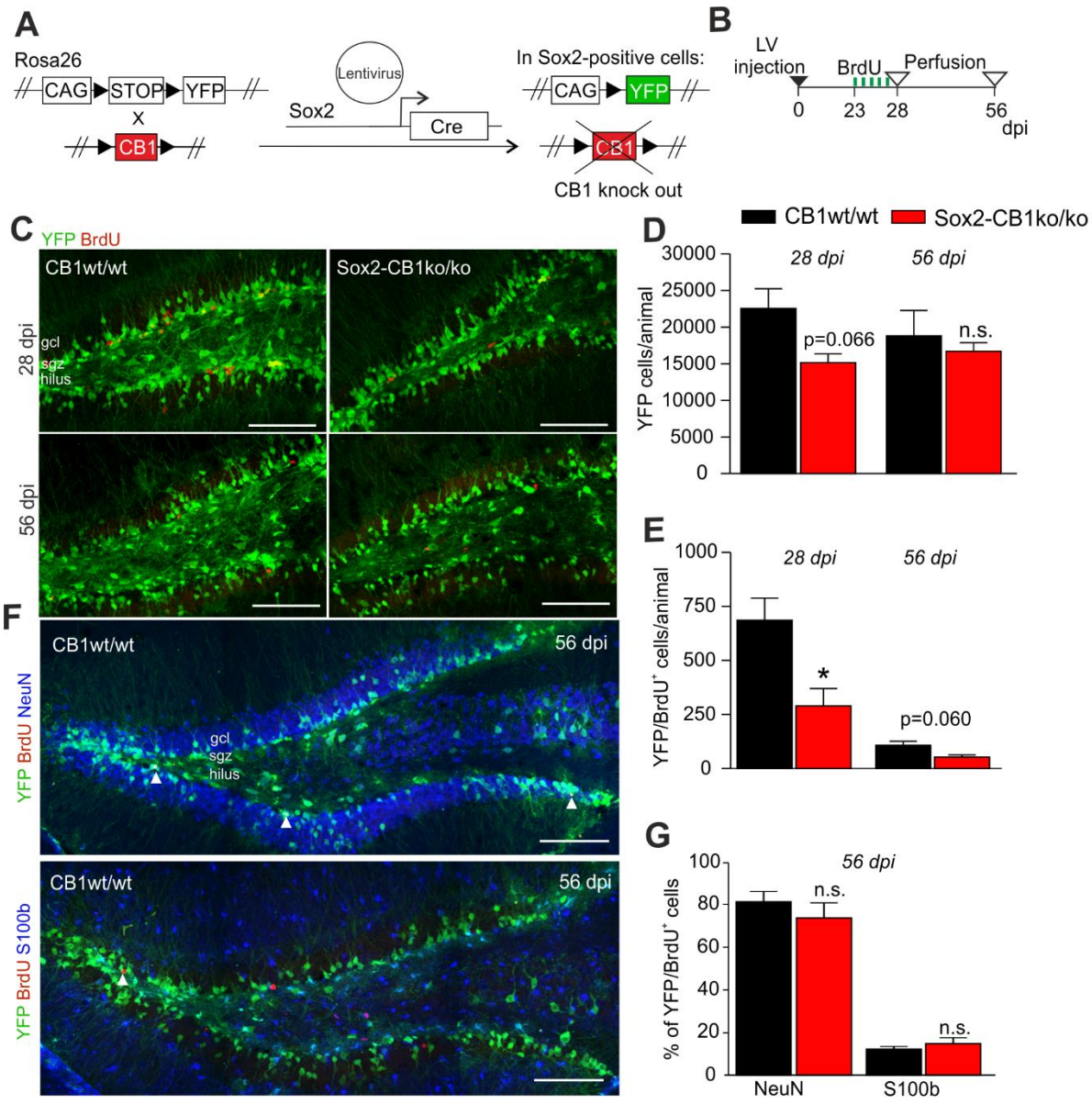

Figure 33. Lentivirus-mediated deletion of CB1 in Sox2-positive cells in the dentate gyrus impairs proliferation of adult neural stem cells. (A) Schematic of the strategy for deletion of CB1 from neural stem cells *in vivo* with a lentivirus containing Cre recombinase under the control of the Sox2 promoter. (B) Timeline of experiment. 8 week old animals were injected with the lentivirus (LV) via stereotactic surgery. BrdU was injected i.p. for 5 consecutive days starting at 23 dpi and animals were perfused at 28 dpi and 56 dpi. (C) Representative micrographs of CB1wt/wt and Sox2-CB1ko/ko mice show recombined cells in the subgranular zone (SGZ) expressing YFP (green) after lentivirus injection and a fraction of it colocalizing with BrdU (red) 28 dpi and 56 dpi. (D) Quantification of YFP cells reveals an almost significant decrease (p=0.066) in YFP positive cells 28 dpi, whereas YFP cell numbers are unaltered 56 dpi. (E) Quantification of YFP/BrdU double positive cells shows that loss of CB1 impairs significantly cell proliferation (28 dpi), but maintenance (56 dpi) of YFP/BrdU cells is only slightly (but not significantly) decreased upon CB1 deletion (p=0.060). (F) Exemplary immunofluorescence images of CB1wt/wt animals for YFP (green) cells colocalizing with BrdU (red) and S100b or NeuN (blue) in the dentate gyrus 56 dpi. (G) Bar graph indicates percentage of YFP/BrdU/marker of total YFP/BrdU cells (marker=S100b or NeuN) 56 dpi. Differentiation into the astroglial or neuronal lineage is not affected. N=3-4 animals/group, *p<0.05, Student's t-test. n.s. not significant. Values represent mean ± SEM. Scale bar, 100 µm.

4.3.4 CB1 is required for neurogenesis-dependent LTP in the hippocampus

Adult neurogenesis is comprised of incorporating new neurons in the existing circuitry. Since we manipulated the proliferation potential of newborn neurons and the number of targeted neuroblasts and neurons, we were wondering if CB1 deletion has an impact on physiological properties such as synaptic plasticity in the hippocampus. We performed electrophysiological analysis at two structures of the hippocampus by a theta burst stimulation paradigm to elicit LTP (Figure 34): 1) stimulation of MPP and recording fEPSPs in the medial molecular layer of the upper blade of the DG (green) and 2) stimulation of Schaffer collateral axons of area CA3 and recording fEPSPs in the CA1 region (red) 28 to 42 dptm.

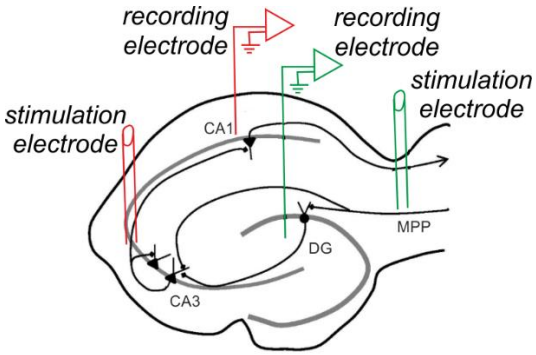

Figure 34. Schematic overview of electrophysiology measurements including stimulation and recording electrodes in the different paradigms. Green: to record long-term potentiation (LTP) in the dentate gyrus (DG), the stimulation electrode was placed in the medial molecular layer of the upper blade of the DG to stimulate the afferent fibers of the medial perforant path (MPP) and the signals were recorded in the DG. Red: to record LTP in the CA1 region, a stimulation electrode was placed in the CA3 region stimulating Schaffer collaterals.

To unmask the potentiation of existing granule cells we investigated LTP in the presence of picrotoxin, a GABAR antagonist. Here, LTP was indistinguishable between both groups (Figure 35A, B). This implies that CB1 deletion does not change potentiation of existing granule neurons.

New neurons in the DG have been shown to elicit a form of LTP, which is specific for activation of NR2b and insensitive to inhibition of GABAergic transmission (Snyder et al., 2001). After tetanic stimulation of MPP in slices, control mice displayed a potentiation lasting for 60 min, which was blocked when NR2b antagonist ifenprodil was applied. In contrast, potentiation levels in nes-CB1ko/ko mice were lower than in control mice and exhibited a similar decay of potentiation when slices from control mice were incubated with ifenprodil (Figure 35C). Averaged potentiation levels of the last 5 min displayed significant different

fEPSP slopes in nes-CB1ko/ko (103.5 ± 2.4%, p=0.007) and CB1wt/wt+ifenprodil (99.4 ± 2.2%, p=0.008) mice compared to CB1wt/wt mice (120.1 ± 3.1%) (Figure 35D).

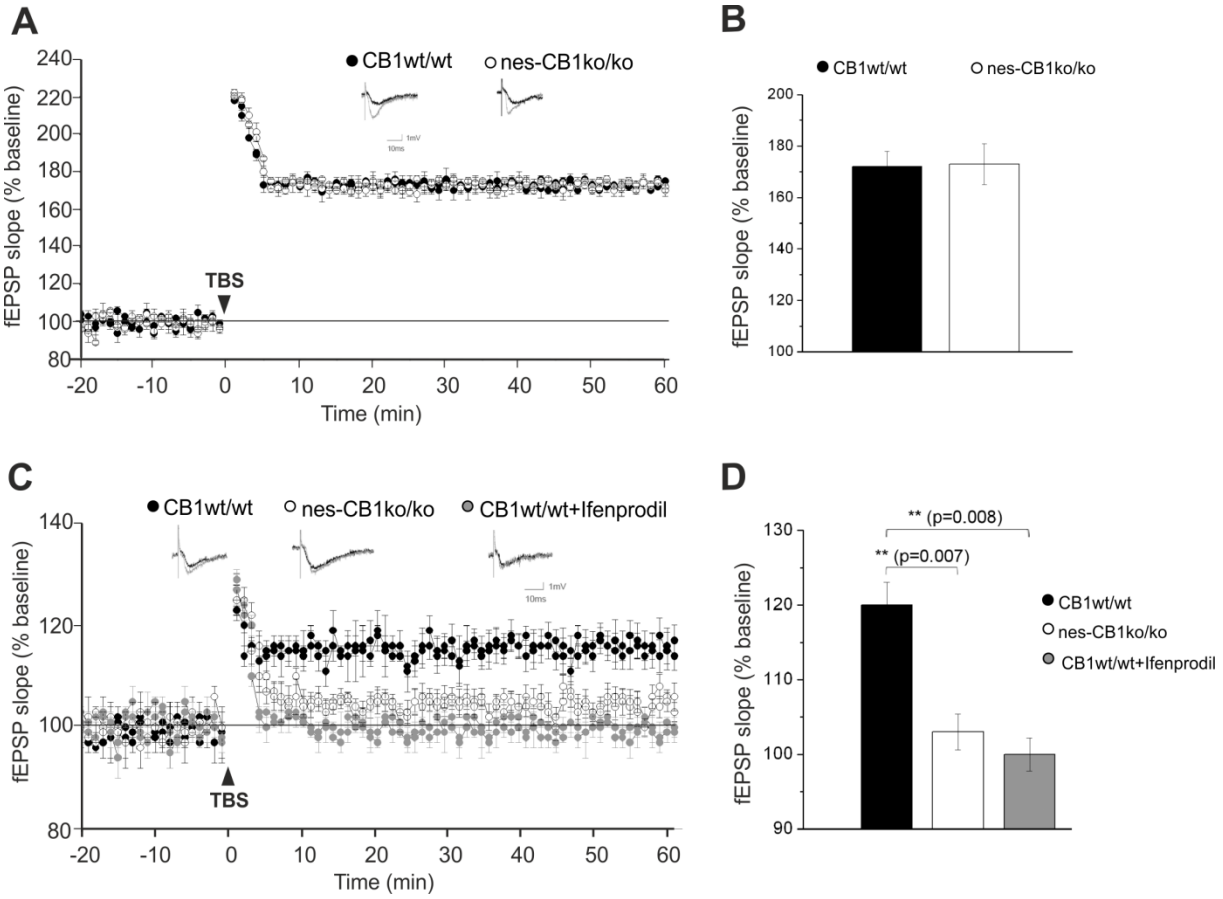

Figure 35. CB1 deletion in adult-born neurons impairs LTP in the dentate gyrus. (A) fEPSP slope of CB1wt/wt (n=9, 3 animals) and nes-CB1ko/ko (n=8, 2 animals) mice in presence of picrotoxin, 28 to 42 dptm. (B) Averaged potentiation levels of the last 5 minutes of LTP in presence of picrotoxin were not significantly different. (C) Summary plots of the field EPSP (fEPSP) slope elicited in response to a test stimulus before (-20 to 0 min) and after (0 to 60 min) tetanic stimulation of the medial perforant path (MPP) in nes-CB1ko/ko (n=12, 4 animals) and in CB1wt/wt in absence (n=11, 4 animals) or presence (n=8, 3 animals) of ifenprodil, 28 to 42 dptm. (D) Averaged potentiation levels of the last 5 minutes of LTP were significantly lower in slices of nes-CB1ko/ko mice and in CB1wt/wt mice treated with ifenprodil. **p<0.01, one-way ANOVA. Data are represented as mean ± SEM. Electrophysiology recordings were performed in the lab of Prof. Ivan Soltesz by Mattia Maroso at the Department of Neurosurgery (Standford University, USA).

To even further analyze physiological changes in synaptic plasticity, we stimulated Schaffer collaterals of CA3 by theta burst stimulation and recorded fEPSPs in CA1, which resulted in a LTP curve that is significantly different to that of littermate controls (Figure 36A). Averaged potentiation levels of the 5 min displayed significant different (p=0.042) fEPSP slopes in nes-CB1ko/ko (132.47 ± 2.04%) mice compared to CB1wt/wt mice (141.01 ± 2.98%) (Figure 36B). This shows that changes in the DG can promote acquisition of the phenotype at synapses in the whole hippocampus (e.g. at CA3-CA1 synapses).

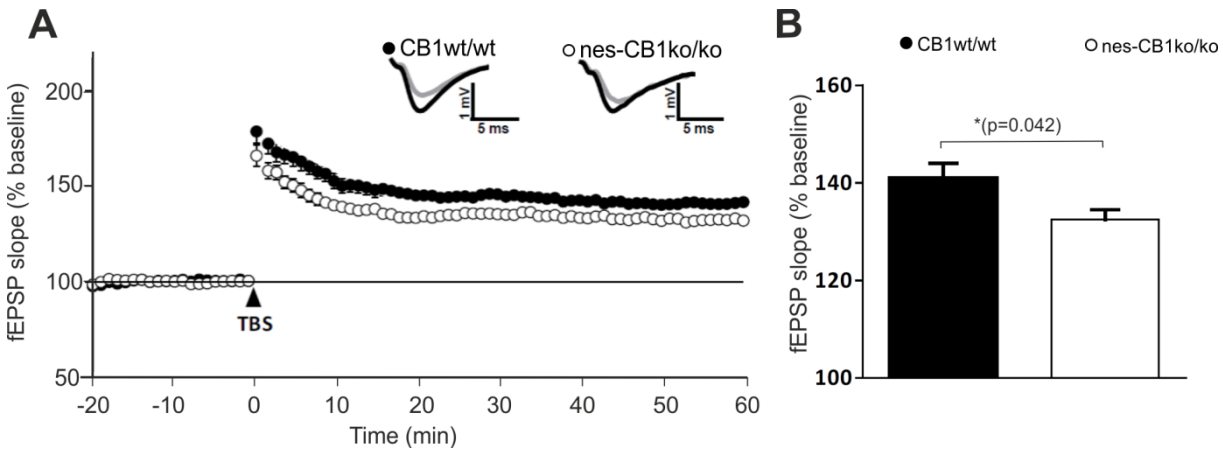

Figure 36. CB1 deletion in adult-born neurons impairs LTP in the CA3-CA1 region. (A) fEPSPs were recorded in CA1 region by stimulating Schaffer collateral axons of area CA3. Acute slices of nes-CB1ko/ko mice (n=16, 4 animals) displayed an LTP curve that is significantly different to that of littermate controls (n=23, 5 animals). (B) Averaged potentiation levels of the last 5 minutes of LTP were significantly lower in nes-CB1ko/ko mice. *p<0.05, Student's t-test. Data are represented as mean ± SEM. Recordings were carried out in the lab of Prof. Martin Korte by Susann Ludewig at the Zoological Institute, Division Cellular Neurobiology (Technische Universität Braunschweig, Germany).

Synaptic transmission was evaluated in all paradigms by testing input-output responses and short-term plasticity was tested by paired-pulse depression (Figure 37). Basal synaptic properties were unaltered when slices were treated with pircotoxin (Figure 37A). Untreated slices from nes-CB1ko/ko animals showed significant alterations at fiber volley amplitudes 0.3 to 0.5 mV (0.3 mV: p=0.034, 0.4 mV: p=0.039, 0.5 mV: p=0.025, Figure 37B, middle panel). In the CA1 region analyzed input-output strength revealed significant alterations between groups at fiber volley amplitudes 0.4 to 0.8 mV (0.4 mV: p=0.032, 0.5 mV: p=0.039, 0.6 mV: p=0.006, 0.7 mV: p=0.003, 0.8 mV: p=0.011, Figure 37C, middle panel).

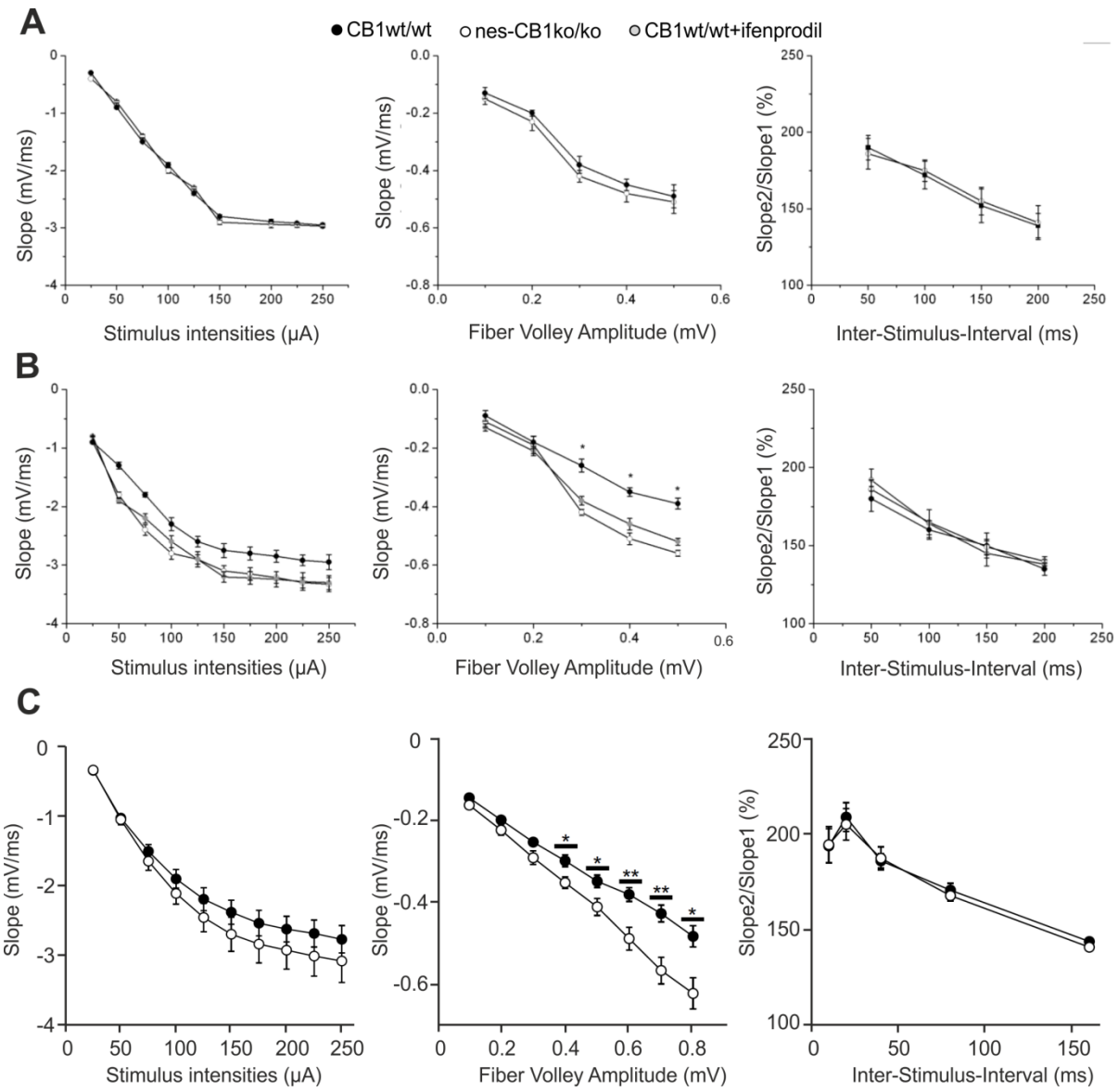

Figure 37. Basal synaptic properties of CB1-wildtype and CB1-deficient mice. (A) In the DG in the presence of picrotoxin neuronal excitability was statistical indistinguishable at all stimulus intensities (25 – 250 µA) between genotypes. Analyzing the Input-Output strength in slices showed no significant alterations between groups and paired pulse facilitation was unaltered (CB1wt/wt (n=9/n=3 animals), nes-CB1ko/ko(n=8/n=2 animals)). (B) In the DG neuronal excitability was statistically indistinguishable at all stimulus intensities (25 – 250 µA) between genotypes and treatment with ifenprodil. Analyzing Input-Output strength revealed significant alterations between all three groups at fiber volley amplitudes 0.3 to 0.5 mV. Paired pulse facilitation was unaltered (CB1wt/wt(n=11/n=4 animals), nes-CB1ko/ko(n=14/n=4 animals), CB1wt/wt+ifenprodil(n=8/n=3 animals)). (C) In the CA1 region neuronal excitability was statistical indistinguishable at all stimulus intensities (25 – 250 µA) between genotypes (CB1wt/wt(n=18/n=5 animals), nes-CB1ko/ko(n=17/n=4 animals)). Analyzing the Input-Output strength revealed significant alterations between groups at fiber volley amplitudes 0.4 to 0.8 mV (CB1wt/wt(n=15/n=5), nes-CB1ko/ko(n=15/n=4)). Paired pulse facilitation was unaltered (CB1wt/wt(n=20/n=5), nes-CB1ko/ko(n=18/n=4)). *p<0.05, **p<0.01, Values represent mean ± SEM.

4.3.5 Spatial memory function and behavioral despair are regulated by CB1 in adult-born neurons

Deletion of CB1 led to a decrease in proliferation of new neurons and to an impairment in LTP specifically in newborn neurons in the DG. We therefore next explored what impact this impaired hippocampal function has on neurogenesis-related behavior in nes-CB1ko/ko mice. We tested the animals in behavioral tasks corresponding to hippocampus-dependent learning and memory and to emotional regulation like anxiety or behavioral despair.

Mice were tested 28 dptm (Figure 38A), starting with the spatial object recognition test (SORT) in a Y-maze. Here, nes-CB1ko/ko mice showed a significant decrease ($p=0.038$) in the index of recognition (CB1wt/wt: 61.1 ± 2.1%, nes-CB1ko/ko: 52.9 ± 3.4%), while total exploration time and distance moved were unaltered (Figure 38B). This implies deletion of CB1 from neural stem cells deteriorates cognitive performance. When testing animals in the Morris water maze (MWM) test (Figure 38C), both groups were able to find the visible platform. During training with the hidden platform nes-CB1ko/ko mice displayed higher escape latencies ($p=0.036$) over the time course of 8 days, indicating that CB1 deletion leads to an aggravation of spatial memory. However, during the probe trial all animals spent the same amount of time in the target quadrant (CB1wt/wt: 28.5 ± 1.5 s, nes-CB1ko/ko: 27.9 ± 2.4 s).

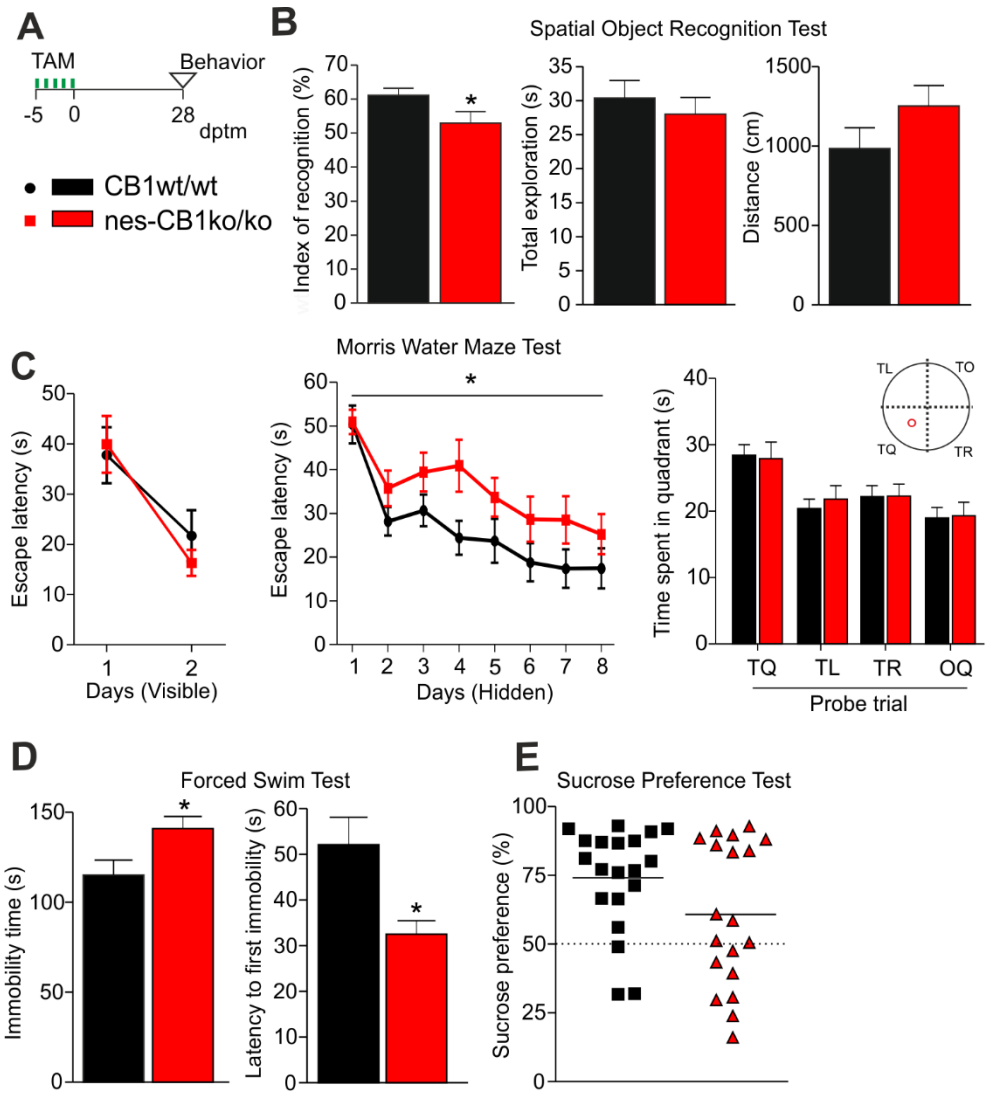

Figure 38. Effect of CB1 loss in adult neural stem cells on hippocampus-dependent learning and memory and emotional regulation. (A) Timeline. Behavior of CB1wt/wt and nes-CB1ko/ko mice was analyzed 28 dptm. (B) CB1-deficient mice in the spatial object recognition test display a decrease in the index of recognition, whereas total exploration and total distance travelled are not impaired. N=19 (CB1wt/wt), n=13 (nes-CB1ko/ko), *p<0.05, Student's t-test. (C) Animals in the Morris water maze test exhibit no difference in escape latency during visible platform training days among groups. nes-CB1ko/ko mice show a worse performance in MWM training during hidden platform days (n=20 (CB1wt/wt, n=19 (nes-CB1ko/ko), *p<0.05, repeated measure 2-way ANOVA; Bonferroni post-test). After 8 days of training animals spent the same time in the target quadrant (TQ) during the probe trial as CB1wt/wt mice. (D) Animals lacking CB1 display an increase in immobility time and a decrease in latency to first immobility in the forced swim test. N=19 (CB1wt/wt), n=13 (nes-CB1ko/ko), *p<0.05, Student's t-test. (E) CB1 deficient mice (n=19) show a reduced, but not significant preference for sucrose compared to CB1wt/wt mice (n=20). Graphs show mean ± SEM.

Additionally, it has been shown that the process of adult neurogenesis is regulating behavioral despair. We tested animals in the forced swim test (Figure 38D), which has been used as a test to assess depressive-like states or antidepressant efficacy. Animals lacking CB1 displayed an increase (p=0.031) in immobility time (CB1wt/wt: 115.2 ± 8.2 s, nes-CB1ko/ko: 141.0 ± 6.7 s) and a decrease (p=0.017) in latency to first immobility (CB1wt/wt: 52.1 ± 6.0 s, nes-CB1ko/ko: 32.5 ± 2.9 s). To support our results of an involvement of CB1

on adult neural stem cells in depressive-like behavior, we measured the preference of animals for sucrose (Figure 38E). Here, CB1 deficient mice showed a decreased, but not significant (p=0.075) preference for sucrose (CB1wt/wt: 74.1 ± 4.2%, nes-CB1ko/ko: 60.8 ± 6.0%).

CB1 deletion did not affect body weight, locomotion, nor anxiety-like behavior in the open field and light dark test (Figure 39A-C). In contrast to the decrease of spatial learning and memory in the SORT and the MWM, CB1 deletion did not have an influence on contextual or cued fear conditioning (Figure 39D). Since nes-CB1ko/ko mice showed an increase in behavioral despair in the forced swim test, we tested the animals in the tail suspension test (Figure 39E), which was unaltered.

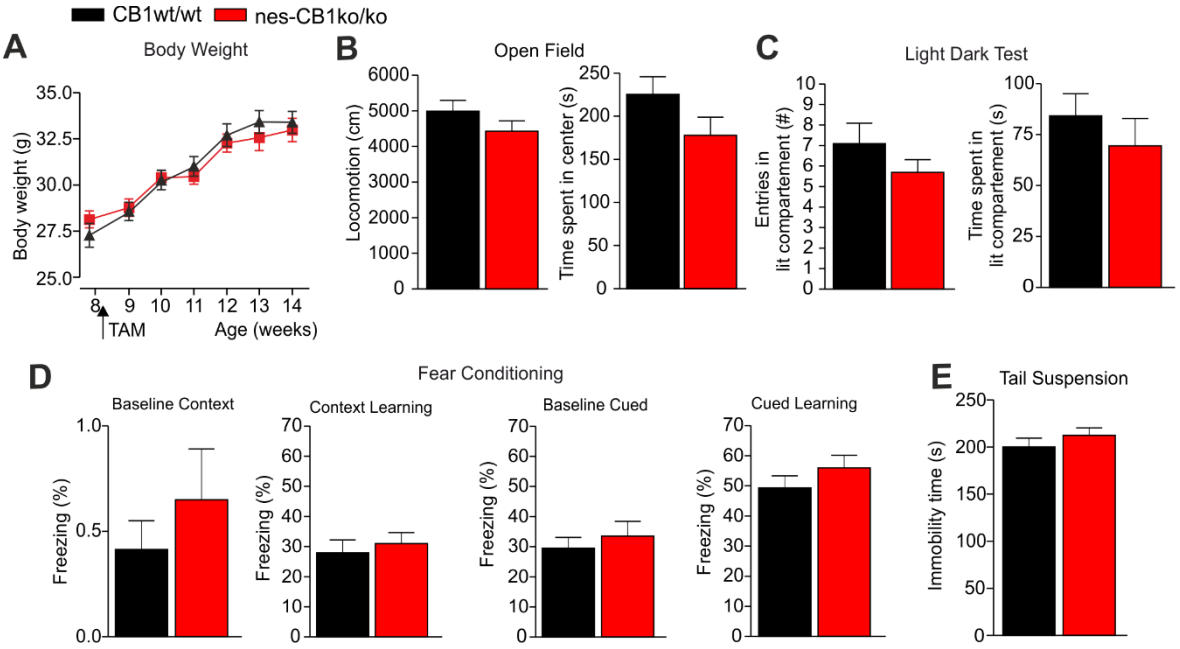

Figure 39. CB1 deletion in nestin positive cells does not affect locomotion, anxiety, body weight, contextual fear memory, nor immobility time in the tail suspension test. (A) Locomotion of animals and time spent in the center was assessed in the open field test 28 dptm and revealed no difference (n=19 (CB1wt/wt), n=13 (nes-CB1ko/ko)). (B) In the light dark test (n=19 (CB1wt/wt), n=13 (nes-CB1ko/ko)) nes-CB1ko/ko animals entered the lit compartment equally frequent and spent the same amount of time in the lit compartment. (C) Nes-CB1ko/ko mice gain the same weight as their wildtype littermates (n=19 (CB1wt/wt), n=13 (nes-CB1ko/ko)). (D) In the fear conditioning task (n=20 (CB1wt/wt), n=19 (nes-CB1ko/ko)) percentage of baseline freezing in the respective context and percentage of freezing during extinction in the context were similar in control and nes-CB1ko/ko mice. During cued fear conditioning CB1wt/wt and nes-CB1ko/ko animals exhibited equivalent freezing levels (baseline and learning). (E) In the tail suspension test (n=20 (CB1wt/wt), n=19 (nes-CB1ko/ko)), immobility time was equivalent in both groups. Data represent mean ± SEM.

In conclusion, CB1-induced impairment on the cellular level led to a severe physiological deterioration in spatial learning and memory, as well as to an enhancement of behavioral despair.

4.3.6 RNA levels of CB1 and BDNF are unaltered in the hippocampus or dentate gyrus of CB1-deficient mice

To dissect the underlying molecular mechanisms, which are responsible for the reduced proliferation rate and the behavioral phenotype, we were interested in changed gene expression levels in the regions of interest, the hippocampus and the DG (Figure 40).

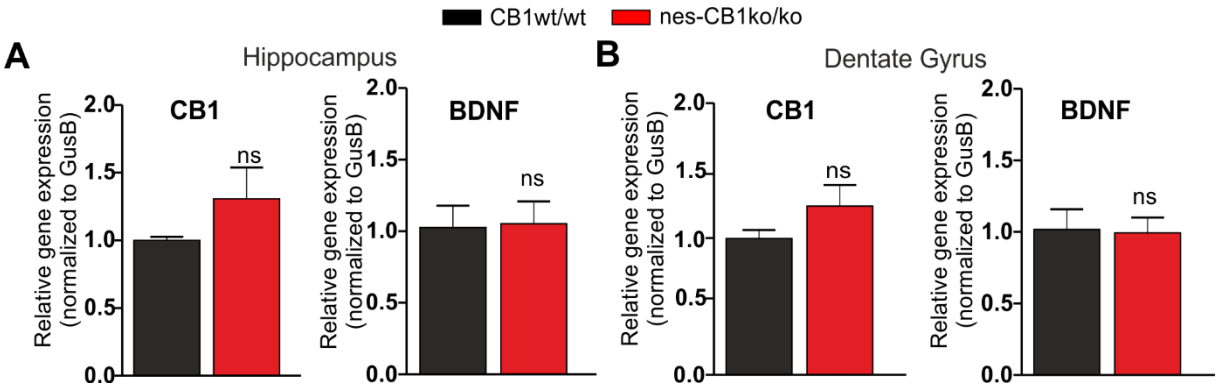

Figure 40. Relative gene expression of CB1 and BDNF in the hippocampus and dentate gyrus is unaltered. RNA from CB1wt/wt and nes-CB1ko/ko mice (n=3). Graphs show mean ± SEM. ns – not significant different.

RNA was isolated from either hippocampus or DG from CB1wt/wt and nes-CB1ko/ko animals and quantified with qPCR. In the hippocampus (Figure 40A), CB1 and BDNF gene expression was not different among groups. Microdissection of the DG (Figure 40B) and subsequent qPCR did not show any differences between groups in CB1 nor BDNF gene expression.

4.3.7 Isolation of adult neural stem cells from nes-CB1ko/ko mice by FACS

Due to the low occurrence of adult NSCs compared to the rest of hippocampal tissue, only few cells have been targeted by our approach using the nestin-CreERT2 mouse line. Thus, any changes in gene expression are very hard to detect. This is why we focused on establishing the isolation of targeted adult NSCs from the SGZ in the laboratory. By following a published protocol (Fischer et al., 2011) for isolation of NSCs from the SVZ, we dissociated the tissue, enriched cells via a sucrose gradient, and immunolabeled isolated cells with fluorescent antibodies (Figure 41). Cells were then sorted based on their expression of YFP (targeted, recombined cells), CD133 (adult NSCs) and PSA-NCAM (adult neuronal progenitor cells) (Figure 42). Afterwards, RNA was isolated and assessed via qPCR.

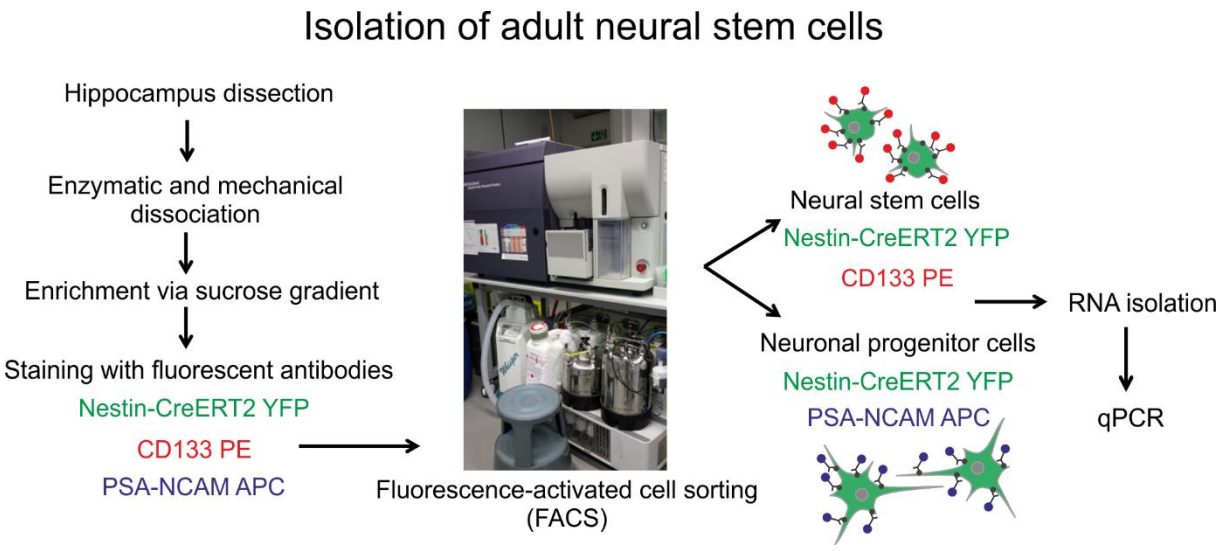

Figure 41. Overview of workflow for isolation of adult NSCs.

From the total population of dissociated cells, 3.8% were selected based on their size in the forward and side scatter and on backgating after completed gating (Figure 42A). Of those cells, 69.5% were selected as single cells in the side scatter and subsequently 83.5% of single cells were isolated living cells (negative for DAPI). This gating has been applied in CB1wt/wt and nes-CB1ko/ko mice, respectively. Only a small fraction of single, living cells from the hippocampus was positive for YFP; 0.35% in CB1wt/wt and 0.34% in nes-CB1ko/ko mice (Figure 42B) as compared to cells from C57BL/6J mice. Our fraction of interest included YFP+/CD133+/PSA-NCAM- cells, the neural stem cells. Flow cytometry analysis showed 35.7% of YFP cells in CB1wt/wt and 41.7% of YFP cells in nes-CB1ko/ko mice were positive for CD133, and 29.4% of YFP cells and 29.8% of YFP cells were positive for PSA-NCAM respectively (Figure 42C). Statistical evaluations between different experiments were not done, since each experiment depended on the quality of the dissociation process.

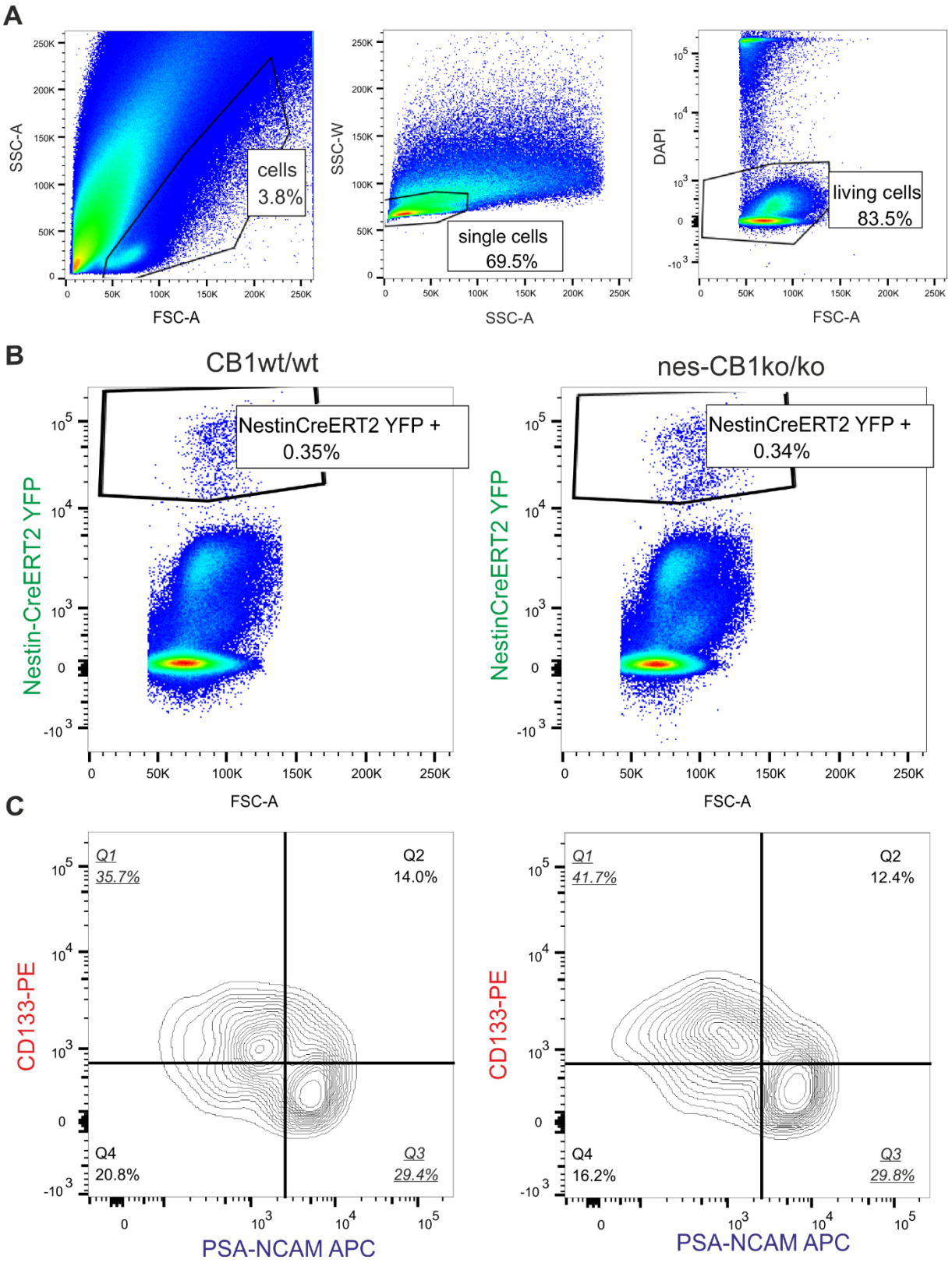

Figure 42. FACS analysis and sorting of isolated NSCs from the hippocampus. (A) Dot plots showing sequential selection of cells, single cells and living cells. (B) Gating for YFP positive cells in CB1wt/wt and nes-CB1ko/ko mice based on negative control. (C) Contour plot of selected YFP cells being positive fo CD133-PE and/or PSA-NCAM-APC. FSC-A; forward scatter-area, SSC-A; side scatter-area, SSC-W; side scatter width, Q; quadrant.

In total, only few cells were isolated (Table 6). Three established experiments/cell sorts were carried out over the course of this thesis. Isolated YFP cells ranged from 505 to 1373 cells. Our fraction of interest, YFP+/CD133+/PSA-NCAM-, contained 155 to 794 cells per genotype. The RNA integrity number (RIN) was assessed in the first two experiments, revealing mostly degraded RNA or below detection limit (RIN=1). The concentration of RNA of those few isolated cells was very low, ranging from 58 pg/µl to 115 pg/µl. When isolating RNA with N-Carriers (to prevent RNA degradation by stabilization with short hairpin RNAs (<100 nt)), RNA concentration was higher, but quality of isolated RNA did not improve. From RNA from our cells of interest we generated and amplified cDNA with an ultra-low input RNA kit, leading to cDNA concentrations ranging from 0.26 ng/µl to 1.47 ng/µl. 0.5 ng/replicate was used for qPCR to assess CB1 and BDNF gene expression. In experiment 1, the CB1 and BDNF RNA level was below the detection limit, thus gene expression changes were not determined. In experiment 2 and 3, CB1 gene expression in nes-CB1ko/ko mice was reduced by half (fold change 0.52 ± 0.31) compared to CB1wt/wt mice. BDNF RNA levels were only determined in experiment 2, revealing a decrease to 0.86 in relative gene expression in nes-CB1ko/ko mice.

In the additional fractions, we tried to transcribe isolated RNA into cDNA using the High Capacity cDNA Reverse Transcription Kit and subjected the whole amount of resulting cDNA to qPCR for CB1 gene expression, to investigate if the CB1 knock-out has occurred in different populations other than our fraction of interest. This resulted in mixed outcomes (very high upregulated versus downregulated in the same population), not representing a clear picture of gene expression changes.

Table 6. Overview of FAC-sorted cells and gene expression changes.

Experiment	Genoytpe	Population	Cell number	RNA [pg/µl]	RIN	cDNA [ng/µl]	CB1 Fold Change	BDNF Fold Change
1 (30.03.16)	CB1 wt/wt	CD133- PSA-NCAM +	131	58.16	1			
		CD133- PSA-NCAM -	102	17.44	1.2			
		CD133+ PSA-NCAM +	69	96.96	1			
		CD133+ PSA-NCAM -	280	107.2	6.8	0.26		
		YFP total	582					
	nes-CB1ko/ko	CD133- PSA-NCAM +	115	24.16	1		1.43	
		CD133- PSA-NCAM -	72	16.56	1		*Undetermined*	
		CD133+ PSA-NCAM +	75	56.96	5.9		13.67	
		CD133+ PSA-NCAM -	279	58.72	N/A	0.66	***Undetermined***	*Undetermined*
		YFP total	541					
2 (31.05.16) (+N-Carrier)	CB1 wt/wt	CD133- PSA-NCAM +	25	116	1			
		CD133- PSA-NCAM -	92	87	1			
		CD133+ PSA-NCAM +	79	209	2.5			
		CD133+ PSA-NCAM -	155	120	1	0.46		
		YFP total	737					
	nes-CB1ko/ko	CD133- PSA-NCAM +	61	157	1		*Undetermined*	
		CD133- PSA-NCAM -	67	224	1		0.11	
		CD133+ PSA-NCAM +	155	388	1		142.22	
		CD133+ PSA-NCAM -	222	197	1.1	0.26	**0.21**	0.86
		YFP total	505					
		YFP negative	500	215	1			
		YFP negative	1000	190	1.1			
3 (20.06.16)	CB1 wt/wt	CD133- PSA-NCAM +	50					
		CD133- PSA-NCAM -	93					
		CD133+ PSA-NCAM +	189					
		CD133+ PSA-NCAM -	291	90		0.6		
		YFP total	623					
	nes-CB1ko/ko	CD133- PSA-NCAM +	93				0.64	
		CD133- PSA-NCAM -	218				1.64	
		CD133+ PSA-NCAM +	268				0.50	
		CD133+ PSA-NCAM -	794	115		1.47	**0.82**	*Undetermined*
		YFP total	1373					

In conclusion, no statement can be given in this thesis about gene expression changes due to technical limitations. Isolation of adult NSCs and their subsequent processing (including RNA isolation of a limited number of cells, stable cDNA generation and qPCR with a very low amount of cDNA) depend on multiple factors that need to be addressed and optimized in further experiments.

4.4 Discussion

In the present study, we developed a transgenic strategy to conditionally delete CB1 from adult neural stem cells and their progeny, and investigated the direct role of CB1 in adult neurogenesis, electrophysiological properties of newborn neurons, and neurogenesis-related behavior. Selective deletion of CB1 from nestin-positive cells led to a decrease in total targeted cells, caused by a reduction in proliferation. Second, CB1 deletion led to an impairment of LTP in the DG and in pyramidal neurons of the CA3-CA1 region. Consistent with these results, hippocampus-dependent spatial learning was deteriorated and depressive-like behavior was induced in CB1-deficient mice.

Our results suggest that CB1 deficiency in a relative small fraction of granule cells is sufficient to produce deficits in neurogenesis-related behavior. Stereological counts revealed that 12,000 - 15,000 newly generated cells were targeted in wildtype mice (concordant with (Lagace et al., 2007)), representing 2.4 - 3% of the total DG granule cell population (500,000 cells (Ihunwo and Schliebs, 2010)). Reduction of neurogenesis in nes-CB1ko/ko mice led to 8,000 - 11,000 cells, constituting only 1.6 – 2.2% of total cells. By using a second approach targeting Sox2-positive NSCs with a lentiviral vector (Suh et al., 2007), we were able to support our results that CB1 deletion leads to a decrease in NSC/NPC proliferation. Here, the results were influenced by the virus injection that involves the technical challenge including heterogeneous labeling, resulting in a widespread population of cell numbers. However, we were not able to show that differentiation of labeled cells into the neuronal or astroglial lineage is affected. In contrast, Aguado et al. demonstrated in CB1 KO mice that progenitor proliferation and astrogliogenesis are impaired *in vitro* (Aguado et al., 2005) and *in vivo* (Aguado et al., 2006). *In vitro* studies involve the use of supplemental growth factors, which by themselves could incidentally affect the potential of differentiation. Concerning the *in vivo* study of complete CB1 KO mice, CB1 deletion on other cells than neural stem cells inside the niche could indirectly induce neurogenesis or reduce astrogliogenesis; e.g. CB1 on glutamatergic or GABAergic neurons and on astrocytes being present in the hippocampus. nestin-CreERT2 mice are not the only model to target adult neural stem cells. Radial glia cells (RGCs) are antigenically heterogeneous (DeCarolis et al., 2013), since not all RGCs in the SGZ zone express nestin. Since the decision between astrocytic or neuronal lineage is presumably made on the level of type-1 cells (Steiner et al., 2006), it would be interesting to see whether deletion of CB1 from type-1 cells only using the astrocyte- and radial glia-specific glutamate aspartate transporter (Glast)-CreERT2 line (GLAST-CreERT2xCB1fl/fl)

could affect the differentiation potential. However, this could also lead to deletion of CB1 from astrocytes, having a rather indirect effect on differentiation later.

Here, we were able to show for the first time, that CB1 on NSCs directly regulates proliferation of NSCs. One mechanism could be that loss of CB1 inhibits activation of quiescent NSCs. Activation of CB1 via endocannabinoid signalling in NPCs involves the proliferative signal transduction pathways PI3K/Akt and ERK, two classical pathways which promote cell survival and proliferation. Downstream targets involve mammalian target of rapamycin complex 1 (mTORC1) and cAMP response element-binding protein (CREB), which are central regulators of IEGs such as cFos, c-jun, zif268, and BDNF (Pagotto et al., 2006), leading to neural cell survival/death decisions (Prenderville et al., 2015). Additionally, CB1 can interact with other growth factors by transactivating e.g. the EGF receptor (Hart et al., 2004). Advances in the technique of FACS and subsequent RNA sequencing should give us an insight on which factors control the process of neurogenesis. To our knowledge, no study has investigated and compared the isolation of stem cells from conditional gene knockout in adult neural stem cells. However, only recently, single-cell transcriptomes of adult hippocampal quiescent NSCs and their immediate progeny have been revealed (Shin et al., 2015), making it a challenging task to extend these discoveries with in the future.

The generation of new neurons in the DG is CB1-dependent, since proliferation is reduced in the early stages of neurogenesis, which then in consequence leads to a reduced number of neuroblasts and mature granule neurons. These newly generated cells compete with existing granule cells for entorhinal cortical input to integrate into the hippocampal circuit. We found that synaptic response strength was decreased in slices from nes-CB1ko/ko animals, revealing a reduced excitability. We then showed that loss of CB1 signaling led to a specific form of strongly impaired LTP in young neurons when comparing with ifenprodil-treated slices from CB1wt/wt mice. Glutamatergic signaling of mature granule neurons was not affected by CB1 deletion, as shown by a further electrophysiological paradigm, where the strong GABAergic inhibition in the DG was blocked with picrotoxin. These results reflect the reduced rate of neurogenesis, because it has already been shown that irradiation of the hippocampus led to the same reduced ifenprodil-sensitive LTP (Snyder et al., 2001). The investigated LTP in the DG in young neurons could be either due to the reduced number of newborn neurons or due to a reduced dendritic arborization and fewer synaptic spines. Literature has already demonstrated that CB1 has an impact on neuronal and synaptic maturation, at least during embryonic development (Berghuis et al., 2007). We are currently investigating the morphology of newborn neurons by retrovirus-mediated labeling of newborn neurons in CB1wt/wt and nes-CB1ko/ko mice. However, one could also use a DCX-CreERT2

(Zhang et al., 2010) mouse line to differentiate the effects of CB1 on either proliferation or dendritic maturation. If LTP in DCX-CB1ko/ko mice would remain unchanged upon CB1 deletion, this would be due to a pure proliferation deficit and a subsequent reduced number of neurons. Nevertheless, when assessing LTP in the CA1 field of the hippocampus in our model, we found a slight decrease of LTP, implicating that the structural modification by the reduced number of new granule cells modified its connectivity by changing the number and strength of synaptic contacts in the whole hippocampal formation.

A decrease in adult neurogenesis has been shown to influence cognitive performance and mood regulation, whereas the dorsal hippocampus is involved in memory processing and the ventral hippocampus in emotional behavior (Fanselow and Dong, 2010). Nes-CB1ko/ko mice display a disrupted hippocampal circuitry, and consequently exhibit a marked decrease in spatial learning in the Morris water maze. Here, the formation of new memories was delayed, because the decreased number of new neurons was not able to remodel the existing circuitry. It has to be considered that animals are placed under a considerable amount of stress through swimming, thereby adding a strong aversive stimulus to the test. A further paradigm to assess spatial learning and memory with a reduced extent of aversive stimulation (bright light) could include the Barnes maze (Barnes, 1979), where performance has also been shown to be impaired with a decrease in neurogenesis (Imayoshi et al., 2008; Shors et al., 2002). Another test could be the radial arm maze (Brown et al., 1976), but this test involves food or water deprivation, also adding a stress component to the test. Nevertheless, we showed that nes-CB1ko/ko mice exhibit a deterioration of cognitive performance and of innate preference for novelty in another hippocampal-dependent test, the SORT. This test requires the hippocampus for encoding, consolidation, and retrieval, and assesses short term spatial memory in the mouse. Our results are in accordance with another study, which showed that the amount of neuroblasts was linear to the reaction to novelty (van Dijk et al., 2016). Another conditional CB1 KO model, which targets astrocytes and a part of adult neural stem cells (GFAP-CreERT2 x CB1fl/fl mice) has been shown to impair spatial working memory (Han et al., 2012). However, here, the authors did not investigate the effect on adult neurogenesis, leaving the hypothesis open that neurogenesis must have also been impaired in these animals.

Notably, in our study, specific CB1 deletion did not affect performance in another hippocampal-dependent task, the context-fear memory. While contextual fear conditioning is dependent on the hippocampus only, cued fear conditioning involves the hippocampus and the amygdala (Phillips and LeDoux, 1992). Decreased levels of neurogenesis by irradiation have been shown to alter fear learning in the contextual fear conditioning paradigm (Saxe et

al., 2006). However, when restricting cell death only to nestin-expressing stem cells, another study could not support the impairment in fear memory (Deng et al., 2009). There are distinct types of hippocampus-dependent long-term memory formation, which differ in their underlying mechanisms, e.g. contextual and spatial mechanisms (Mizuno and Giese, 2005). Here, our results reflect the involvement of CB1 rather in spatial learning and short-term memory than in associative learning, which is highly implicated during contextual fear conditioning.

CB1 is also involved in hippocampal control of the hypothalamic–pituitary–adrenal (HPA) axis (Evanson et al., 2010). CB1-deficiency could therefore account for depressive-like symptoms resulting from an unbalanced HPA axis. Indeed, we found that nes-CB1ko/ko mice displayed an increase in behavioral despair in the forced swim test and a decrease of sucrose preference, which demonstrates an increase in anhedonia, a hallmark of depression (Treadway and Zald, 2011). Surprisingly, we found no differences in the tail suspension test. Both tests target similarly behavioral despair in mice. However, there are multiple important differences in their sensitivity and performance, and the results of one test may not necessarily be replicated by the other (Cryan et al., 2005). BDNF is a significant mediator of effects of antidepressants (e.g. fluoxetine) (Castren and Rantamaki, 2010). Furthermore, there is evidence that CB1 regulates BDNF expression, which then could lead to reduced neurogenesis. Indeed, it has been shown that CB1 regulates BDNF expression (Aso et al., 2008) in the hippocampus, which in turn leads to a decrease in neurogenesis, as it has been assessed in conditional TrkB KO mice (Bergami et al., 2008). The pattern of hypoproliferation in CB1-deficient mice in this study is similar to alterations in neurogenesis in depression, indicating that CB1 could be an *in vivo* modulator of mood regulation. High corticosterone or cortisol levels in mice or humans during chronic stress could lead to downregulation of CB1, thereby inhibit neurogenesis, and increase vulnerability to depression. Interestingly, chronic THC treatment has been shown to decrease proliferation and to impair spatial learning in the MWM (Wolf et al., 2010). However, chronic treatment with the synthetic cannabinoid HU-210 enhanced proliferation and survival in rat DG (Jiang et al., 2005), which means that treatment-related CB1-dependent effects on neurogenesis need further elucidation

CB1 could also be activated by other potent stimulators of adult neurogenesis such as running through increased serum levels of endocannabinoids (Raichlen et al., 2013), which leads to an enhancement of the learning process, but not memory formation. It has been reported in a previous study that voluntary exercise increased endocannabinoid signaling in the hippocampus and subsequently proliferation of progenitor cells. This effect was abrogated by concurrent treatment with the CB1 antagonist AM251, indicating that the

increase in endocannabinoid signaling in the hippocampus is required for the exercise-induced increase in cell proliferation (Hill et al., 2010). Here, we show that specifically CB1 on adult neural stem cells is responsible for the induced hypoproliferation and the subsequent reduced learning performance.

In summary, the results presented in this thesis provide substantial evidence that CB1 is required for accurate proliferation of adult NSCs in the adult DG. CB1 signaling on adult NSCs contributes to hippocampal plasticity and is potentially involved in regulating depressive-like behavior and spatial memory function. Different clinical manipulations of CB1 related to adult neurogenesis could lead to functional recovery in mood or memory disorders.

5 Conclusion / Outlook

Stem cells are a powerful tool for neurobiological research, as they can either be used for cell replacement therapies in neurodegenerative diseases or they can be studied to unravel their influencing properties in adult brain function. This thesis aimed to answer two questions: first, if BDNF-overexpressing embryonic stem cells can be applied as a combination cell replacement therapy for HD, and second, how CB1 is regulating the NSC fate in the SGZ.

By transplanting BDNF-overexpressing NPCs, which had been derived from ESCs, we found robust motor improvements in the QA-lesioned mouse model, whereas grafting of BDNF-progenitors in the R6/2 and N171-82Q model resulted only in minor general NPC effects. Tumor formation after transplantation was absent, and the rescue of motor deficits was attributed to enhanced neuronal and striatal differentiation of BDNF-NPCs. Furthermore, adult neurogenesis was preserved in a BDNF-dependent manner. This study highlights the importance of choosing the right model for transplantation studies and the significance of BDNF in regenerating the striatum.

To translate this therapy into human patients and monitor cell survival and engraftment, it would be particularly interesting to use a non-invasive method of cell tracing. Transplanted cells could be traced with magnetic resonance imaging by labeling cells *in vitro* with iron oxide nanoparticles which would allow for repetitive, real-time observation (Berman et al., 2011). Recent studies in HD cell transplantation research took advantage of iPSC technology. Human iPSCs derived from fibroblasts of HD patients were genetically corrected to remove the mutation in htt and showed reversal of the HD phenotype *in vitro* (An et al., 2012). Corrected iPSCs survived in the R6/2 model and differentiated into striatal neurons. To date, the functional relevance in assessing mouse behavior is lacking, but these human iPSCs could provide a potential donor source for cell replacement therapy in humans. Manipulating these corrected stem cells by overexpressing BDNF may fulfill the promise of using human iPSCs as a potential cell therapy for HD patients. Another application of our BDNF-NPCs could be the transplantation into traumatic brain injury (TBI). TBI is one of the leading cause of death and disability worldwide (Bruns and Hauser, 2003), which is accompanied by cell death, brain atrophy, and functional neurological impairment (Rolfe and Sun, 2015). Indeed, a recent study isolated NSCs, genetically engineered them to overexpress BDNF, and grafted them into the injury cavity of TBI brains, which lead to a short-term functional improvement (Ma et al., 2012a). Using our approach we aim at a long-term recovery of functional behavior. In addition, other neurodegenerative diseases like

Parkinson's and Alzheimer's disease or stroke could be a target of our combinatory stem cell therapy, since they display prominent cell loss. Here, our BDNF-NPCs could be used to promote synaptic repair in specific brain regions (Lu et al., 2013).

In the second part of this thesis, we aimed at characterizing the role of CB1 on NSCs in the hippocampus of the adult brain. We found that NSC-specific deletion of the CB1 receptor led to a decrease in neural stem cell proliferation, which resulted in a decreased number of newborn neuroblasts and neurons, whereas the differentiation potential of targeted cells was not affected. Animals with the specific NSC-deletion of CB1 displayed an impairment in LTP specifically in newborn neurons in the dentate gyrus, which is contributed by a decreased pool of new neurons. Animals lacking a functional CB1 receptor in newborn neurons displayed a decrease in learning, short-term spatial memory function, and an increase in behavioral despair. Ongoing studies involve analysis of dendritic arborization and spine formation of newborn neurons. To identify downstream targets of CB1 specifically in NSCs, it might be interesting to optimize single-cell sorts of SGZ adult NSCs and assess gene expression via single-cell RNA sequencing. One might also crossbreed loxP-floxSTOP-Sun1-GFP mice with T2-nestin-Cre and CB1flox/flox animals to isolate nuclei from the SGZ and perform RNA sequencing, to obtain new target genes of CB1. One potential downstream target of CB1 involves BDNF, which already has been described as IEG of CB1 and which could hypothetically rescue the proliferation deficits if being overexpressed in NSCs. Taken together, our results suggest that CB1 deficiency in a relative small fraction of granule cells is sufficient to produce deficits in neurogenesis-related behavior. In the future, neuropsychiatric diseases are predicted to be one of the highest causes of global disease burden (Murray et al., 2012). Depression, anxiety, and schizophrenia patients have a disruptive function of the DG and treatments focus on regulating neurogenesis. With this study we conclude that distinct clinical manipulations of CB1 linked to adult neurogenesis may lead to functional recovery in mood and memory disorders.

6 References

Abboussi, O., Tazi, A., Paizanis, E., and El Ganouni, S. (2014). Chronic exposure to WIN55,212-2 affects more potently spatial learning and memory in adolescents than in adult rats via a negative action on dorsal hippocampal neurogenesis. Pharmacol Biochem Behav *120*, 95-102.

Aguado, T., Monory, K., Palazuelos, J., Stella, N., Cravatt, B., Lutz, B., Marsicano, G., Kokaia, Z., Guzman, M., and Galve-Roperh, I. (2005). The endocannabinoid system drives neural progenitor proliferation. FASEB J *19*, 1704-1706.

Aguado, T., Palazuelos, J., Monory, K., Stella, N., Cravatt, B., Lutz, B., Marsicano, G., Kokaia, Z., Guzman, M., and Galve-Roperh, I. (2006). The endocannabinoid system promotes astroglial differentiation by acting on neural progenitor cells. J Neurosci *26*, 1551-1561.

Aguado, T., Romero, E., Monory, K., Palazuelos, J., Sendtner, M., Marsicano, G., Lutz, B., Guzman, M., and Galve-Roperh, I. (2007). The CB1 cannabinoid receptor mediates excitotoxicity-induced neural progenitor proliferation and neurogenesis. J Biol Chem *282*, 23892-23898.

Aimone, J.B., Li, Y., Lee, S.W., Clemenson, G.D., Deng, W., and Gage, F.H. (2014). Regulation and function of adult neurogenesis: from genes to cognition. Physiol Rev *94*, 991-1026.

Aimone, J.B., Wiles, J., and Gage, F.H. (2009). Computational influence of adult neurogenesis on memory encoding. Neuron *61*, 187-202.

Akers, K.G., Martinez-Canabal, A., Restivo, L., Yiu, A.P., De Cristofaro, A., Hsiang, H.L., Wheeler, A.L., Guskjolen, A., Niibori, Y., Shoji, H.*, et al.* (2014). Hippocampal neurogenesis regulates forgetting during adulthood and infancy. Science *344*, 598-602.

Alexander, G.E., Crutcher, M.D., and DeLong, M.R. (1990). Basal ganglia-thalamocortical circuits: parallel substrates for motor, oculomotor, "prefrontal" and "limbic" functions. Prog Brain Res *85*, 119-146.

Altman, J., and Das, G.D. (1965). Post-natal origin of microneurones in the rat brain. Nature *207*, 953-956.

Ambrosetti, D.C., Basilico, C., and Dailey, L. (1997). Synergistic activation of the fibroblast growth factor 4 enhancer by Sox2 and Oct-3 depends on protein-protein interactions facilitated by a specific spatial arrangement of factor binding sites. Mol Cell Biol *17*, 6321-6329.

An, M.C., Zhang, N., Scott, G., Montoro, D., Wittkop, T., Mooney, S., Melov, S., and Ellerby, L.M. (2012). Genetic correction of Huntington's disease phenotypes in induced pluripotent stem cells. Cell Stem Cell *11*, 253-263.

Arvidsson, A., Collin, T., Kirik, D., Kokaia, Z., and Lindvall, O. (2002). Neuronal replacement from endogenous precursors in the adult brain after stroke. Nat Med *8*, 963-970.

Asano, T., Ageyama, N., Takeuchi, K., Momoeda, M., Kitano, Y., Sasaki, K., Ueda, Y., Suzuki, Y., Kondo, Y., Torii, R.*, et al.* (2003). Engraftment and tumor formation after allogeneic in utero transplantation of primate embryonic stem cells. Transplantation *76*, 1061-1067.

Aso, E., Ozaita, A., Valdizan, E.M., Ledent, C., Pazos, A., Maldonado, R., and Valverde, O. (2008). BDNF impairment in the hippocampus is related to enhanced despair behavior in CB1 knockout mice. J Neurochem *105*, 565-572.

Aubry, L., Bugi, A., Lefort, N., Rousseau, F., Peschanski, M., and Perrier, A.L. (2008). Striatal progenitors derived from human ES cells mature into DARPP32 neurons in vitro and in quinolinic acid-lesioned rats. Proc Natl Acad Sci U S A *105*, 16707-16712.

Bachoud-Levi, A.C., Gaura, V., Brugieres, P., Lefaucheur, J.P., Boisse, M.F., Maison, P., Baudic, S., Ribeiro, M.J., Bourdet, C., Remy, P.*, et al.* (2006). Effect of fetal neural transplants in patients with Huntington's disease 6 years after surgery: a long-term follow-up study. Lancet Neurol *5*, 303-309.

Bagutti, C., Wobus, A.M., Fassler, R., and Watt, F.M. (1996). Differentiation of embryonal stem cells into keratinocytes: comparison of wild-type and beta 1 integrin-deficient cells. Dev Biol *179*, 184-196.

Bain, G., Kitchens, D., Yao, M., Huettner, J.E., and Gottlieb, D.I. (1995). Embryonic stem cells express neuronal properties in vitro. Dev Biol *168*, 342-357.

Bambico, F.R., Katz, N., Debonnel, G., and Gobbi, G. (2007). Cannabinoids elicit antidepressant-like behavior and activate serotonergic neurons through the medial prefrontal cortex. J Neurosci *27*, 11700-11711.

Barberi, T., Klivenyi, P., Calingasan, N.Y., Lee, H., Kawamata, H., Loonam, K., Perrier, A.L., Bruses, J., Rubio, M.E., Topf, N.*, et al.* (2003). Neural subtype specification of fertilization and nuclear transfer embryonic stem cells and application in parkinsonian mice. Nat Biotechnol *21*, 1200-1207.

Barnes, C.A. (1979). Memory deficits associated with senescence: a neurophysiological and behavioral study in the rat. J Comp Physiol Psychol *93*, 74-104.

Bates, G.P., Dorsey, R., Gusella, J.F., Hayden, M.R., Kay, C., Leavitt, B.R., Nance, M., Ross, C.A., Scahill, R.I., Wetzel, R.*, et al.* (2015). Huntington disease. Nat Rev Dis Primers *1*, 15005.

Baydyuk, M., Russell, T., Liao, G.Y., Zang, K., An, J.J., Reichardt, L.F., and Xu, B. (2011). TrkB receptor controls striatal formation by regulating the number of newborn striatal neurons. Proc Natl Acad Sci U S A *108*, 1669-1674.

Beal, M.F., Ferrante, R.J., Swartz, K.J., and Kowall, N.W. (1991). Chronic quinolinic acid lesions in rats closely resemble Huntington's disease. J Neurosci *11*, 1649-1659.

Beal, M.F., Kowall, N.W., Swartz, K.J., Ferrante, R.J., and Martin, J.B. (1989). Differential sparing of somatostatin-neuropeptide Y and cholinergic neurons following striatal excitotoxin lesions. Synapse *3*, 38-47.

Behrstock, S., Ebert, A.D., Klein, S., Schmitt, M., Moore, J.M., and Svendsen, C.N. (2008). Lesion-induced increase in survival and migration of human neural progenitor cells releasing GDNF. Cell Transplant *17*, 753-762.

Benito, C., Romero, J.P., Tolon, R.M., Clemente, D., Docagne, F., Hillard, C.J., Guaza, C., and Romero, J. (2007). Cannabinoid CB1 and CB2 receptors and fatty acid amide hydrolase are specific markers of plaque cell subtypes in human multiple sclerosis. J Neurosci *27*, 2396-2402.

Benraiss, A., Chmielnicki, E., Lerner, K., Roh, D., and Goldman, S.A. (2001). Adenoviral brain-derived neurotrophic factor induces both neostriatal and olfactory neuronal

recruitment from endogenous progenitor cells in the adult forebrain. J Neurosci *21*, 6718-6731.

Bergami, M., Rimondini, R., Santi, S., Blum, R., Gotz, M., and Canossa, M. (2008). Deletion of TrkB in adult progenitors alters newborn neuron integration into hippocampal circuits and increases anxiety-like behavior. Proc Natl Acad Sci U S A *105*, 15570-15575.

Berghuis, P., Rajnicek, A.M., Morozov, Y.M., Ross, R.A., Mulder, J., Urban, G.M., Monory, K., Marsicano, G., Matteoli, M., Canty, A.*, et al.* (2007). Hardwiring the brain: endocannabinoids shape neuronal connectivity. Science *316*, 1212-1216.

Berman, S.M., Walczak, P., and Bulte, J.W. (2011). MRI of transplanted neural stem cells. Methods Mol Biol *711*, 435-449.

Bernreuther, C., Dihne, M., Johann, V., Schiefer, J., Cui, Y., Hargus, G., Schmid, J.S., Xu, J., Kosinski, C.M., and Schachner, M. (2006). Neural cell adhesion molecule L1-transfected embryonic stem cells promote functional recovery after excitotoxic lesion of the mouse striatum. J Neurosci *26*, 11532-11539.

Bertrand, N., Castro, D.S., and Guillemot, F. (2002). Proneural genes and the specification of neural cell types. Nat Rev Neurosci *3*, 517-530.

Binder, D.K., and Scharfman, H.E. (2004). Brain-derived neurotrophic factor. Growth Factors *22*, 123-131.

Bjornebekk, A., Mathe, A.A., and Brene, S. (2005). The antidepressant effect of running is associated with increased hippocampal cell proliferation. Int J Neuropsychopharmacol *8*, 357-368.

Bortolato, M., Bini, V., and Tambaro, S. (2010). Vulnerability Factors for the Psychiatric and Behavioral Effects of Cannabis. Pharmaceuticals (Basel) *3*, 2799-2820.

Brown, M.F., Farley, R.F., and Lorek, E.J. (1976). Remembrance of places you passed: social spatial working memory in rats. J Exp Psychol Anim Behav Process *33*, 213-224.

Bruns, J., Jr., and Hauser, W.A. (2003). The epidemiology of traumatic brain injury: a review. Epilepsia *44 Suppl 10*, 2-10.

Buckley, N.J., Johnson, R., Zuccato, C., Bithell, A., and Cattaneo, E. (2010). The role of REST in transcriptional and epigenetic dysregulation in Huntington's disease. Neurobiol Dis *39*, 28-39.

Butenschon, J., Zimmermann, T., Schmarowski, N., Nitsch, R., Fackelmeier, B., Friedemann, K., Radyushkin, K., Baumgart, J., Lutz, B., and Leschik, J. (2016). PSA-NCAM positive neural progenitors stably expressing BDNF promote functional recovery in a mouse model of spinal cord injury. Stem Cell Res Ther *7*, 11.

Campos, A.C., Ortega, Z., Palazuelos, J., Fogaca, M.V., Aguiar, D.C., Diaz-Alonso, J., Ortega-Gutierrez, S., Vazquez-Villa, H., Moreira, F.A., Guzman, M.*, et al.* (2013). The anxiolytic effect of cannabidiol on chronically stressed mice depends on hippocampal neurogenesis: involvement of the endocannabinoid system. Int J Neuropsychopharmacol *16*, 1407-1419.

Capecchi, M.R. (1989). Altering the genome by homologous recombination. Science *244*, 1288-1292.

Castren, E., and Rantamaki, T. (2010). The role of BDNF and its receptors in depression and antidepressant drug action: Reactivation of developmental plasticity. Dev Neurobiol *70*, 289-297.

Cattaneo, E. (2003). Dysfunction of wild-type huntingtin in Huntington disease. News Physiol Sci *18*, 34-37.

Chambers, I., Colby, D., Robertson, M., Nichols, J., Lee, S., Tweedie, S., and Smith, A. (2003). Functional expression cloning of Nanog, a pluripotency sustaining factor in embryonic stem cells. Cell *113*, 643-655.

Cheng, M.F. (2013). Hypothalamic neurogenesis in the adult brain. Front Neuroendocrinol *34*, 167-178.

Chiang, M.C., Chen, C.M., Lee, M.R., Chen, H.W., Chen, H.M., Wu, Y.S., Hung, C.H., Kang, J.J., Chang, C.P., Chang, C.*, et al.* (2010). Modulation of energy deficiency in Huntington's disease via activation of the peroxisome proliferator-activated receptor gamma. Hum Mol Genet *19*, 4043-4058.

Chiarlone, A., Bellocchio, L., Blazquez, C., Resel, E., Soria-Gomez, E., Cannich, A., Ferrero, J.J., Sagredo, O., Benito, C., Romero, J.*, et al.* (2014). A restricted population of CB1 cannabinoid receptors with neuroprotective activity. Proc Natl Acad Sci U S A *111*, 8257-8262.

Chmielnicki, E., Benraiss, A., Economides, A.N., and Goldman, S.A. (2004). Adenovirally expressed noggin and brain-derived neurotrophic factor cooperate to induce new medium spiny neurons from resident progenitor cells in the adult striatal ventricular zone. J Neurosci *24*, 2133-2142.

Connor, B., Sun, Y., von Hieber, D., Tang, S.K., Jones, K.S., and Maucksch, C. (2016). AAV1/2-mediated BDNF gene therapy in a transgenic rat model of Huntington's disease. Gene Ther *23*, 283-295.

Consiglio, A., Gritti, A., Dolcetta, D., Follenzi, A., Bordignon, C., Gage, F.H., Vescovi, A.L., and Naldini, L. (2004). Robust in vivo gene transfer into adult mammalian neural stem cells by lentiviral vectors. Proc Natl Acad Sci U S A *101*, 14835-14840.

Crick, C., and Miranker, W. (2006). Apoptosis, neurogenesis, and information content in Hebbian networks. Biol Cybern *94*, 9-19.

Cryan, J.F., and Holmes, A. (2005). The ascent of mouse: advances in modelling human depression and anxiety. Nat Rev Drug Discov *4*, 775-790.

Cryan, J.F., Mombereau, C., and Vassout, A. (2005). The tail suspension test as a model for assessing antidepressant activity: review of pharmacological and genetic studies in mice. Neurosci Biobehav Rev *29*, 571-625.

Curtis, R., Adryan, K.M., Stark, J.L., Park, J.S., Compton, D.L., Weskamp, G., Huber, L.J., Chao, M.V., Jaenisch, R., Lee, K.F.*, et al.* (1995). Differential role of the low affinity neurotrophin receptor (p75) in retrograde axonal transport of the neurotrophins. Neuron *14*, 1201-1211.

Dani, C., Smith, A.G., Dessolin, S., Leroy, P., Staccini, L., Villageois, P., Darimont, C., and Ailhaud, G. (1997). Differentiation of embryonic stem cells into adipocytes in vitro. J Cell Sci *110 (Pt 11)*, 1279-1285.

Danjo, T., Eiraku, M., Muguruma, K., Watanabe, K., Kawada, M., Yanagawa, Y., Rubenstein, J.L., and Sasai, Y. (2011). Subregional specification of embryonic stem

cell-derived ventral telencephalic tissues by timed and combinatory treatment with extrinsic signals. J Neurosci *31*, 1919-1933.

DeCarolis, N.A., Mechanic, M., Petrik, D., Carlton, A., Ables, J.L., Malhotra, S., Bachoo, R., Gotz, M., Lagace, D.C., and Eisch, A.J. (2013). In vivo contribution of nestin- and GLAST-lineage cells to adult hippocampal neurogenesis. Hippocampus *23*, 708-719.

Delli Carri, A., Onorati, M., Lelos, M.J., Castiglioni, V., Faedo, A., Menon, R., Camnasio, S., Vuono, R., Spaiardi, P., Talpo, F.*, et al.* (2013). Developmentally coordinated extrinsic signals drive human pluripotent stem cell differentiation toward authentic DARPP-32+ medium-sized spiny neurons. Development *140*, 301-312.

Deng, W., Saxe, M.D., Gallina, I.S., and Gage, F.H. (2009). Adult-born hippocampal dentate granule cells undergoing maturation modulate learning and memory in the brain. J Neurosci *29*, 13532-13542.

Desbaillets, I., Ziegler, U., Groscurth, P., and Gassmann, M. (2000). Embryoid bodies: an in vitro model of mouse embryogenesis. Exp Physiol *85*, 645-651.

Devane, W.A., Dysarz, F.A., 3rd, Johnson, M.R., Melvin, L.S., and Howlett, A.C. (1988). Determination and characterization of a cannabinoid receptor in rat brain. Mol Pharmacol *34*, 605-613.

Devane, W.A., Hanus, L., Breuer, A., Pertwee, R.G., Stevenson, L.A., Griffin, G., Gibson, D., Mandelbaum, A., Etinger, A., and Mechoulam, R. (1992). Isolation and structure of a brain constituent that binds to the cannabinoid receptor. Science *258*, 1946-1949.

Di, S., Boudaba, C., Popescu, I.R., Weng, F.J., Harris, C., Marcheselli, V.L., Bazan, N.G., and Tasker, J.G. (2005). Activity-dependent release and actions of endocannabinoids in the rat hypothalamic supraoptic nucleus. J Physiol *569*, 751-760.

Diaz-Alonso, J., Aguado, T., Wu, C.S., Palazuelos, J., Hofmann, C., Garcez, P., Guillemot, F., Lu, H.C., Lutz, B., Guzman, M.*, et al.* (2012). The CB(1) cannabinoid receptor drives corticospinal motor neuron differentiation through the Ctip2/Satb2 transcriptional regulation axis. J Neurosci *32*, 16651-16665.

Dimitropoulou, A., and Bixby, J.L. (2000). Regulation of retinal neurite growth by alterations in MAPK/ERK kinase (MEK) activity. Brain Res *858*, 205-214.

Doetsch, F., Caille, I., Lim, D.A., Garcia-Verdugo, J.M., and Alvarez-Buylla, A. (1999). Subventricular zone astrocytes are neural stem cells in the adult mammalian brain. Cell *97*, 703-716.

Doetschman, T., Gregg, R.G., Maeda, N., Hooper, M.L., Melton, D.W., Thompson, S., and Smithies, O. (1987). Targetted correction of a mutant HPRT gene in mouse embryonic stem cells. Nature *330*, 576-578.

Dupret, D., Montaron, M.F., Drapeau, E., Aurousseau, C., Le Moal, M., Piazza, P.V., and Abrous, D.N. (2005). Methylazoxymethanol acetate does not fully block cell genesis in the young and aged dentate gyrus. Eur J Neurosci *22*, 778-783.

Dupret, D., Revest, J.M., Koehl, M., Ichas, F., De Giorgi, F., Costet, P., Abrous, D.N., and Piazza, P.V. (2008). Spatial relational memory requires hippocampal adult neurogenesis. PLoS One *3*, e1959.

Ebert, A.D., Barber, A.E., Heins, B.M., and Svendsen, C.N. (2010). Ex vivo delivery of GDNF maintains motor function and prevents neuronal loss in a transgenic mouse model of Huntington's disease. Exp Neurol *224*, 155-162.

El-Akabawy, G., Rattray, I., Johansson, S.M., Gale, R., Bates, G., and Modo, M. (2012). Implantation of undifferentiated and pre-differentiated human neural stem cells in the R6/2 transgenic mouse model of Huntington's disease. BMC Neurosci *13*, 97.

Esposito, M.S., Piatti, V.C., Laplagne, D.A., Morgenstern, N.A., Ferrari, C.C., Pitossi, F.J., and Schinder, A.F. (2005). Neuronal differentiation in the adult hippocampus recapitulates embryonic development. J Neurosci *25*, 10074-10086.

Evans, J., Sumners, C., Moore, J., Huentelman, M.J., Deng, J., Gelband, C.H., and Shaw, G. (2002). Characterization of mitotic neurons derived from adult rat hypothalamus and brain stem. J Neurophysiol *87*, 1076-1085.

Evans, M.J., and Kaufman, M.H. (1981). Establishment in culture of pluripotential cells from mouse embryos. Nature *292*, 154-156.

Evanson, N.K., Tasker, J.G., Hill, M.N., Hillard, C.J., and Herman, J.P. (2010). Fast feedback inhibition of the HPA axis by glucocorticoids is mediated by endocannabinoid signaling. Endocrinology *151*, 4811-4819.

Fanselow, M.S., and Dong, H.W. (2010). Are the dorsal and ventral hippocampus functionally distinct structures? Neuron *65*, 7-19.

Ferrari, F., Ottani, A., Vivoli, R., and Giuliani, D. (1999). Learning impairment produced in rats by the cannabinoid agonist HU 210 in a water-maze task. Pharmacol Biochem Behav *64*, 555-561.

Filippov, V., Kronenberg, G., Pivneva, T., Reuter, K., Steiner, B., Wang, L.P., Yamaguchi, M., Kettenmann, H., and Kempermann, G. (2003). Subpopulation of nestin-expressing progenitor cells in the adult murine hippocampus shows electrophysiological and morphological characteristics of astrocytes. Mol Cell Neurosci *23*, 373-382.

Fink, K.D., Rossignol, J., Crane, A.T., Davis, K.K., Bombard, M.C., Bavar, A.M., Clerc, S., Lowrance, S.A., Song, C., Lescaudron, L.*, et al.* (2013). Transplantation of umbilical cord-derived mesenchymal stem cells into the striata of R6/2 mice: behavioral and neuropathological analysis. Stem Cell Res Ther *4*, 130.

Fischer, J., Beckervordersandforth, R., Tripathi, P., Steiner-Mezzadri, A., Ninkovic, J., and Gotz, M. (2011). Prospective isolation of adult neural stem cells from the mouse subependymal zone. Nat Protoc *6*, 1981-1989.

Fisher, E.R., and Hayden, M.R. (2014). Multisource ascertainment of Huntington disease in Canada: prevalence and population at risk. Mov Disord *29*, 105-114.

Folstein, S.E., Jensen, B., Leigh, R.J., and Folstein, M.F. (1983). The measurement of abnormal movement: methods developed for Huntington's disease. Neurobehav Toxicol Teratol *5*, 605-609.

Fraichard, A., Chassande, O., Bilbaut, G., Dehay, C., Savatier, P., and Samarut, J. (1995). In vitro differentiation of embryonic stem cells into glial cells and functional neurons. J Cell Sci *108 (Pt 10)*, 3181-3188.

Gaetani, S., Dipasquale, P., Romano, A., Righetti, L., Cassano, T., Piomelli, D., and Cuomo, V. (2009). The endocannabinoid system as a target for novel anxiolytic and antidepressant drugs. Int Rev Neurobiol *85*, 57-72.

Gage, F.H. (2000). Mammalian neural stem cells. Science *287*, 1433-1438.

Gallina, P., Paganini, M., Lombardini, L., Mascalchi, M., Porfirio, B., Gadda, D., Marini, M., Pinzani, P., Salvianti, F., Crescioli, C.*, et al.* (2010). Human striatal neuroblasts

develop and build a striatal-like structure into the brain of Huntington's disease patients after transplantation. Exp Neurol *222*, 30-41.

Galve-Roperh, I., Aguado, T., Palazuelos, J., and Guzman, M. (2008). Mechanisms of control of neuron survival by the endocannabinoid system. Curr Pharm Des *14*, 2279-2288.

Galve-Roperh, I., Palazuelos, J., Aguado, T., and Guzman, M. (2009). The endocannabinoid system and the regulation of neural development: potential implications in psychiatric disorders. Eur Arch Psychiatry Clin Neurosci *259*, 371-382.

Gao, Y., Vasilyev, D.V., Goncalves, M.B., Howell, F.V., Hobbs, C., Reisenberg, M., Shen, R., Zhang, M.Y., Strassle, B.W., Lu, P.*, et al.* (2010). Loss of retrograde endocannabinoid signaling and reduced adult neurogenesis in diacylglycerol lipase knock-out mice. J Neurosci *30*, 2017-2024.

Gaoni, Y., and Mechoulam, R. (1964). Isolation, Structure, and Partial Synthesis of an Active Constituent of Hashish. Journal of the American Chemical Society *86*, 1646-1647.

Garcia, A.D., Doan, N.B., Imura, T., Bush, T.G., and Sofroniew, M.V. (2004). GFAP-expressing progenitors are the principal source of constitutive neurogenesis in adult mouse forebrain. Nat Neurosci *7*, 1233-1241.

Gauthier, L.R., Charrin, B.C., Borrell-Pages, M., Dompierre, J.P., Rangone, H., Cordelieres, F.P., De Mey, J., MacDonald, M.E., Lessmann, V., Humbert, S.*, et al.* (2004). Huntingtin controls neurotrophic support and survival of neurons by enhancing BDNF vesicular transport along microtubules. Cell *118*, 127-138.

Ge, S., Goh, E.L., Sailor, K.A., Kitabatake, Y., Ming, G.L., and Song, H. (2006). GABA regulates synaptic integration of newly generated neurons in the adult brain. Nature *439*, 589-593.

Ge, S., Yang, C.H., Hsu, K.S., Ming, G.L., and Song, H. (2007). A critical period for enhanced synaptic plasticity in newly generated neurons of the adult brain. Neuron *54*, 559-566.

Gerrard, L., Rodgers, L., and Cui, W. (2005). Differentiation of human embryonic stem cells to neural lineages in adherent culture by blocking bone morphogenetic protein signaling. Stem Cells *23*, 1234-1241.

Giralt, A., Friedman, H.C., Caneda-Ferron, B., Urban, N., Moreno, E., Rubio, N., Blanco, J., Peterson, A., Canals, J.M., and Alberch, J. (2010). BDNF regulation under GFAP promoter provides engineered astrocytes as a new approach for long-term protection in Huntington's disease. Gene Ther *17*, 1294-1308.

Gokce, O., Runne, H., Kuhn, A., and Luthi-Carter, R. (2009). Short-term striatal gene expression responses to brain-derived neurotrophic factor are dependent on MEK and ERK activation. PLoS One *4*, e5292.

Goncalves, J.T., Schafer, S.T., and Gage, F.H. (2016). Adult Neurogenesis in the Hippocampus: From Stem Cells to Behavior. Cell *167*, 897-914.

Goncalves, M.B., Suetterlin, P., Yip, P., Molina-Holgado, F., Walker, D.J., Oudin, M.J., Zentar, M.P., Pollard, S., Yanez-Munoz, R.J., Williams, G.*, et al.* (2008). A diacylglycerol lipase-CB2 cannabinoid pathway regulates adult subventricular zone neurogenesis in an age-dependent manner. Mol Cell Neurosci *38*, 526-536.

Group, T.H.s.D.C.R. (1993). A novel gene containing a trinucleotide repeat that is expanded and unstable on Huntington's disease chromosomes. The Huntington's Disease Collaborative Research Group. Cell *72*, 971-983.

Han, J., Kesner, P., Metna-Laurent, M., Duan, T., Xu, L., Georges, F., Koehl, M., Abrous, D.N., Mendizabal-Zubiaga, J., Grandes, P.*, et al.* (2012). Acute cannabinoids impair working memory through astroglial CB1 receptor modulation of hippocampal LTD. Cell *148*, 1039-1050.

Haring, M., Grieb, M., Monory, K., Lutz, B., and Moreira, F.A. (2013). Cannabinoid CB(1) receptor in the modulation of stress coping behavior in mice: the role of serotonin and different forebrain neuronal subpopulations. Neuropharmacology *65*, 83-89.

Harkany, T., Guzman, M., Galve-Roperh, I., Berghuis, P., Devi, L.A., and Mackie, K. (2007). The emerging functions of endocannabinoid signaling during CNS development. Trends Pharmacol Sci *28*, 83-92.

Hart, S., Fischer, O.M., and Ullrich, A. (2004). Cannabinoids induce cancer cell proliferation via tumor necrosis factor alpha-converting enzyme (TACE/ADAM17)-mediated transactivation of the epidermal growth factor receptor. Cancer Res *64*, 1943-1950.

Hegert, C., Kramer, J., Hargus, G., Muller, J., Guan, K., Wobus, A.M., Muller, P.K., and Rohwedel, J. (2002). Differentiation plasticity of chondrocytes derived from mouse embryonic stem cells. J Cell Sci *115*, 4617-4628.

Hemmati-Brivanlou, A., and Melton, D. (1997). Vertebrate embryonic cells will become nerve cells unless told otherwise. Cell *88*, 13-17.

Herkenham, M., Lynn, A.B., Little, M.D., Johnson, M.R., Melvin, L.S., de Costa, B.R., and Rice, K.C. (1990). Cannabinoid receptor localization in brain. Proc Natl Acad Sci U S A *87*, 1932-1936.

Hikabe, O., Hamazaki, N., Nagamatsu, G., Obata, Y., Hirao, Y., Hamada, N., Shimamoto, S., Imamura, T., Nakashima, K., Saitou, M.*, et al.* (2016). Reconstitution in vitro of the entire cycle of the mouse female germ line. Nature.

Hill, M.N., Carrier, E.J., McLaughlin, R.J., Morrish, A.C., Meier, S.E., Hillard, C.J., and Gorzalka, B.B. (2008). Regional alterations in the endocannabinoid system in an animal model of depression: effects of concurrent antidepressant treatment. J Neurochem *106*, 2322-2336.

Hill, M.N., Kambo, J.S., Sun, J.C., Gorzalka, B.B., and Galea, L.A. (2006). Endocannabinoids modulate stress-induced suppression of hippocampal cell proliferation and activation of defensive behaviours. Eur J Neurosci *24*, 1845-1849.

Hill, M.N., Patel, S., Carrier, E.J., Rademacher, D.J., Ormerod, B.K., Hillard, C.J., and Gorzalka, B.B. (2005). Downregulation of endocannabinoid signaling in the hippocampus following chronic unpredictable stress. Neuropsychopharmacology *30*, 508-515.

Hill, M.N., Titterness, A.K., Morrish, A.C., Carrier, E.J., Lee, T.T., Gil-Mohapel, J., Gorzalka, B.B., Hillard, C.J., and Christie, B.R. (2010). Endogenous cannabinoid signaling is required for voluntary exercise-induced enhancement of progenitor cell proliferation in the hippocampus. Hippocampus *20*, 513-523.

Hogan, B. (1994). Manipulating the Mouse Embryo: A Laboratory Manual (Cold Spring Harbor Laboratory Press).

Howlett, A.C. (1985). Cannabinoid inhibition of adenylate cyclase. Biochemistry of the response in neuroblastoma cell membranes. Mol Pharmacol *27*, 429-436.

Howlett, A.C., Barth, F., Bonner, T.I., Cabral, G., Casellas, P., Devane, W.A., Felder, C.C., Herkenham, M., Mackie, K., Martin, B.R.*, et al.* (2002). International Union of Pharmacology. XXVII. Classification of cannabinoid receptors. Pharmacol Rev *54*, 161-202.

Howlett, A.C., Qualy, J.M., and Khachatrian, L.L. (1986). Involvement of Gi in the inhibition of adenylate cyclase by cannabimimetic drugs. Mol Pharmacol *29*, 307-313.

Hua, T., Vemuri, K., Pu, M., Qu, L., Han, G.W., Wu, Y., Zhao, S., Shui, W., Li, S., Korde, A.*, et al.* (2016). Crystal Structure of the Human Cannabinoid Receptor CB1. Cell *167*, 750-762 e714.

Huang, E.J., and Reichardt, L.F. (2001). Neurotrophins: roles in neuronal development and function. Annu Rev Neurosci *24*, 677-736.

Huntington, G. (1872). On chorea. George Huntington, M.D. J Neuropsychiatry Clin Neurosci *15*, 109-112.

Ihunwo, A.O., and Schliebs, R. (2010). Cell proliferation and total granule cell number in dentate gyrus of transgenic Tg2576 mouse. Acta Neurobiol Exp (Wars) *70*, 362-369.

Imayoshi, I., Sakamoto, M., Ohtsuka, T., Takao, K., Miyakawa, T., Yamaguchi, M., Mori, K., Ikeda, T., Itohara, S., and Kageyama, R. (2008). Roles of continuous neurogenesis in the structural and functional integrity of the adult forebrain. Nat Neurosci *11*, 1153-1161.

Itsykson, P., Ilouz, N., Turetsky, T., Goldstein, R.S., Pera, M.F., Fishbein, I., Segal, M., and Reubinoff, B.E. (2005). Derivation of neural precursors from human embryonic stem cells in the presence of noggin. Mol Cell Neurosci *30*, 24-36.

Ivkovic, S., and Ehrlich, M.E. (1999). Expression of the striatal DARPP-32/ARPP-21 phenotype in GABAergic neurons requires neurotrophins in vivo and in vitro. J Neurosci *19*, 5409-5419.

Jessberger, S., Clark, R.E., Broadbent, N.J., Clemenson, G.D., Jr., Consiglio, A., Lie, D.C., Squire, L.R., and Gage, F.H. (2009). Dentate gyrus-specific knockdown of adult neurogenesis impairs spatial and object recognition memory in adult rats. Learn Mem *16*, 147-154.

Jiang, W., Zhang, Y., Xiao, L., Van Cleemput, J., Ji, S.P., Bai, G., and Zhang, X. (2005). Cannabinoids promote embryonic and adult hippocampus neurogenesis and produce anxiolytic- and antidepressant-like effects. J Clin Invest *115*, 3104-3116.

Jin, K., Xie, L., Kim, S.H., Parmentier-Batteur, S., Sun, Y., Mao, X.O., Childs, J., and Greenberg, D.A. (2004). Defective adult neurogenesis in CB1 cannabinoid receptor knockout mice. Mol Pharmacol *66*, 204-208.

Jin, W., Brown, S., Roche, J.P., Hsieh, C., Celver, J.P., Kovoor, A., Chavkin, C., and Mackie, K. (1999). Distinct domains of the CB1 cannabinoid receptor mediate desensitization and internalization. J Neurosci *19*, 3773-3780.

Jones, K.R., Farinas, I., Backus, C., and Reichardt, L.F. (1994). Targeted disruption of the BDNF gene perturbs brain and sensory neuron development but not motor neuron development. Cell *76*, 989-999.

Kano, M., Ohno-Shosaku, T., Hashimotodani, Y., Uchigashima, M., and Watanabe, M. (2009). Endocannabinoid-mediated control of synaptic transmission. Physiol Rev *89*, 309-380.

Kaplan, D.R., and Miller, F.D. (2000). Neurotrophin signal transduction in the nervous system. Curr Opin Neurobiol *10*, 381-391.

Katona, I., and Freund, T.F. (2012). Multiple functions of endocannabinoid signaling in the brain. Annu Rev Neurosci *35*, 529-558.

Kawasaki, H., Mizuseki, K., Nishikawa, S., Kaneko, S., Kuwana, Y., Nakanishi, S., Nishikawa, S.I., and Sasai, Y. (2000). Induction of midbrain dopaminergic neurons from ES cells by stromal cell-derived inducing activity. Neuron *28*, 31-40.

Kee, N., Teixeira, C.M., Wang, A.H., and Frankland, P.W. (2007). Preferential incorporation of adult-generated granule cells into spatial memory networks in the dentate gyrus. Nat Neurosci *10*, 355-362.

Khaspekov, L.G., Brenz Verca, M.S., Frumkina, L.E., Hermann, H., Marsicano, G., and Lutz, B. (2004). Involvement of brain-derived neurotrophic factor in cannabinoid receptor-dependent protection against excitotoxicity. Eur J Neurosci *19*, 1691-1698.

Kheirbek, M.A., Drew, L.J., Burghardt, N.S., Costantini, D.O., Tannenholz, L., Ahmari, S.E., Zeng, H., Fenton, A.A., and Hen, R. (2013). Differential control of learning and anxiety along the dorsoventral axis of the dentate gyrus. Neuron *77*, 955-968.

Kim, J., Isokawa, M., Ledent, C., and Alger, B.E. (2002). Activation of muscarinic acetylcholine receptors enhances the release of endogenous cannabinoids in the hippocampus. J Neurosci *22*, 10182-10191.

Kim, S.H., Won, S.J., Mao, X.O., Ledent, C., Jin, K., and Greenberg, D.A. (2006). Role for neuronal nitric-oxide synthase in cannabinoid-induced neurogenesis. J Pharmacol Exp Ther *319*, 150-154.

Knoth, R., Singec, I., Ditter, M., Pantazis, G., Capetian, P., Meyer, R.P., Horvat, V., Volk, B., and Kempermann, G. (2010). Murine features of neurogenesis in the human hippocampus across the lifespan from 0 to 100 years. PLoS One *5*, e8809.

Kochman, L.J., dos Santos, A.A., Fornal, C.A., and Jacobs, B.L. (2006). Despite strong behavioral disruption, Delta9-tetrahydrocannabinol does not affect cell proliferation in the adult mouse dentate gyrus. Brain Res *1113*, 86-93.

Koller, W.C., and Trimble, J. (1985). The gait abnormality of Huntington's disease. Neurology *35*, 1450-1454.

Kramer, J., Hegert, C., Guan, K., Wobus, A.M., Muller, P.K., and Rohwedel, J. (2000). Embryonic stem cell-derived chondrogenic differentiation in vitro: activation by BMP-2 and BMP-4. Mech Dev *92*, 193-205.

Kronenberg, G., Reuter, K., Steiner, B., Brandt, M.D., Jessberger, S., Yamaguchi, M., and Kempermann, G. (2003). Subpopulations of proliferating cells of the adult hippocampus respond differently to physiologic neurogenic stimuli. J Comp Neurol *467*, 455-463.

Labandeira-Garcia, J.L., Wictorin, K., Cunningham, E.T., Jr., and Bjorklund, A. (1991). Development of intrastriatal striatal grafts and their afferent innervation from the host. Neuroscience *42*, 407-426.

Lagace, D.C., Whitman, M.C., Noonan, M.A., Ables, J.L., DeCarolis, N.A., Arguello, A.A., Donovan, M.H., Fischer, S.J., Farnbauch, L.A., Beech, R.D.*, et al.* (2007). Dynamic

contribution of nestin-expressing stem cells to adult neurogenesis. J Neurosci *27*, 12623-12629.

Landles, C., and Bates, G.P. (2004). Huntingtin and the molecular pathogenesis of Huntington's disease. Fourth in molecular medicine review series. EMBO Rep *5*, 958-963.

Langa, F., Kress, C., Colucci-Guyon, E., Khun, H., Vandormael-Pournin, S., Huerre, M., and Babinet, C. (2000). Teratocarcinomas induced by embryonic stem (ES) cells lacking vimentin: an approach to study the role of vimentin in tumorigenesis. J Cell Sci *113 Pt 19*, 3463-3472.

Langbehn, D.R., Hayden, M.R., Paulsen, J.S., and Group, P.-H.I.o.t.H.S. (2010). CAG-repeat length and the age of onset in Huntington disease (HD): a review and validation study of statistical approaches. Am J Med Genet B Neuropsychiatr Genet *153B*, 397-408.

Lee, S.H., Lumelsky, N., Studer, L., Auerbach, J.M., and McKay, R.D. (2000). Efficient generation of midbrain and hindbrain neurons from mouse embryonic stem cells. Nat Biotechnol *18*, 675-679.

Lee, S.T., Chu, K., Jung, K.H., Im, W.S., Park, J.E., Lim, H.C., Won, C.H., Shin, S.H., Lee, S.K., Kim, M.*, et al.* (2009). Slowed progression in models of Huntington disease by adipose stem cell transplantation. Ann Neurol *66*, 671-681.

Lee, Y.W., Cho, H.J., Lee, W.H., and Sonntag, W.E. (2012). Whole brain radiation-induced cognitive impairment: pathophysiological mechanisms and therapeutic targets. Biomol Ther (Seoul) *20*, 357-370.

Lehmbrock, C. (2011). Cre-Rekombinase-vermittelte Inaktivierung des CB1-Rezeptors in adulten neuralen Stammzellen. Diplomarbeit der Johannes Gutenberg Universität Mainz.

Lemberger, L. (1980). Potential therapeutic usefulness of marijuana. Annu Rev Pharmacol Toxicol *20*, 151-172.

Leschik, J., Eckenstaler, R., Nieweg, K., Lichtenecker, P., Brigadski, T., Gottmann, K., Lessmann, V., and Lutz, B. (2013). Embryonic stem cells stably expressing BDNF-GFP exhibit a BDNF-release-dependent enhancement of neuronal differentiation. J Cell Sci *126*, 5062-5073.

Li, D.M. (1973). Cardiovascular and respiratory effects of cannabis extracts and 1-tetra-hydrocannabinol (1-THC). Br J Pharmacol *47*, 627P.

Li, X.J., Du, Z.W., Zarnowska, E.D., Pankratz, M., Hansen, L.O., Pearce, R.A., and Zhang, S.C. (2005). Specification of motoneurons from human embryonic stem cells. Nat Biotechnol *23*, 215-221.

Lichtman, A.H., Dimen, K.R., and Martin, B.R. (1995). Systemic or intrahippocampal cannabinoid administration impairs spatial memory in rats. Psychopharmacology (Berl) *119*, 282-290.

Livak, K.J., and Schmittgen, T.D. (2001). Analysis of relative gene expression data using real-time quantitative PCR and the 2(-Delta Delta C(T)) Method. Methods *25*, 402-408.

Lu, B., Nagappan, G., Guan, X., Nathan, P.J., and Wren, P. (2013). BDNF-based synaptic repair as a disease-modifying strategy for neurodegenerative diseases. Nat Rev Neurosci *14*, 401-416.

Lupien, S.J., Maheu, F., Tu, M., Fiocco, A., and Schramek, T.E. (2007). The effects of stress and stress hormones on human cognition: Implications for the field of brain and cognition. Brain Cogn *65*, 209-237.

Lutz, B., Marsicano, G., Maldonado, R., and Hillard, C.J. (2015). The endocannabinoid system in guarding against fear, anxiety and stress. Nat Rev Neurosci *16*, 705-718.

Ma, D.K., Bonaguidi, M.A., Ming, G.L., and Song, H. (2009). Adult neural stem cells in the mammalian central nervous system. Cell Res *19*, 672-682.

Ma, H., Yu, B., Kong, L., Zhang, Y., and Shi, Y. (2012a). Neural stem cells over-expressing brain-derived neurotrophic factor (BDNF) stimulate synaptic protein expression and promote functional recovery following transplantation in rat model of traumatic brain injury. Neurochem Res *37*, 69-83.

Ma, L., Hu, B., Liu, Y., Vermilyea, S.C., Liu, H., Gao, L., Sun, Y., Zhang, X., and Zhang, S.C. (2012b). Human embryonic stem cell-derived GABA neurons correct locomotion deficits in quinolinic acid-lesioned mice. Cell Stem Cell *10*, 455-464.

Mackie, K. (2005). Distribution of cannabinoid receptors in the central and peripheral nervous system. Handb Exp Pharmacol, 299-325.

Maejima, T., Hashimoto, K., Yoshida, T., Aiba, A., and Kano, M. (2001). Presynaptic inhibition caused by retrograde signal from metabotropic glutamate to cannabinoid receptors. Neuron *31*, 463-475.

Malberg, J.E., Eisch, A.J., Nestler, E.J., and Duman, R.S. (2000). Chronic antidepressant treatment increases neurogenesis in adult rat hippocampus. J Neurosci *20*, 9104-9110.

Maltsev, V.A., Rohwedel, J., Hescheler, J., and Wobus, A.M. (1993). Embryonic stem cells differentiate in vitro into cardiomyocytes representing sinusnodal, atrial and ventricular cell types. Mech Dev *44*, 41-50.

Maltsev, V.A., Wobus, A.M., Rohwedel, J., Bader, M., and Hescheler, J. (1994). Cardiomyocytes differentiated in vitro from embryonic stem cells developmentally express cardiac-specific genes and ionic currents. Circ Res *75*, 233-244.

Mangiarini, L., Sathasivam, K., Seller, M., Cozens, B., Harper, A., Hetherington, C., Lawton, M., Trottier, Y., Lehrach, H., Davies, S.W*., et al.* (1996). Exon 1 of the HD gene with an expanded CAG repeat is sufficient to cause a progressive neurological phenotype in transgenic mice. Cell *87*, 493-506.

Marchalant, Y., Brothers, H.M., and Wenk, G.L. (2009). Cannabinoid agonist WIN-55,212-2 partially restores neurogenesis in the aged rat brain. Mol Psychiatry *14*, 1068-1069.

Marsicano, G., Goodenough, S., Monory, K., Hermann, H., Eder, M., Cannich, A., Azad, S.C., Cascio, M.G., Gutierrez, S.O., van der Stelt, M*., et al.* (2003). CB1 cannabinoid receptors and on-demand defense against excitotoxicity. Science *302*, 84-88.

Marsicano, G., and Kuner, R. (2008). Anatomical Distribution of Receptors, Ligands and Enzymes in the Brain and in the Spinal Cord: Circuitries and Neurochemistry. In Cannabinoids and the Brain, A. Köfalvi, ed. (Boston, MA: Springer US), pp. 161-201.

Marsicano, G., and Lutz, B. (1999). Expression of the cannabinoid receptor CB1 in distinct neuronal subpopulations in the adult mouse forebrain. Eur J Neurosci *11*, 4213-4225.

Marsicano, G., Wotjak, C.T., Azad, S.C., Bisogno, T., Rammes, G., Cascio, M.G., Hermann, H., Tang, J., Hofmann, C., Zieglgansberger, W*., et al.* (2002). The endogenous cannabinoid system controls extinction of aversive memories. Nature *418*, 530-534.

Martin, G.R. (1981). Isolation of a pluripotent cell line from early mouse embryos cultured in medium conditioned by teratocarcinoma stem cells. Proc Natl Acad Sci U S A *78*, 7634-7638.

Masana, M., Su, Y.A., Liebl, C., Wang, X.D., Jansen, L., Westerholz, S., Wagner, K.V., Labermaier, C., Scharf, S.H., Santarelli, S.*, et al.* (2014). The stress-inducible actin-interacting protein DRR1 shapes social behavior. Psychoneuroendocrinology *48*, 98-110.

McBride, J.L., Ramaswamy, S., Gasmi, M., Bartus, R.T., Herzog, C.D., Brandon, E.P., Zhou, L., Pitzer, M.R., Berry-Kravis, E.M., and Kordower, J.H. (2006). Viral delivery of glial cell line-derived neurotrophic factor improves behavior and protects striatal neurons in a mouse model of Huntington's disease. Proc Natl Acad Sci U S A *103*, 9345-9350.

Mechoulam, R., Ben-Shabat, S., Hanus, L., Ligumsky, M., Kaminski, N.E., Schatz, A.R., Gopher, A., Almog, S., Martin, B.R., Compton, D.R.*, et al.* (1995). Identification of an endogenous 2-monoglyceride, present in canine gut, that binds to cannabinoid receptors. Biochem Pharmacol *50*, 83-90.

Mechoulam, R., Braun, P., and Gaoni, Y. (1967). A stereospecific synthesis of (-)-delta 1- and (-)-delta 1(6)-tetrahydrocannabinols. J Am Chem Soc *89*, 4552-4554.

Menalled, L.L., C.; Ramboz, S.; Brunner, D.; Lager, B.; Noble, S.; Park, L.; Howland, D. (2014). A Field Guide to Working with Mouse Models of Huntington's Disease. CHDI, The Jackson Laboratory, PsychoGenics, Inc.

Metna-Laurent, M., and Marsicano, G. (2015). Rising stars: modulation of brain functions by astroglial type-1 cannabinoid receptors. Glia *63*, 353-364.

Michoulam, R., and Shvo, Y. (1963). Hashish. I. The structure of cannabidiol. Tetrahedron *19*, 2073-2078.

Mizuno, K., and Giese, K.P. (2005). Hippocampus-dependent memory formation: do memory type-specific mechanisms exist? J Pharmacol Sci *98*, 191-197.

Monje, M.L., Mizumatsu, S., Fike, J.R., and Palmer, T.D. (2002). Irradiation induces neural precursor-cell dysfunction. Nat Med *8*, 955-962.

Monje, M.L., Toda, H., and Palmer, T.D. (2003). Inflammatory blockade restores adult hippocampal neurogenesis. Science *302*, 1760-1765.

Monory, K., Massa, F., Egertova, M., Eder, M., Blaudzun, H., Westenbroek, R., Kelsch, W., Jacob, W., Marsch, R., Ekker, M.*, et al.* (2006). The endocannabinoid system controls key epileptogenic circuits in the hippocampus. Neuron *51*, 455-466.

Moreira, F.A., and Lutz, B. (2008). The endocannabinoid system: emotion, learning and addiction. Addict Biol *13*, 196-212.

Morris, R.G., Garrud, P., Rawlins, J.N., and O'Keefe, J. (1982). Place navigation impaired in rats with hippocampal lesions. Nature *297*, 681-683.

Mu, Y., Lee, S.W., and Gage, F.H. (2010). Signaling in adult neurogenesis. Curr Opin Neurobiol *20*, 416-423.

Mulder, J., Aguado, T., Keimpema, E., Barabas, K., Ballester Rosado, C.J., Nguyen, L., Monory, K., Marsicano, G., Di Marzo, V., Hurd, Y.L.*, et al.* (2008). Endocannabinoid signaling controls pyramidal cell specification and long-range axon patterning. Proc Natl Acad Sci U S A *105*, 8760-8765.

Murray, C.J., Vos, T., Lozano, R., Naghavi, M., Flaxman, A.D., Michaud, C., Ezzati, M., Shibuya, K., Salomon, J.A., Abdalla, S.*, et al.* (2012). Disability-adjusted life years (DALYs) for 291 diseases and injuries in 21 regions, 1990-2010: a systematic analysis for the Global Burden of Disease Study 2010. Lancet *380*, 2197-2223.

Navarrete, M., and Araque, A. (2010). Endocannabinoids potentiate synaptic transmission through stimulation of astrocytes. Neuron *68*, 113-126.

Navarrete, M., Diez, A., and Araque, A. (2014). Astrocytes in endocannabinoid signalling. Philos Trans R Soc Lond B Biol Sci *369*, 20130599.

Nichols, J., and Smith, A. (2012). Pluripotency in the embryo and in culture. Cold Spring Harb Perspect Biol *4*, a008128.

Nunez, E., Benito, C., Pazos, M.R., Barbachano, A., Fajardo, O., Gonzalez, S., Tolon, R.M., and Romero, J. (2004). Cannabinoid CB2 receptors are expressed by perivascular microglial cells in the human brain: an immunohistochemical study. Synapse *53*, 208-213.

O'Connor, T.P., and Crystal, R.G. (2006). Genetic medicines: treatment strategies for hereditary disorders. Nat Rev Genet *7*, 261-276.

O'Sullivan, S.E. (2007). Cannabinoids go nuclear: evidence for activation of peroxisome proliferator-activated receptors. Br J Pharmacol *152*, 576-582.

Okabe, S., Forsberg-Nilsson, K., Spiro, A.C., Segal, M., and McKay, R.D. (1996). Development of neuronal precursor cells and functional postmitotic neurons from embryonic stem cells in vitro. Mech Dev *59*, 89-102.

Okamoto, K., Okazawa, H., Okuda, A., Sakai, M., Muramatsu, M., and Hamada, H. (1990). A novel octamer binding transcription factor is differentially expressed in mouse embryonic cells. Cell *60*, 461-472.

Ortega, J.A., and Alcantara, S. (2010). BDNF/MAPK/ERK-induced BMP7 expression in the developing cerebral cortex induces premature radial glia differentiation and impairs neuronal migration. Cereb Cortex *20*, 2132-2144.

Oudin, M.J., Hobbs, C., and Doherty, P. (2011). DAGL-dependent endocannabinoid signalling: roles in axonal pathfinding, synaptic plasticity and adult neurogenesis. Eur J Neurosci *34*, 1634-1646.

Pagotto, U., Marsicano, G., Cota, D., Lutz, B., and Pasquali, R. (2006). The emerging role of the endocannabinoid system in endocrine regulation and energy balance. Endocr Rev *27*, 73-100.

Palazuelos, J., Davoust, N., Julien, B., Hatterer, E., Aguado, T., Mechoulam, R., Benito, C., Romero, J., Silva, A., Guzman, M.*, et al.* (2008). The CB(2) cannabinoid receptor controls myeloid progenitor trafficking: involvement in the pathogenesis of an animal model of multiple sclerosis. J Biol Chem *283*, 13320-13329.

Palazuelos, J., Ortega, Z., Diaz-Alonso, J., Guzman, M., and Galve-Roperh, I. (2012). CB2 cannabinoid receptors promote neural progenitor cell proliferation via mTORC1 signaling. J Biol Chem *287*, 1198-1209.

Palmer, T.D., Willhoite, A.R., and Gage, F.H. (2000). Vascular niche for adult hippocampal neurogenesis. J Comp Neurol *425*, 479-494.

Pamplona, F.A., and Takahashi, R.N. (2006). WIN 55212-2 impairs contextual fear conditioning through the activation of CB1 cannabinoid receptors. Neurosci Lett *397*, 88-92.

Papp, M., Willner, P., and Muscat, R. (1991). An animal model of anhedonia: attenuation of sucrose consumption and place preference conditioning by chronic unpredictable mild stress. Psychopharmacology (Berl) *104*, 255-259.

Pencea, V., Bingaman, K.D., Wiegand, S.J., and Luskin, M.B. (2001). Infusion of brain-derived neurotrophic factor into the lateral ventricle of the adult rat leads to new neurons in the parenchyma of the striatum, septum, thalamus, and hypothalamus. J Neurosci *21*, 6706-6717.

Perrier, A.L., Tabar, V., Barberi, T., Rubio, M.E., Bruses, J., Topf, N., Harrison, N.L., and Studer, L. (2004). Derivation of midbrain dopamine neurons from human embryonic stem cells. Proc Natl Acad Sci U S A *101*, 12543-12548.

Phillips, R.G., and LeDoux, J.E. (1992). Differential contribution of amygdala and hippocampus to cued and contextual fear conditioning. Behav Neurosci *106*, 274-285.

Pineda, J.R., Rubio, N., Akerud, P., Urban, N., Badimon, L., Arenas, E., Alberch, J., Blanco, J., and Canals, J.M. (2007). Neuroprotection by GDNF-secreting stem cells in a Huntington's disease model: optical neuroimage tracking of brain-grafted cells. Gene Ther *14*, 118-128.

Plotkin, J.L., Day, M., Peterson, J.D., Xie, Z., Kress, G.J., Rafalovich, I., Kondapalli, J., Gertler, T.S., Flajolet, M., Greengard, P.*, et al.* (2014). Impaired TrkB receptor signaling underlies corticostriatal dysfunction in Huntington's disease. Neuron *83*, 178-188.

Plumpe, T., Ehninger, D., Steiner, B., Klempin, F., Jessberger, S., Brandt, M., Romer, B., Rodriguez, G.R., Kronenberg, G., and Kempermann, G. (2006). Variability of doublecortin-associated dendrite maturation in adult hippocampal neurogenesis is independent of the regulation of precursor cell proliferation. BMC Neurosci *7*, 77.

Porsolt, R.D., Bertin, A., and Jalfre, M. (1977). Behavioral despair in mice: a primary screening test for antidepressants. Arch Int Pharmacodyn Ther *229*, 327-336.

Prenderville, J.A., Kelly, A.M., and Downer, E.J. (2015). The role of cannabinoids in adult neurogenesis. Br J Pharmacol *172*, 3950-3963.

Raber, J., Rola, R., LeFevour, A., Morhardt, D., Curley, J., Mizumatsu, S., VandenBerg, S.R., and Fike, J.R. (2004). Radiation-induced cognitive impairments are associated with changes in indicators of hippocampal neurogenesis. Radiat Res *162*, 39-47.

Radyushkin, K., Anokhin, K., Meyer, B.I., Jiang, Q., Alvarez-Bolado, G., and Gruss, P. (2005). Genetic ablation of the mammillary bodies in the Foxb1 mutant mouse leads to selective deficit of spatial working memory. Eur J Neurosci *21*, 219-229.

Raichlen, D.A., Foster, A.D., Seillier, A., Giuffrida, A., and Gerdeman, G.L. (2013). Exercise-induced endocannabinoid signaling is modulated by intensity. Eur J Appl Physiol *113*, 869-875.

Ramaswamy, S., McBride, J.L., and Kordower, J.H. (2007). Animal models of Huntington's disease. ILAR J *48*, 356-373.

Rauskolb, S., Zagrebelsky, M., Dreznjak, A., Deogracias, R., Matsumoto, T., Wiese, S., Erne, B., Sendtner, M., Schaeren-Wiemers, N., Korte, M.*, et al.* (2010). Global deprivation of brain-derived neurotrophic factor in the CNS reveals an area-specific requirement for dendritic growth. J Neurosci *30*, 1739-1749.

Ray, J., Peterson, D.A., Schinstine, M., and Gage, F.H. (1993). Proliferation, differentiation, and long-term culture of primary hippocampal neurons. Proc Natl Acad Sci U S A *90*, 3602-3606.

Reiner, A., Albin, R.L., Anderson, K.D., D'Amato, C.J., Penney, J.B., and Young, A.B. (1988). Differential loss of striatal projection neurons in Huntington disease. Proc Natl Acad Sci U S A *85*, 5733-5737.

Reubinoff, B.E., Itsykson, P., Turetsky, T., Pera, M.F., Reinhartz, E., Itzik, A., and Ben-Hur, T. (2001). Neural progenitors from human embryonic stem cells. Nat Biotechnol *19*, 1134-1140.

Revest, J.M., Dupret, D., Koehl, M., Funk-Reiter, C., Grosjean, N., Piazza, P.V., and Abrous, D.N. (2009). Adult hippocampal neurogenesis is involved in anxiety-related behaviors. Mol Psychiatry *14*, 959-967.

Rey, A.A., Purrio, M., Viveros, M.P., and Lutz, B. (2012). Biphasic effects of cannabinoids in anxiety responses: CB1 and GABA(B) receptors in the balance of GABAergic and glutamatergic neurotransmission. Neuropsychopharmacology *37*, 2624-2634.

Reynolds, B.A., and Weiss, S. (1992). Generation of neurons and astrocytes from isolated cells of the adult mammalian central nervous system. Science *255*, 1707-1710.

Rivera, P., Romero-Zerbo, Y., Pavon, F.J., Serrano, A., Lopez-Avalos, M.D., Cifuentes, M., Grondona, J.M., Bermudez-Silva, F.J., Fernandez-Llebrez, P., de Fonseca, F.R.*, et al.* (2011). Obesity-dependent cannabinoid modulation of proliferation in adult neurogenic regions. Eur J Neurosci *33*, 1577-1586.

Rohwedel, J., Maltsev, V., Bober, E., Arnold, H.H., Hescheler, J., and Wobus, A.M. (1994). Muscle cell differentiation of embryonic stem cells reflects myogenesis in vivo: developmentally regulated expression of myogenic determination genes and functional expression of ionic currents. Dev Biol *164*, 87-101.

Rolfe, A., and Sun, D. (2015). Stem Cell Therapy in Brain Trauma: Implications for Repair and Regeneration of Injured Brain in Experimental TBI Models. In Brain Neurotrauma: Molecular, Neuropsychological, and Rehabilitation Aspects, F.H. Kobeissy, ed. (Boca Raton (FL)).

Ross, C.A., Aylward, E.H., Wild, E.J., Langbehn, D.R., Long, J.D., Warner, J.H., Scahill, R.I., Leavitt, B.R., Stout, J.C., Paulsen, J.S.*, et al.* (2014). Huntington disease: natural history, biomarkers and prospects for therapeutics. Nat Rev Neurol *10*, 204-216.

Ross, R.A. (2009). The enigmatic pharmacology of GPR55. Trends Pharmacol Sci *30*, 156-163.

Sambrook, J., and Russell, D. (2001). Molecular Cloning: A Laboratory Manual (Cold Spring Harbor Laboratory Press).

Sanai, N., Nguyen, T., Ihrie, R.A., Mirzadeh, Z., Tsai, H.H., Wong, M., Gupta, N., Berger, M.S., Huang, E., Garcia-Verdugo, J.M.*, et al.* (2011). Corridors of migrating neurons in the human brain and their decline during infancy. Nature *478*, 382-386.

Sanberg, P.R., and Coyle, J.T. (1984). Scientific approaches to Huntington's disease. CRC Crit Rev Clin Neurobiol *1*, 1-44.

Santarelli, L., Saxe, M., Gross, C., Surget, A., Battaglia, F., Dulawa, S., Weisstaub, N., Lee, J., Duman, R., Arancio, O.*, et al.* (2003). Requirement of hippocampal neurogenesis for the behavioral effects of antidepressants. Science *301*, 805-809.

Sari, Y. (2011). Huntington's Disease: From Mutant Huntingtin Protein to Neurotrophic Factor Therapy. Int J Biomed Sci *7*, 89-100.

Saxe, M.D., Battaglia, F., Wang, J.W., Malleret, G., David, D.J., Monckton, J.E., Garcia, A.D., Sofroniew, M.V., Kandel, E.R., Santarelli, L.*, et al.* (2006). Ablation of hippocampal neurogenesis impairs contextual fear conditioning and synaptic plasticity in the dentate gyrus. Proc Natl Acad Sci U S A *103*, 17501-17506.

Scharfman, H., Goodman, J., Macleod, A., Phani, S., Antonelli, C., and Croll, S. (2005). Increased neurogenesis and the ectopic granule cells after intrahippocampal BDNF infusion in adult rats. Exp Neurol *192*, 348-356.

Schilling, G., Becher, M.W., Sharp, A.H., Jinnah, H.A., Duan, K., Kotzuk, J.A., Slunt, H.H., Ratovitski, T., Cooper, J.K., Jenkins, N.A.*, et al.* (1999). Intranuclear inclusions and neuritic aggregates in transgenic mice expressing a mutant N-terminal fragment of huntingtin. Hum Mol Genet *8*, 397-407.

Schmidt-Hieber, C., Jonas, P., and Bischofberger, J. (2004). Enhanced synaptic plasticity in newly generated granule cells of the adult hippocampus. Nature *429*, 184-187.

Schmitt, R.M., Bruyns, E., and Snodgrass, H.R. (1991). Hematopoietic development of embryonic stem cells in vitro: cytokine and receptor gene expression. Genes Dev *5*, 728-740.

Scholer, H.R., Ruppert, S., Suzuki, N., Chowdhury, K., and Gruss, P. (1990). New type of POU domain in germ line-specific protein Oct-4. Nature *344*, 435-439.

Schroeder, I.S., Rolletschek, A., Blyszczuk, P., Kania, G., and Wobus, A.M. (2006). Differentiation of mouse embryonic stem cells to insulin-producing cells. Nat Protoc *1*, 495-507.

Seki, T., and Arai, Y. (1993). Highly polysialylated neural cell adhesion molecule (NCAM-H) is expressed by newly generated granule cells in the dentate gyrus of the adult rat. J Neurosci *13*, 2351-2358.

Seri, B., Garcia-Verdugo, J.M., Collado-Morente, L., McEwen, B.S., and Alvarez-Buylla, A. (2004). Cell types, lineage, and architecture of the germinal zone in the adult dentate gyrus. J Comp Neurol *478*, 359-378.

Seri, B., Garcia-Verdugo, J.M., McEwen, B.S., and Alvarez-Buylla, A. (2001). Astrocytes give rise to new neurons in the adult mammalian hippocampus. J Neurosci *21*, 7153-7160.

Shin, E., Palmer, M.J., Li, M., and Fricker, R.A. (2012). GABAergic neurons from mouse embryonic stem cells possess functional properties of striatal neurons in vitro, and develop into striatal neurons in vivo in a mouse model of Huntington's disease. Stem Cell Rev *8*, 513-531.

Shin, J., Berg, D.A., Zhu, Y., Shin, J.Y., Song, J., Bonaguidi, M.A., Enikolopov, G., Nauen, D.W., Christian, K.M., Ming, G.L.*, et al.* (2015). Single-Cell RNA-Seq with Waterfall Reveals Molecular Cascades underlying Adult Neurogenesis. Cell Stem Cell *17*, 360-372.

Shors, T.J., Miesegaes, G., Beylin, A., Zhao, M., Rydel, T., and Gould, E. (2001). Neurogenesis in the adult is involved in the formation of trace memories. Nature *410*, 372-376.

Shors, T.J., Townsend, D.A., Zhao, M., Kozorovitskiy, Y., and Gould, E. (2002). Neurogenesis may relate to some but not all types of hippocampal-dependent learning. Hippocampus *12*, 578-584.

Smith, A.G., Heath, J.K., Donaldson, D.D., Wong, G.G., Moreau, J., Stahl, M., and Rogers, D. (1988). Inhibition of pluripotential embryonic stem cell differentiation by purified polypeptides. Nature *336*, 688-690.

Snyder, B.R., Chiu, A.M., Prockop, D.J., and Chan, A.W. (2010). Human multipotent stromal cells (MSCs) increase neurogenesis and decrease atrophy of the striatum in a transgenic mouse model for Huntington's disease. PLoS One *5*, e9347.

Snyder, J.S., Hong, N.S., McDonald, R.J., and Wojtowicz, J.M. (2005). A role for adult neurogenesis in spatial long-term memory. Neuroscience *130*, 843-852.

Snyder, J.S., Kee, N., and Wojtowicz, J.M. (2001). Effects of adult neurogenesis on synaptic plasticity in the rat dentate gyrus. J Neurophysiol *85*, 2423-2431.

Squinto, S.P., Stitt, T.N., Aldrich, T.H., Davis, S., Bianco, S.M., Radziejewski, C., Glass, D.J., Masiakowski, P., Furth, M.E., Valenzuela, D.M.*, et al.* (1991). trkB encodes a functional receptor for brain-derived neurotrophic factor and neurotrophin-3 but not nerve growth factor. Cell *65*, 885-893.

Squitieri, F., Andrew, S.E., Goldberg, Y.P., Kremer, B., Spence, N., Zeisler, J., Nichol, K., Theilmann, J., Greenberg, J., Goto, J.*, et al.* (1994). DNA haplotype analysis of Huntington disease reveals clues to the origins and mechanisms of CAG expansion and reasons for geographic variations of prevalence. Hum Mol Genet *3*, 2103-2114.

Srinivas, S., Watanabe, T., Lin, C.S., William, C.M., Tanabe, Y., Jessell, T.M., and Costantini, F. (2001). Cre reporter strains produced by targeted insertion of EYFP and ECFP into the ROSA26 locus. BMC Dev Biol *1*, 4.

Stack, E.C., Kubilus, J.K., Smith, K., Cormier, K., Del Signore, S.J., Guelin, E., Ryu, H., Hersch, S.M., and Ferrante, R.J. (2005). Chronology of behavioral symptoms and neuropathological sequela in R6/2 Huntington's disease transgenic mice. J Comp Neurol *490*, 354-370.

Steindel, F., Lerner, R., Haring, M., Ruehle, S., Marsicano, G., Lutz, B., and Monory, K. (2013). Neuron-type specific cannabinoid-mediated G protein signalling in mouse hippocampus. J Neurochem *124*, 795-807.

Steiner, B., Klempin, F., Wang, L., Kott, M., Kettenmann, H., and Kempermann, G. (2006). Type-2 cells as link between glial and neuronal lineage in adult hippocampal neurogenesis. Glia *54*, 805-814.

Steiner, B., Kronenberg, G., Jessberger, S., Brandt, M.D., Reuter, K., and Kempermann, G. (2004). Differential regulation of gliogenesis in the context of adult hippocampal neurogenesis in mice. Glia *46*, 41-52.

Stella, N. (2004). Cannabinoid signaling in glial cells. Glia *48*, 267-277.

Stella, N. (2009). Endocannabinoid signaling in microglial cells. Neuropharmacology *56 Suppl 1*, 244-253.

Steru, L., Chermat, R., Thierry, B., and Simon, P. (1985). The tail suspension test: a new method for screening antidepressants in mice. Psychopharmacology (Berl) *85*, 367-370.

Stevens, L.C., and Varnum, D.S. (1974). The development of teratomas from parthenogenetically activated ovarian mouse eggs. Dev Biol *37*, 369-380.

Strubing, C., Ahnert-Hilger, G., Shan, J., Wiedenmann, B., Hescheler, J., and Wobus, A.M. (1995). Differentiation of pluripotent embryonic stem cells into the neuronal lineage in vitro gives rise to mature inhibitory and excitatory neurons. Mech Dev *53*, 275-287.

Suh, H., Consiglio, A., Ray, J., Sawai, T., D'Amour, K.A., and Gage, F.H. (2007). In vivo fate analysis reveals the multipotent and self-renewal capacities of Sox2+ neural stem cells in the adult hippocampus. Cell Stem Cell *1*, 515-528.

Suh, H., Deng, W., and Gage, F.H. (2009). Signaling in adult neurogenesis. Annu Rev Cell Dev Biol *25*, 253-275.

Sun, K., and Lai, E.C. (2013). Adult-specific functions of animal microRNAs. Nat Rev Genet *14*, 535-548.

Takahashi, K., and Yamanaka, S. (2006). Induction of pluripotent stem cells from mouse embryonic and adult fibroblast cultures by defined factors. Cell *126*, 663-676.

Tattersfield, A.S., Croon, R.J., Liu, Y.W., Kells, A.P., Faull, R.L., and Connor, B. (2004). Neurogenesis in the striatum of the quinolinic acid lesion model of Huntington's disease. Neuroscience *127*, 319-332.

Thomas, K.R., and Capecchi, M.R. (1987). Site-directed mutagenesis by gene targeting in mouse embryo-derived stem cells. Cell *51*, 503-512.

Thomson, J.A., Itskovitz-Eldor, J., Shapiro, S.S., Waknitz, M.A., Swiergiel, J.J., Marshall, V.S., and Jones, J.M. (1998). Embryonic stem cell lines derived from human blastocysts. Science *282*, 1145-1147.

Thored, P., Arvidsson, A., Cacci, E., Ahlenius, H., Kallur, T., Darsalia, V., Ekdahl, C.T., Kokaia, Z., and Lindvall, O. (2006). Persistent production of neurons from adult brain stem cells during recovery after stroke. Stem Cells *24*, 739-747.

Toth, A., Blumberg, P.M., and Boczan, J. (2009). Anandamide and the vanilloid receptor (TRPV1). Vitam Horm *81*, 389-419.

Tozuka, Y., Fukuda, S., Namba, T., Seki, T., and Hisatsune, T. (2005). GABAergic excitation promotes neuronal differentiation in adult hippocampal progenitor cells. Neuron *47*, 803-815.

Treadway, M.T., and Zald, D.H. (2011). Reconsidering anhedonia in depression: lessons from translational neuroscience. Neurosci Biobehav Rev *35*, 537-555.

Tropepe, V., Hitoshi, S., Sirard, C., Mak, T.W., Rossant, J., and van der Kooy, D. (2001). Direct neural fate specification from embryonic stem cells: a primitive mammalian neural stem cell stage acquired through a default mechanism. Neuron *30*, 65-78.

Trzaska, K.A., and Rameshwar, P. (2011). Dopaminergic neuronal differentiation protocol for human mesenchymal stem cells. Methods Mol Biol *698*, 295-303.

Vaillant, A.R., Mazzoni, I., Tudan, C., Boudreau, M., Kaplan, D.R., and Miller, F.D. (1999). Depolarization and neurotrophins converge on the phosphatidylinositol 3-kinase-Akt pathway to synergistically regulate neuronal survival. J Cell Biol *146*, 955-966.

van Dijk, R.M., Lazic, S.E., Slomianka, L., Wolfer, D.P., and Amrein, I. (2016). Large-scale phenotyping links adult hippocampal neurogenesis to the reaction to novelty. Hippocampus *26*, 646-657.

Vandeputte, C., Taymans, J.M., Casteels, C., Coun, F., Ni, Y., Van Laere, K., and Baekelandt, V. (2010). Automated quantitative gait analysis in animal models of movement disorders. BMC Neurosci *11*, 92.

Varma, N., Carlson, G.C., Ledent, C., and Alger, B.E. (2001). Metabotropic glutamate receptors drive the endocannabinoid system in hippocampus. J Neurosci *21*, RC188.

Varvel, S.A., and Lichtman, A.H. (2002). Evaluation of CB1 receptor knockout mice in the Morris water maze. J Pharmacol Exp Ther *301*, 915-924.

Vilar, M., and Mira, H. (2016). Regulation of Neurogenesis by Neurotrophins during Adulthood: Expected and Unexpected Roles. Front Neurosci *10*, 26.

Vonsattel, J.P., Myers, R.H., Stevens, T.J., Ferrante, R.J., Bird, E.D., and Richardson, E.P., Jr. (1985). Neuropathological classification of Huntington's disease. J Neuropathol Exp Neurol *44*, 559-577.

Watts, C., and Dunnett, S.B. (1998). Effects of severity of host striatal damage on the morphological development of intrastriatal transplants in a rodent model of Huntington's disease: implications for timing of surgical intervention. J Neurosurg *89*, 267-274.

Wetzel, R., and Mishra, R. (2014). Huntington's Disease In Structural Biology: Order, Disorder, and Conformational Flux (Oxford, UK: 'Oxford University Press').

Wichterle, H., and Peljto, M. (2008). Differentiation of mouse embryonic stem cells to spinal motor neurons. Curr Protoc Stem Cell Biol *Chapter 1*, Unit 1H 1 1-1H 1 9.

Williams, R.L., Hilton, D.J., Pease, S., Willson, T.A., Stewart, C.L., Gearing, D.P., Wagner, E.F., Metcalf, D., Nicola, N.A., and Gough, N.M. (1988). Myeloid leukaemia inhibitory factor maintains the developmental potential of embryonic stem cells. Nature *336*, 684-687.

Wobus, A.M., Wallukat, G., and Hescheler, J. (1991). Pluripotent mouse embryonic stem cells are able to differentiate into cardiomyocytes expressing chronotropic responses to adrenergic and cholinergic agents and Ca2+ channel blockers. Differentiation *48*, 173-182.

Wolf, S.A., Bick-Sander, A., Fabel, K., Leal-Galicia, P., Tauber, S., Ramirez-Rodriguez, G., Muller, A., Melnik, A., Waltinger, T.P., Ullrich, O*., et al.* (2010). Cannabinoid receptor CB1 mediates baseline and activity-induced survival of new neurons in adult hippocampal neurogenesis. Cell Commun Signal *8*, 12.

Yun, S., Reynolds, R.P., Masiulis, I., and Eisch, A.J. (2016). Re-evaluating the link between neuropsychiatric disorders and dysregulated adult neurogenesis. Nat Med *22*, 1239-1247.

Zhang, C.L., Zou, Y., He, W., Gage, F.H., and Evans, R.M. (2008). A role for adult TLX-positive neural stem cells in learning and behaviour. Nature *451*, 1004-1007.

Zhang, J., Giesert, F., Kloos, K., Vogt Weisenhorn, D.M., Aigner, L., Wurst, W., and Couillard-Despres, S. (2010). A powerful transgenic tool for fate mapping and functional analysis of newly generated neurons. BMC Neurosci *11*, 158.

Zhao, C., Deng, W., and Gage, F.H. (2008). Mechanisms and functional implications of adult neurogenesis. Cell *132*, 645-660.

Zhao, C., Teng, E.M., Summers, R.G., Jr., Ming, G.L., and Gage, F.H. (2006). Distinct morphological stages of dentate granule neuron maturation in the adult mouse hippocampus. J Neurosci *26*, 3-11.

Zhou, J.M., Chu, J.X., and Chen, X.J. (2008). An improved protocol that induces human embryonic stem cells to differentiate into neural cells in vitro. Cell Biol Int *32*, 80-85.

Zlomuzica, A., Viggiano, D., Degen, J., Binder, S., Ruocco, L.A., Sadile, A.G., Willecke, K., Huston, J.P., and Dere, E. (2012). Behavioral alterations and changes in Ca/calmodulin kinase II levels in the striatum of connexin36 deficient mice. Behav Brain Res *226*, 293-300.

Zuccato, C., and Cattaneo, E. (2009). Brain-derived neurotrophic factor in neurodegenerative diseases. Nat Rev Neurol *5*, 311-322.

Zuccato, C., and Cattaneo, E. (2014). Huntington's disease. Handb Exp Pharmacol *220*, 357-409.

Zuccato, C., Ciammola, A., Rigamonti, D., Leavitt, B.R., Goffredo, D., Conti, L., MacDonald, M.E., Friedlander, R.M., Silani, V., Hayden, M.R.*, et al.* (2001). Loss of huntingtin-mediated BDNF gene transcription in Huntington's disease. Science *293*, 493-498.

Zuccato, C., Marullo, M., Conforti, P., MacDonald, M.E., Tartari, M., and Cattaneo, E. (2008). Systematic assessment of BDNF and its receptor levels in human cortices affected by Huntington's disease. Brain Pathol *18*, 225-238.

7 Appendix

7.1 Abbreviations

2-AG	2-arachidonoylglycerol
ABHD6	α/β-hydrolase domain 6
ACSF	Artificial cerebrospinal fluid
AEA	N-arachidonoylethanolamine/ anandamide
ANOVA	Analysis of variance
APC	Allophycocyanin
AraC	Cytosine-β-D-arabinofuranoside
ASPA	Aspartoacylase
BDNF	Brain-derived neurotrophic factor
BrdU	Bromdesoxyuridin
BSA	Bovine serum albumin
CA	Cornu Ammonis region
CAG	Cytosine adenine guanine triplet
CB1	Cannabinoid 1 receptor
CBD	Cannabidiol
CD133	Cluster of differentiation 133
CNS	Central nervous system
CREB	cAMP response element-binding protein
DAGL	Diacyl glycerol lipase-α
DAPI	4',6-diamidino-2-phenylindole
DARPP32	Dopamine- and cAMP-regulated neuronal phosphoprotein
DCX	Doublecortin
DG	Dentate gyrus
Dpi	Days post infection
Dptm	Days post tamoxifen
DSE	Depolarization-induced suppression of excitation
DSI	Depolarization-induced suppression of inhibition
EB	Embryoid body
EBSS	Earl’s balanced salt solution
eCB-LTD	eCB-mediated long-term depression
eCB-STD	eCB-mediated short-term depression

EGF	Epidermal growth factor
ESC	Embryonic stem cell
FAAH	Fatty acid amide hydrolase
FACS	Fluorescence-activated cell sorting
fEPSP	Field excitatory postsynaptic potential
FGF2	Fibroblast growth factor 2
FOXG1	Forkhead box protein G1
FOXP1	Forkhead box protein 1
FSC	Forward scatter
GABA	Gamma-aminobutyric acid
GAPDH	Glyceraldehyde 3-phosphate dehydrogenase
GFAP	Glial fibrillary acidic protein
GFP	Green fluorescent protein
Glast	Glutamate aspartate transporter
GPCR	G-protein coupled receptors
GusB	Glucoronidase beta
HBSS	Hanks' balanced salt solution
HD	Huntington’s disease
HPA	Hypothalamic–pituitary–adrenal
HTT	Huntingtin
IPSC	Induced pluripotent stem cell
ISI	Inter-stimulus-interval
ITSFn	Insulin, transferrin, selenium chloride, fibronectin
IVF	*In vitro* fertilization
KO	Knockout
LF	Left forepaw
LH	Left hindpaw
LIF	Leukemia inhibitory factor
LTP	Long-term potentiation
MACS	Magnetic-activated cell sorting
MAGL	Monoacyl-glycerol lipase
MAM	Methylazoxymethanol acetate
MAP2	Microtubule-associated protein 2
MPP	Medial perforant path
MSN	Medium spiny neuron
mTORC1	Mammalian target of rapamycin complex 1
MWM	Morris water maze

NAPE-PLD	N-acyl phosphatidylethanolamine phospholipase D
NDS	Normal donkey serum
NeuN	Neuronal nuclei
NGF	Nerve growth factor
NMDA	N-methyl-D-aspartat
NPC	Neural progenitor cell
NR2B	N-methyl-D-aspartat receptor subunit 2B
NSC	Neural stem cell
NT	Neurotrophin
Oct-4	Octamer binding transcription factor 4
OLIG2	Oligodendrocyte transcription factor 2
p75NTR	p75 neurotrophin receptor
PBS	Phosphate buffered saline
PCR	Polymerase chain reaction
PE	Phycoerythrin
PFA	Paraformaldehyde
PI3K	Phosphoinositide 3-kinase
PKA	Protein kinase A
PLC	Phospholipase C
PSA-NCAM	Polysialylated-neural cell adhesion molecule
QA	Quinolinic acid
qPCR	Quantitative polymerase chain reaction
R26	Rosa26
RA	Retinoic acid
REST	RE1 silencing transcription factor
RF	Right forepaw
RGC	Radial glia cell
RH	Right hindpaw
RIN	RNA integrity number
RMS	Rostral migratory stream
S100B	S100 calcium-binding protein B
SGZ	Subgranular zone
Shc	Src homology 2 domain-containing adapter protein
SORT	Spatial object recognition test
SSC	Side scatter
SSEA-1	Stage-specific embryonic antigen 1
SSRI	Selective serotonin reuptake inhibitor

Sox2	SRY-box transcription factor 2
SVZ	Subventricular zone
TAM	Tamoxifen
TBI	Traumatic brain injury
TBS	Tris buffered saline
THC	Δ^9-tetrahydrocannabinol
TK	Thymidine kinase
TrkB	Tropomyosin-receptor kinase B
TRPV1	Transient receptor potential vanilloid type 1
TX	Triton X-100
UTR	Untranslated region
YFP	Yellow fluorescent protein

7.2 List of figures

7.3 List of tables